Investigation of a wool measurement device for determining the mean diameter of a sample consisting of multiple wool fibres

by
Dirk-Mathys Spangenberg

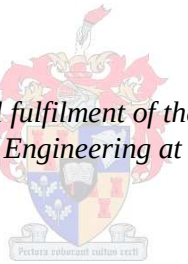

Thesis presented in partial fulfilment of the requirements for the degree Master of Science in Engineering at Stellenbosch University

Supervisor: Prof. Willem Jacobus Perold
Co-Supervisors: Dr. Johan Burger and Prof. Hubertus von Bergmann
Department of Electrical and Electronic Engineering in collaboration with the Department of Physics

March 2012

Stellenbosch University http://scholar.sun.ac.za

Declaration

By submitting this thesis electronically, I declare that the entirety of the work contained therein is my own, original work, that I am the owner of the copyright thereof (save to the extent explicitly otherwise stated), that reproduction and publication thereof by Stellenbosch University will not infringe any third party rights and that I have not previously in its entirety or in part submitted it for obtaining any qualification.

Date: March 2012

Copyright © 2012 Stellenbosch University

All rights reserved

Stellenbosch University http://scholar.sun.ac.za

Abstract

Investigation of a wool measurement device for determining the mean diameter of a sample consisting of multiple wool fibers

D. Spangenberg

Supervisors: Dr. Johan Burger and Prof. Hubertus von Bergmann
Co-Supervisor: Prof. Willem Jacobus Perold
Department of Electrical and Electronic Engineering in collaboration with the Department of Physics

Thesis: MScEng (Electronic Engineering)

March 2012

In the wool trade the mean diameter of wool is a primary indicator of wool quality. It is currently standard practice for a wool grower to send samples to a laboratory for classification before and after shearing. The devices used to make measurements on samples are often big and bulky and sensitive to the environment, thus they are not ideally suited for on site testing. A brief discussion of the industry is given with background information on existing devices as well as information about organic fibres in general.

We test an experimental device which has the potential to be robust and compact based on the Fourier optical principle. Two initial designs are considered and the transmission design is further developed into a working system. The working system is evaluated in a sample measurement experiment. In our sample measurement experiment we determine the mean diameter of a set of samples which has been analysed by an external testing body such that the measurements could be compared.

Stellenbosch University http://scholar.sun.ac.za

Uittreksel

'n Ondersoek na die navorsing en ontwikkeling van 'n meetinstrument om die gemiddelde dikte van veelvoudige wolhaar vesels te bepaal

("Wool measurement: An Investigation into Research & Development")

D. Spangenberg

Supervisors: Dr. Johan Burger and Prof. Hubertus von Bergmann
Co-Supervisor: Prof. Willem Jacobus Perold
Department of Electrical and Electronic Engineering in collaboration with the Department of Physics

Tesis: MScIng (Elektroniese Ingenieurswese)

Maart 2012

In die wol bedryf word die gemiddelde diameter van wol as 'n primêre kwaliteitindeks gebruik. Dit is tans gebruiklik om wol monsters na 'n laboratorium te stuur vir klassifikasie voor en na die skape geskeer word. Die toestel wat gebruik word om die wol monsters te klassifiseer is geneig om groot, lomp en sensitief vir die omgewing te wees en is sodoende nie ideaal vir veld gebruik nie. 'n Kort uitleg van die industrie word gegee tesame met agtergrond inligting van bestaande toestelle asook agtergrond oor organiese vesels in die algemeen.

Ons toets 'n eksperimentele toestel wat potensieel kompak en aanpasbaar kan wees en gebaseer is op die Fourier optiese prinsiep. Twee aanvanklike ontwerpe word oorweeg en eindelik word die transmissie ontwerp verder ontwikkel tot 'n werkende sisteem. Die sisteem word geëvalueer in 'n monster meting eksperiment. In die monster meting eksperiment bepaal ons die gemiddelde diameter van 'n stel monsters waarvan die gemiddelde diameter deur 'n eksterne liggaam bepaal is om sodoende die metings te kan vergelyk.

Stellenbosch University http://scholar.sun.ac.za

Acknowledgements

I would like to express my sincere gratitude to the following people and organisations without whom this research would not have been possible.

- The National Reasearch Foundation who supplied the funding for the project
- Dr. Burger, Prof von Bergmann and Prof W.J. Perold
- Johanna Oosthuizen of Cape Mohair and Wool who supplied me with reference test samples
- Mr. Van der Leij and Mr. Phindile at Innovus

Stellenbosch University http://scholar.sun.ac.za

Dedications

Ek dra hierdie tesis op aan almal wat my ondersteun het en bygedra het tydens die studie.

Stellenbosch University http://scholar.sun.ac.za

Contents

Stellenbosch University http://scholar.sun.ac.za

Stellenbosch University http://scholar.sun.ac.za

Stellenbosch University http://scholar.sun.ac.za

List of Figures

Stellenbosch University http://scholar.sun.ac.za

Stellenbosch University http://scholar.sun.ac.za

Stellenbosch University http://scholar.sun.ac.za

Stellenbosch University http://scholar.sun.ac.za

Stellenbosch University http://scholar.sun.ac.za

List of Tables

Stellenbosch University http://scholar.sun.ac.za

Nomenclature & Abbreviations

Constants

$\pi =$	3.141 592 654	
e =	2.718 281 828	
$j =$	$\sqrt{-1}$	
$c =$	299 792 458 Speed of light	[m/s]

Variables

I	Current Coordinate	[Ampere]
V	Voltage Coordinate	[Volt]
x	Coordinate	[m]
λ	Wavelength	[m]

Subscripts

c	Complex valued function

Abbreviations

CSIRO	Commonwealth Scientific and Research Organization
IWTO	International Wool Textile Organisation
AWTA	Australian Wool Testing Authority
OFDA	Optical Fibre Diameter Analyser
FFDA	Fibre Fineness Distribution Analyser

Stellenbosch University http://scholar.sun.ac.za

FDA Fibre Distribution Analyser

TME Test Method under Evaluation

WIRA Wool Industries Research Association

CL Confidence Limit

SD Standard Deviation

CCD Charge Coupled Device

EFL Effective Focal Length

OPL Optical path length

OPD Optical path distance

DFT Discrete Fourier Transform

LTI Linear Time Invariant

Stellenbosch University http://scholar.sun.ac.za

1 Introduction

1.1 Motivation

This thesis is based on the study of a potential method to determine specific properties of wool. We will be looking at a Fourier optical system to determine the mean diameter of wool fibres. In this thesis the challenge will be to determine the obstacles in building a Fourier optical system which must meet specific demands in terms of measurement range and physical size. Many different devices exist to determine the properties of wool. Standardized techniques to measure the properties of wool are enforced by the International Wool Trade Organisation (IWTO) who evaluates devices and determine set procedures to follow when measurements are made with said devices to ensure a uniform standard across the market. The measurement technique we will look at could potentially be adopted by the IWTO for wool classification purposes or potentially it could be developed into a hand held device which farmers could use for breeding purposes or possibly to classify wool prior to shearing.

1.2 Research Objectives

The main objective of this thesis is to investigate a potential method which could be used to determine the mean thickness of a random sample of wool fibres, outlining all the difficulties encountered. This project aims to experimentally prove that a device could be built to determine the mean thickness of a random sample of wool by means of the Fourier optical principle. We further wish to verify resultant measurements obtained by the device from a single wool sample set against measurements from a laboratory certified by the IWTO on the same wool sample set.

Stellenbosch University http://scholar.sun.ac.za

1.3 Thesis Outline

Chapter One serves as an introduction.

Chapter Two serves as a literature study giving background theory related to light and its application in this thesis.

Chapter Three serves as a literature study which gives an overview of the wool industry and wool measurement techniques.

Chapter Four is dedicated to theoretically finding and solving design parameters in order to design a Fourier optical system.

Chapter Five is dedicated to the testing of the Fourier optical systems developed in Chapter Four and finding solutions to practical problems encountered in order to have a working experimental Fourier optical setup.

Chapter Six is dedicated to defining the system parameters and defining the method used to do pattern analysis and all required parameters which are needed to do the pattern analysis.

Chapter Seven is dedicated to determine comparative results between our Fourier optical system and samples obtained from an external laboratory.

Chapter Eight serves as a conclusion considering the results from the comparative sample experiment and discusses future development and the possible market segments within which such a device could compete.

Stellenbosch University http://scholar.sun.ac.za

2

The properties of light

This chapter will serve as the foundation of theory describing and explaining the principles upon which Fourier optics is based. As such we will look at the implications of linear time invariance on wave theory and how it is applied to electromagnetic theory. From electromagnetic theory we highlight the applicability of the ray which is widely used in geometric optics. The ray is then applied to geometric optics and extrapolated to demonstrate the working of Fourier optics and give insight into aberrations. Diffraction is then discussed in order to describe how electromagnetic waves are affected by obstructions and finally we examine specific simplifications which is applicable to the theory for our application.

2.1 Linear time invariant systems

Linear time invariant systems allow one to break input functions and output solutions modified by a system into a set of simple base functions which could easily be individually analysed. In this section we will define systems in general and define and discuss what linear time invariance means and how it applies to the wave equation. The discussion follows from Gaskill [13][1].

2.1.1 Systems

Let's first look at systems, linearity and time invariance and discuss the implications thereof.

A system transforms a function or set of functions into a new set of functions such that for a given set of input functions $\{f_1(x), f_2(x), .., f_n(x)\}$ one has a corresponding set of output functions $\{g_1(x), g_2(x), ..., g_n(x)\}$ through the $\mathcal{S}\{\}$

[1] Gaskill [13] on page 135

Stellenbosch University http://scholar.sun.ac.za

operator, thus

$$\mathcal{S}\{f_i(x)\} = g_i(x), \qquad i = 1, 2, ..., n, . \tag{2.1}$$

It is not immediately obvious from the notation of Eq. (2.1) what is meant by a system. The following example gives a better understanding of the concept,

$$\frac{d^2}{dx^2}g_i(x) + Kg_i(x) = f_i(x). \tag{2.2}$$

The function $f_i(x)$ acts as a forcing function and the function $g_i(x)$ is the solution and the output. We will refer to the input and output functions as input and output signals in the following sections.

2.1.2 Linearity

A system $\mathcal{S}\{f(x)\}$ is said to be linear if for the given input signals $f_1(x)$ and $f_2(x)$ if the following property holds,

$$\mathcal{S}\{a_1 f_1(x) + a_2 f_2(x)\} = a_1 g_1(x) + a_2 g_2(x). \tag{2.3}$$

Linearity implies that an input signal could be split into the sum of a set of signals which could each be individually processed by the system to give a resultant set of output solutions, the sum of which is the solution of the original input signal.

2.1.3 Time invariance

A system $\mathcal{S}\{f(x)\}$ is said to be time or shift invariant if given

$$\mathcal{S}\{f(x)\} = g(x) \tag{2.4}$$

then

$$\mathcal{S}\{f(x - x_0)\} = g(x - x_0). \tag{2.5}$$

Time invariance implies that the response of a system to a signal would be the same regardless of when that signal is applied to the system.

Stellenbosch University http://scholar.sun.ac.za

2.1.4 Waves in the framework of systems

In this section we will show that waves are linear time invariant systems. In order to do so we view the wave equation as a system. Consider the generic wave equation,

$$\nabla^2\psi - \frac{1}{v^2}\frac{\partial^2}{\partial t^2}\psi = 0 \tag{2.6}$$

where

$$\begin{aligned} \nabla^2 &= \text{The Laplacian operator in Cartesian coordinates} \\ v &= \text{The wave velocity} \\ t &= \text{Time} \\ \psi &= \text{The function describing the wave.} \end{aligned}$$

The Laplacian operator ∇^2 is defined as,

$$\nabla^2 = \frac{\partial^2}{\partial x^2} + \frac{\partial^2}{\partial y^2} + \frac{\partial^2}{\partial z^2}. \tag{2.7}$$

One can view Eq. (2.6) in terms of a system as follows

$$\mathcal{S}\{\psi(x,t)\} = 0 = f(x,t). \tag{2.8}$$

With the system as defined by Eq. (2.8) it can be shown that any solution to the wave function is linear and time invariant.

Given two equations describing waves

$$\nabla^2\psi_1 - \frac{1}{v^2}\frac{\partial^2}{\partial t^2}\psi_1 = 0 = f_1 \tag{2.9}$$

$$\nabla^2\psi_2 - \frac{1}{v^2}\frac{\partial^2}{\partial t^2}\psi_2 = 0 = f_2. \tag{2.10}$$

one can add them together to find,

$$\nabla^2(\psi_1 + \psi_2) - \frac{1}{v^2}\frac{\partial^2}{\partial t^2}(\psi_1 + \psi_2) = f_1 + f_2 = 0. \tag{2.11}$$

Thus the generic wave equation, Eq. (2.6), is linear as illustrated by Eq. (2.11). In the same way it can be shown that Eq. (2.6) is time invariant, since the right

Stellenbosch University http://scholar.sun.ac.za

hand side of Eq. (2.6) is zero the time invariant property is directly implied, thus

$$\nabla^2\psi(x+\phi,t) - \frac{1}{v^2}\frac{\partial^2}{\partial t^2}\psi(x+\phi,t) = f(x+\phi,t) = 0 \tag{2.12}$$

$$\nabla^2\psi(x,t+\phi) - \frac{1}{v^2}\frac{\partial^2}{\partial t^2}\psi(x,t+\phi) = f(x,t+\phi) = 0. \tag{2.13}$$

As demonstrated the wave equation is a linear time invariant system. Fourier theory could be used to break up any input to such a system into the sum of sinusoidal functions with varying phase frequency and amplitude each of which could easily be analysed giving a resultant set of output signals which can simply be added together to find the output solution.

It has to be noted that a wave disturbance has both a temporal and spatial dependence, see Fig. 2.1. In terms of Fourier theory this implies that the signal can be seen as the sum of it's temporal frequency components and the sum of it's spatial frequency components.

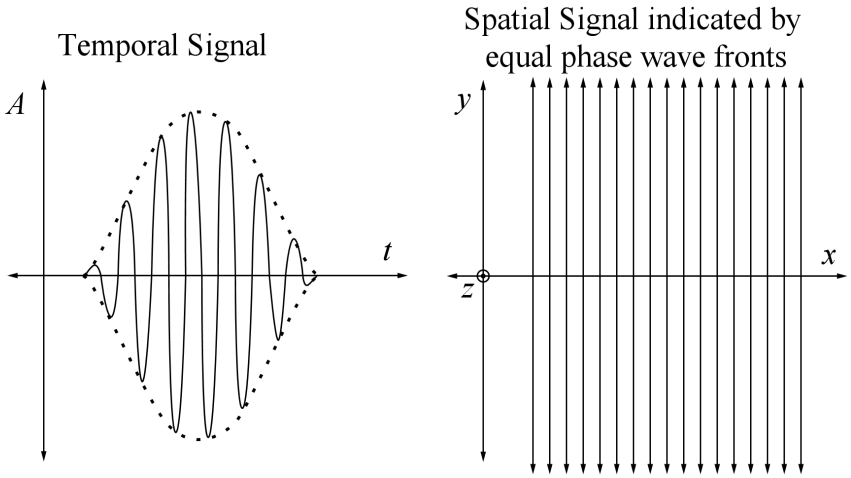

Figure 2.1: An exaggerated disturbance signal split up into it's temporal and spatial components. The intensity A along each wave front is constant and conforms to the temporal signal

In terms of the temporal frequency components it is simple to understand, as the signal is viewed only in terms of time and amplitude. It should be understood that the time axis of the temporal signal is always perpendicular to the wave front.

From the above statement it is apparent that spatial frequency components does not refer to temporal frequency. The spatial geometry of the system is considered and the signal is broken down into a set of plane waves each propagating at different angles, this is referred to as the angular spectrum. The angular spec-

Stellenbosch University http://scholar.sun.ac.za

trum will be discussed in more detail in Section 2.5.2.

This implies that for each temporal frequency component there exist a spatial frequency spectrum and the sum of all of these determines the final resultant disturbance.

2.1.5 The complex wave function

Since linear time invariance implies through Fourier theory that any wave signal is the sum of sinusoidal waves with varying frequency and phases, let's consider the general sinusoidal wave. The following follows from Goodman [2][2] modified only slightly such that we consider waves in general. The equation for any single frequency wave disturbance at a position P and time t is

$$u(P,t) = U(P)\cos[2\pi vt + \phi(P)] \tag{2.14}$$

where

$$\begin{aligned} U(P) &= \text{The amplitude modulation as a function of position} \\ v &= \text{The frequency of the disturbance} \\ t &= \text{Time} \\ \phi(P) &= \text{Position dependant phase contribution.} \end{aligned}$$

Rewriting (2.14) in complex notation one finds

$$u_c(P,t) = U(P)\,e^{-j\phi(P)}e^{-j2\pi vt} \tag{2.15}$$

where

$$u(P,t) = \Re[u_c(P,t)]. \tag{2.16}$$

One can substitute Eq. (2.15) into the wave equation, Eq. (2.17),

$$\nabla^2 u - \frac{1}{c^2}\frac{\partial^2 u}{\partial t^2} = 0 \tag{2.17}$$

where ∇^2 is the Laplacian operator

$$\nabla^2 = \frac{\partial^2}{\partial x^2} + \frac{\partial^2}{\partial y^2} + \frac{\partial^2}{\partial z^2} \tag{2.18}$$

[2]Goodman [2] on page 33

Stellenbosch University http://scholar.sun.ac.za

and if one defines

$$k = \frac{2\pi}{\lambda} \tag{2.19}$$

and

$$U_c = U(P)\, e^{-j\phi(P)} \tag{2.20}$$

then it can be seen that the complex disturbance U_c must satisfy the time-independent equation

$$\left(\nabla^2 + k^2\right) U_c = 0 \tag{2.21}$$

where

$$\begin{aligned} c &= \text{The speed of light} \\ U_c &= \text{The complex disturbance at } P \\ k &= \text{The wave number.} \end{aligned}$$

See Appendix A.1 for a more detailed derivation of Eq. (2.21). Eq. (2.21) is known as the Helmholtz equation. The complex disturbance of any monochromatic wave source must satisfy such a relation, linear time invariance is implied through the wave equation. The Helmholtz equation affords a simpler method to view complex wave disturbances and will serve as a useful starting point for further derivations and discussions.

2.2 Light as electromagnetic radiation

In the previous sections waves in general had been discussed, in this section it will be shown that electromagnetic radiation conforms to the wave equations through Maxwell's equations. Maxwell's equations which describe electromagnetic phenomenon are very generally defined, thus it helps to be able to restrict the set of solutions to the specific application. In optics the spectrum of electromagnetic radiation which applies is referred to as 'light' and roughly spans the visible and near visible range of the electromagnetic spectrum. In the application of optics in this thesis we limit the discussion to electromagnetic radiation through homogenous, isotropic dielectric materials. In this section we define these properties and look at the resultant application with regard to Maxwell's

Stellenbosch University http://scholar.sun.ac.za

equations.

In material sciences the word **homogenous** is used to imply uniformity of the materials density properties, see Hibbeler [14][3]. In terms of light and optics the word implies uniformity with respect to optical properties of a medium as is indicated by the following statement from Carlson [15][4] with respect to light rays, *"In homogeneous media, these rays travel in straight lines, independent of each other"*.

A material is said to be **isotropic**, *"when it's physical properties at each point are independent of direction"*, Born and Wolf [16][5].

Materials with negligibly small specific conductivity are insulators also referred to as **dielectrics**, see Born and Wolf [16][6]. A detailed discussion of how electromagnetic waves propagates through a dielectric material is beyond the scope of this thesis. One only needs to understand that certain dielectric materials such as glass allows electromagnetic waves of certain wavelengths to propagate through it at a lower velocity.

2.2.1 Maxwell's equations for light

Since light is electromagnetic radiation one can use Maxwell's equations to find the wave equations for the electric as well as the magnetic fields. The derivation follows from Carlson [15][7]

Given the time-dependant form of Maxwell's equations,

$$\nabla \times \mathbf{E} = -\frac{\partial \mathbf{B}}{\partial t} \tag{2.22}$$

$$\nabla \times \mathbf{H} = \mathbf{J} + \frac{\partial D}{\partial t} \tag{2.23}$$

$$\nabla \cdot \mathbf{D} = \varrho \tag{2.24}$$

$$\nabla \cdot \mathbf{B} = 0 \tag{2.25}$$

[3] Hibbeler [14] on page 248
[4] Carlson [15] on page 6
[5] Born and Wolf [16] on page 3
[6] Born and Wolf [16] on page 3
[7] Carlson [15] on page 2

Stellenbosch University http://scholar.sun.ac.za

where

$$\begin{aligned} \mathbf{E} &= \text{The electric field} \\ \mathbf{H} &= \text{The magnetic vector} \\ \mathbf{D} &= \text{Electric flux density} \\ \mathbf{B} &= \text{The magnetic induction} \\ \mathbf{J} &= \text{Current density} \\ \varrho &= \text{Free electric charge density.} \end{aligned}$$

From Born and Wolf [16][8], if the medium of interest is isotropic and at rest one can define

$$\mathbf{J} = \sigma\mathbf{E} \tag{2.26}$$
$$\mathbf{D} = \varepsilon\mathbf{E} \tag{2.27}$$
$$\mathbf{B} = \mu\mathbf{H} \tag{2.28}$$

where

$$\begin{aligned} \sigma &= \text{Specific conductivity} \\ \varepsilon &= \text{Dielectric constant} \\ \mu &= \text{Magnetic permeability.} \end{aligned}$$

If one further asserts that the medium in question is source free then ϱ and $\mathbf{J}$ are zero. Further assuming a time harmonic solution of the form $e^{-j2\pi vt}$ one can simplify Eq. (2.22) to Eq. (2.25) by substitution of Eq. (2.26) to Eq. (2.28) to find

$$\nabla \times \mathbf{E} = j2\pi v\mu\mathbf{H} \tag{2.29}$$
$$\nabla \times \mathbf{H} = -j2\pi v\varepsilon\mathbf{E} \tag{2.30}$$
$$\nabla \cdot \mathbf{E} = 0 \tag{2.31}$$
$$\nabla \cdot \mathbf{H} = 0 \tag{2.32}$$

where

$$v = \text{The frequency also referred to as the optical frequency.}$$

[8] Born and Wolf [16] on page 3

Stellenbosch University http://scholar.sun.ac.za

For the purpose of the discussion let's define

$$\omega = 2\pi v. \tag{2.33}$$

One can now rewrite Eq. (2.29) by substituting Eq. (2.33) and taking the divergence on both sides

$$\nabla \times \nabla \times \mathbf{E} = j\omega\mu(\nabla \times \mathbf{H}) \tag{2.34}$$

and substitute Eq. (2.30) into Eq. (2.34) to find

$$\nabla \times \nabla \times \mathbf{E} = \omega^2\mu\varepsilon\mathbf{E}. \tag{2.35}$$

From the identity for an arbitrary vector function $\mathbf{F}$ given as

$$\nabla \times \nabla \times \mathbf{F} = \nabla(\nabla \cdot \mathbf{F}) - \nabla^2\mathbf{F} \tag{2.36}$$

one can manipulate Eq. (2.35) by substitution of Eq. (2.31) and application of the identity given in Eq. (2.36) to find,

$$\nabla^2\mathbf{E} + \omega^2\mu\varepsilon\mathbf{E} = 0. \tag{2.37}$$

In a similar fashion we can find

$$\nabla^2\mathbf{H} + \omega^2\mu\varepsilon\mathbf{H} = 0. \tag{2.38}$$

Carlson [15][9] defines $\mathbf{k}$ as the propagation vector and defines

$$k^2 = \omega^2\mu\varepsilon. \tag{2.39}$$

It is know that,

$$v_\mathrm{p} = \frac{1}{\sqrt{\mu\varepsilon}} \tag{2.40}$$

where

$$v_\mathrm{p} = \text{The velocity of propagation}$$

[9] Carlson [15] on page 4

Stellenbosch University http://scholar.sun.ac.za

and that,

$$\lambda = \frac{2\pi}{\omega} v_{\mathrm{p}} \tag{2.41}$$

thus one can substitute Eq. (2.40) into Eq. (2.39) and substitute Eq. (2.41) into the resultant equation to find,

$$k^2 = \left(\frac{2\pi}{\lambda}\right)^2. \tag{2.42}$$

It can be seen that Eq. (2.42) is the square of the wave number as previously defined by Eq. (2.19).

If one substitutes Eq. (2.39) into Eq. (2.37) and Eq. (2.38) one finds,

$$\left(\nabla^2 + k^2\right)\mathbf{E} = 0 \tag{2.43}$$

$$\left(\nabla^2 + k^2\right)\mathbf{H} = 0. \tag{2.44}$$

The resultant equations, given by Eq. (2.43) and Eq. (2.44), are in the form of the Helmholtz equation for both the **E** and **H** fields.

Both Eq. (2.43) and Eq. (2.44) result in a rule which any electromagnetic disturbance propagating through free space must obey.

As is shown in Section 2.1.4 any disturbance which conforms to the wave equation is linear and time invariant thus enabling us to view electromagnetic radiation as a linear combination of functions to which Fourier theory applies.

2.2.2 Optical paths and rays

In classical optics the ray was used mainly to estimate the position and scaling properties of an optical system. In the previous section it was shown that both the **E** and the **H** fields conform to the complex wave equation and are therefore LTI systems. Thus a light source could be broken up into an infinite number of point sources and further the wave front of each point source can be viewed as the sum of an infinite number of infinitely small areas across the surface of the wave front. If a wave front is divided into an infinite number of infinitely small areas, each of these areas could be represented by a plane wave. In an isotropic homogenous dielectric medium, a ray is defined as the optical path perpendicularly through the centre of such a small section of the wave front, see Hecht [1][10]. From this

[10] Hecht [1] on page 85

Stellenbosch University http://scholar.sun.ac.za

definition it is apparent that the ray is a powerful and accurate tool if used within this context and that it conforms to Maxwell's equations.

Solutions and calculations are easily found and performed for plane waves using electromagnetic theory. By viewing a ray as the optical path normal to a small section of a planar wave front one can calculate the law of refraction across boundaries for such a planar wave. The law of reflection and refraction derived from electromagnetic principles then becomes as given in Hecht [1][11].

In the case of reflection the angle of propagation of a ray, as defined in Fig. 2.2, is described by

$$\theta_i = \theta_r \tag{2.45}$$

where

θ_i = Angle between the interface normal and the incident plane wave
θ_r = Angle between the interface normal and the reflected plane wave.

With respect to refraction the angle of propagation of a ray, as defined in Fig. 2.2, is described by

$$n_i \sin\theta_i = n_t \sin\theta_t \tag{2.46}$$

where

n_i = Refractive index of medium before the interface
n_t = Refractive index of medium after the interface
θ_t = Angle between the interface normal and the transmitted plane wave.

Eq. (2.46) is known as Snell's law of refraction.

The amplitude scaling factors for the electric field can also be calculated for

[11] Hecht [1] on page 92

Stellenbosch University http://scholar.sun.ac.za

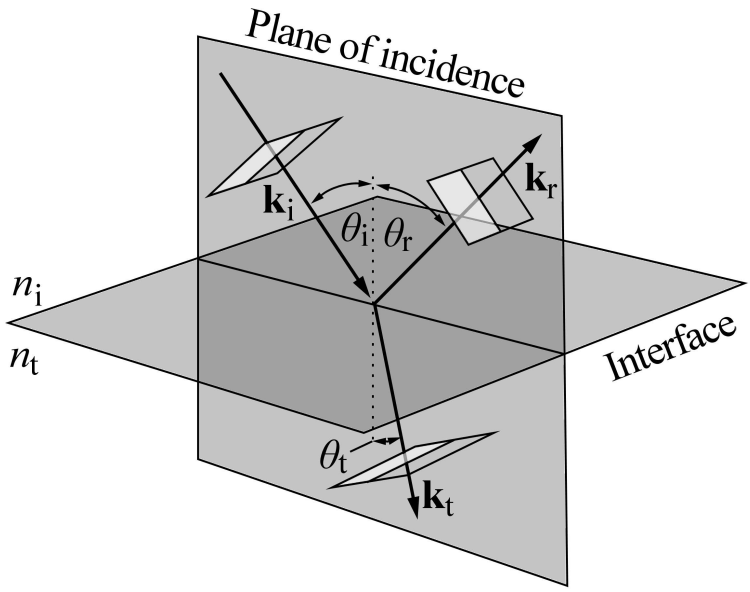

Figure 2.2: Plane waves incident on the boundary between two homogeneous, isotropic, loss less dielectric media from Hecht [1]

plane waves as is done by Hecht [1][12]. These are given as

$$r_\perp = -\frac{\sin(\theta_i - \theta_t)}{\sin(\theta_i + \theta_t)} \tag{2.47}$$

$$r_\parallel = +\frac{\tan(\theta_i - \theta_t)}{\tan(\theta_i + \theta_t)} \tag{2.48}$$

$$t_\perp = +\frac{2\sin\theta_t \cos\theta_i}{\sin(\theta_i + \theta_t)} \tag{2.49}$$

$$t_\parallel = +\frac{2\sin\theta_t \cos\theta_i}{\sin(\theta_i + \theta_t)\cos(\theta_i - \theta_t)} \tag{2.50}$$

where

$r_\perp =$ Amplitude reflection coefficient for **E** perpendicular to plane of incidence

$t_\perp =$ Amplitude transmission coefficient for **E** perpendicular to plane of incidence

$r_\parallel =$ Amplitude reflection coefficient for **E** parallel to the plane of incidence

$t_\parallel =$ Amplitude transmission coefficient for **E** parallel to the plane of incidence.

[12] Hecht [1] on page 94

Stellenbosch University http://scholar.sun.ac.za

In our optical system reflection is either planned or unwanted. The transmission equations are therefore of academic interest only. Generally one can use anti-reflection coatings in order to minimise unwanted reflections.

The **E** and the **H** fields are coupled via Maxwell's equations making calculations complicated. Fortunately work done by Silver [17] shows that under certain conditions one can view the **E** field as a scalar component thereby ignoring the coupling imposed by Maxwell's equations. The conditions under which this simplification is valid, referred to in the following sections as the *scalar conditions*, are as follows

1. The diffracting aperture is large with respect to the wavelength of the incident light.

2. The diffracted fields are not observed close to the aperture.

Work done in this thesis is in accordance with the scalar conditions.

2.3 Geometric optics

Geometric optics in the classic sense is concerned with imaging systems relying primarily on ray tracing as a tool to determine position and scaling properties of optical systems. The computational complexity which results when tracing rays through an optical system gave rise to simplified models of lenses which can be used to estimate the imaging properties of simple optical systems quickly. The simplifications allows us to gain qualitative insight into Fourier optical phenomena.

In this section we will traverse through the simplifications which leads to the ideal model for a lensing system and show how such a lensing system performs an optical Fourier transform.

2.3.1 Basic concepts in optics

In order to follow the discussions related to geometric optics we define some arbitrary terms related to optics. We will restrict definitions to those which are relevant to the terms and concepts in this thesis.

A perfect optical system is capable of forming a perfect image. Deviation from the perfect model is referred to as aberrations. If the aberrations calculated from the optical geometry is smaller than the limitations imposed by diffraction then

Stellenbosch University http://scholar.sun.ac.za

a system is said to be diffraction limited. Diffraction will be discussed in more detail in Section 2.5.

The optical axis could be viewed as a ray which goes through the centre of the optical system or optical systems undeviated except in special cases such as beam splitters and mirrors which serve to redirect or split the optical axis.

The optical centre of an optical system is defined as the point at which an undeviated ray crosses the optical axis while traversing the optical system. It is implicitly defined that such a ray must not be parallel to the optical axis and must be travelling in a plane perpendicular to the optical axis.

Any ray travelling through the optical centre of an optical system is referred to as the principle ray. If such a ray traverses a single lens in air then it's entrance angle and exit angles will be equal, see Hecht [1][13].

Focal length is defined as the distance between the intersection point on the x-axis of a ray parallel to the optical axis traversing through an optical system and the optical centre of the optical system. It is implicitly defined that rays can be extended in the forward and backward direction to find the focal length.

A spherical lens is made of a material with a specific index of refraction bound by two spherical surfaces with finite or infinite diameter. The definition of an aspheric lens is similar except any or both of it's surfaces could be described by an aspheric equation.

2.3.2 The first order approximation in optics

First order geometric optics is based on the assertion that one only considers the case where rays are incident with small angles on the optical surfaces. This leads to the simplification of Snell's law of refraction, which gives rise to thin lens theory. Further assumptions allows us to approximate thick lenses as thin lenses. As computing power became readily available, the need for first order approximations of Snell's law or indeed any approximation faded. The following statement by Hecht [1][14] is made in reference to the design of systems of optical lenses, *"The advent of computerized lens design requires a certain shift in emphasis - there is litttle need to do what a computer can do better"*. Our focus with regard to the first order approximation is not on the simplification of the ray tracing process but rather to gain insight into the Fourier optical properties of a lens.

[13] Hecht [1] on page 211

[14] Hecht [1] on page 211. I take the spelling of *"litttle"* to be correct in the context used, on the grounds of Figure 3.37 on page 71 in Hecht [1] (see Appendix D), and to be interpreted as such: The more t's you add the smaller the quantity implied

Stellenbosch University http://scholar.sun.ac.za

2.3.3 Snell's law under the first order approximation

Let's examine the effect of simplification of Snell's law specifically with respect to thin lenses in the first order approximation. In Fourier optics one is concerned mainly with the effect of optical elements on the angular spectrum of light. As such we will focus our discussion here in this regard.

Let's start by finding the relationship between the slope of a ray entering and exiting a thin lens.

Consider the series expansion for the arbitrary function $\sin\varphi$ and $\cos\varphi$

$$\sin\varphi = \varphi - \frac{\varphi^3}{3!} + \frac{\varphi^5}{5!} - \frac{\varphi^7}{7!} + \frac{\varphi^9}{9!}\cdots \tag{2.51}$$

$$\cos\varphi = 1 - \frac{\varphi^2}{2!} + \frac{\varphi^4}{4!} - \frac{\varphi^6}{6!} + \frac{\varphi^8}{8!}\cdots \tag{2.52}$$

where

$$\varphi = \text{An arbitrary angle.}$$

For small values of φ one can simplify Eq. (2.51) and Eq. (2.52) to

$$\sin\varphi \cong \varphi \tag{2.53}$$

$$\cos\varphi \cong 1. \tag{2.54}$$

From the definition of $\tan\varphi = \sin\varphi/\cos\varphi$ one can write

$$\tan\varphi \cong \varphi. \tag{2.55}$$

Any ray for which the approximations of Eq. (2.53), Eq. (2.54) and Eq. (2.55) are accurate is defined as a paraxial ray and further the region where paraxial rays originating from a point on the optical axis are incident upon a lens are defined as the paraxial region. These definitions hold for small angles, the degree of which must be such that the performance of a lens in it's paraxial region must be diffraction limited.

One can now use Eq. (2.53) and simplify Snells law, Eq. (2.46), to

$$n_1\theta_1 \cong n_2\theta_2 \tag{2.56}$$

Stellenbosch University http://scholar.sun.ac.za

where

n_1 = The refractive index of the first medium
n_2 = The refractive index of the second medium
θ_1 = The angle of incidence before the interface
θ_2 = The angle of incidence after the interface.

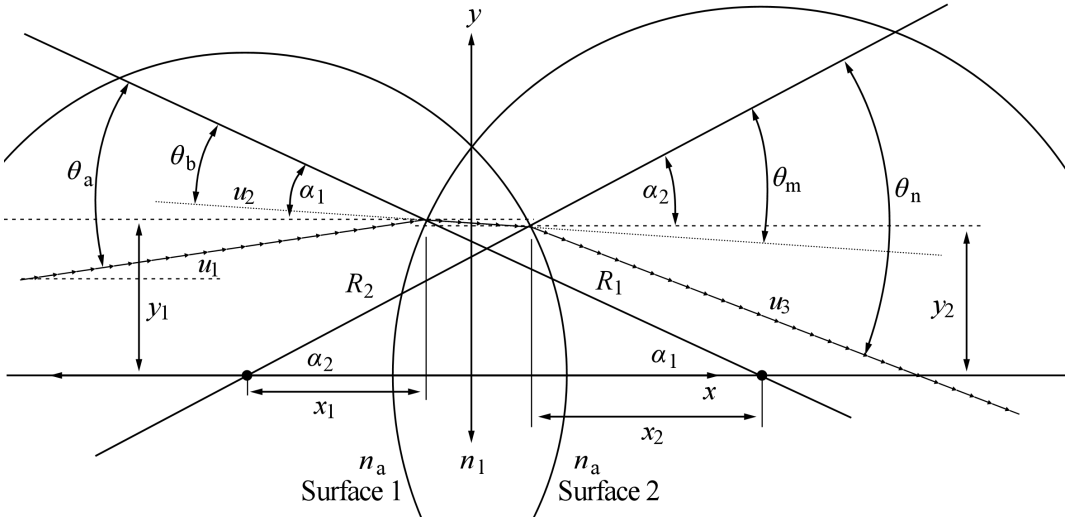

Figure 2.3: Schematic of a thin lens with u denoting gradient and n denoting refractive index

With reference to the first surface of refraction in Fig. 2.3 and the simplified form of the equations given by Eq. (2.53), Eq. (2.54), Eq. (2.55) and Eq. (2.56), one can define the following functions

$$u_2 = \theta_b - \alpha_1 \tag{2.57}$$
$$\theta_a = \alpha_1 + u_1 \tag{2.58}$$
$$\theta_b = \frac{n_a}{n_1}\theta_a \tag{2.59}$$

where, from Fig. 2.3

u_1 = The ray gradient before the lens
u_2 = The ray gradient inside the lens
α_1 = The angle between the optical axis and an interface normal line with the first interface
n_a = The index of refraction of air
n_1 = The index of refraction of the lens

Stellenbosch University http://scholar.sun.ac.za

$\theta_a =$ The angle between the ray before the lens and the interface normal line with the first interface

$\theta_b =$ The angle between the ray inside the lens and the interface normal line with the first interface.

Substituting Eq. (2.58) into Eq. (2.59) and the resultant equation into Eq. (2.57) one finds

$$u_2 = \frac{n_a}{n_l}(\alpha_1 + u_1) - \alpha_1. \tag{2.60}$$

One can repeat the process for the second surface of refraction in Fig. 2.3 to find

$$u_3 = \alpha_2 - \frac{n_l}{n_a}(\alpha_2 - u_2) \tag{2.61}$$

where, from Fig. 2.3,

$u_3 =$ The ray gradient after the lens

$\alpha_2 =$ The angle between the optical axis and an interface normal line with the second interface

$\theta_m =$ The angle between the ray inside the lens and the interface normal line with the second interface

$\theta_n =$ The angle between the ray after the lens and the interface normal line with the second interface.

Substituting Eq. (2.60) into Eq. (2.61) and simplifying one finds

$$u_3 = \left(1 - \frac{n_l}{n_a}\right)(\alpha_1 + \alpha_2) + u_1. \tag{2.62}$$

One can further simplify Eq. (2.62) by assuming that the height at which the ray enters a thin lens is approximately the height at which the ray exits the lens, thus

$$y_1 \cong y_2 = y_h \tag{2.63}$$

where, from Fig. 2.3,

$y_1 =$ The height position on the lens of the ray entering the lens

$y_2 =$ The height position on the lens of the ray exiting the lens

$y_h =$ The approximate height of the ray entering and exiting the lens.

Stellenbosch University http://scholar.sun.ac.za

For small values for α_1 and α_2 one can use the approximation in Eq. (2.54) to find

$$\begin{aligned} \alpha_1 &= \tan^{-1}\left(\frac{y_h}{R_1\cos\alpha_1}\right) \cong \frac{y_h}{R_1} \\ \alpha_2 &= \tan^{-1}\left(\frac{y_h}{-R_2\cos\alpha_2}\right) \cong \frac{y_h}{-R_2} \end{aligned} \tag{2.64}$$

where, from Fig. 2.3,

$$\begin{aligned} R_1 &= \text{The radius of curvature of the first lens surface} \\ R_2 &= \text{The radius of curvature of the second lens surface.} \end{aligned}$$

Substituting the relations in Eq. (2.64) into Eq. (2.62) one finds

$$u_3 = \left(1-\frac{n_l}{n_a}\right)\left(\frac{1}{R_1}-\frac{1}{R_2}\right)y_h + u_1. \tag{2.65}$$

The resultant equation, given as Eq. (2.65), is free from the clutter of the angles introduced by refraction and allows one to predict the gradient of a ray exiting a thin lens, if the gradient of the ray entering the lens is known, the position where the ray enters the lens, the indexes of refraction and both radii of curvature.

One can further simplify Eq. (2.65) by defining the focal length of a thin lens as the distance from the optical centre of the lens to the position where a plane wave would be focused. The rays of a plane wave would be parallel to the optical axis, therefore $u_1 = 0$ and from Eq. (2.65) one can calculate the gradient at which the ray exits the thin lens u_3. From the simple line equation $y = mx + c$ one can calculate the focal length f by noting $m = u_3$ and $y = 0$ when $x = f$ and thus write an expression as

$$0 = \left(1-\frac{n_l}{n_a}\right)\left(\frac{1}{R_1}-\frac{1}{R_2}\right)y_h f + y_h \tag{2.66}$$

where

$$f = \text{The focal length of the lens.}$$

One can rearrange Eq. (2.66) to find,

$$-\frac{1}{f} = \left(1-\frac{n_l}{n_a}\right)\left(\frac{1}{R_1}-\frac{1}{R_2}\right). \tag{2.67}$$

Stellenbosch University http://scholar.sun.ac.za

Substituting Eq. (2.67) into Eq. (2.65) one finds

$$u_3 = u_1 - \frac{y_h}{f}. \tag{2.68}$$

The resulting equation, given in Eq. (2.68), neatly describes the modification in gradient of a ray incident on a thin lens at a position y_h from the optical axis, but it does not give immediate insight into the working of Fourier optics.

In Fourier optics we are interested how light interferes after a lens. It is known that a plane wave front translates to a set of parallel rays and that in an ideal optical system a plane wave would be focused to a diffraction limited spot. To investigate, let's take any two rays which are parallel, thus representing a plane wave, but not parallel with the optical axis and derive an expression for their point of intersection. If this is known we can calculate the resultant effect of interference.

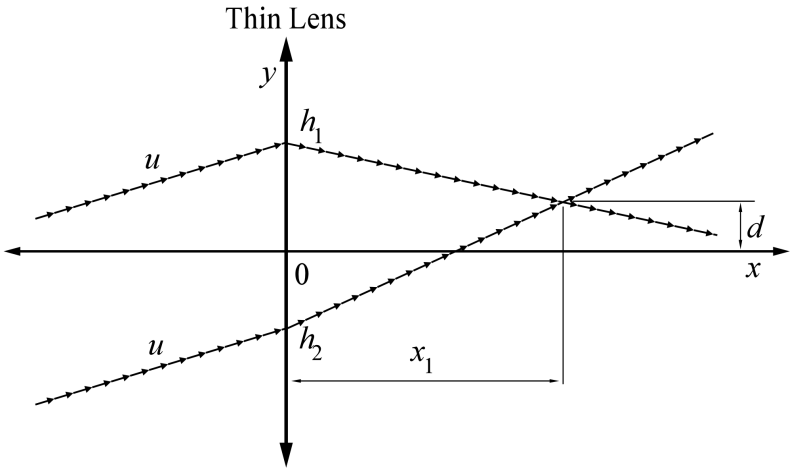

Figure 2.4: Geometry of parallel rays through a thin lens. Note only the perpendicular plane through the optical axis is indicated representing the lens and the heights of the intersection points with the lens plane.

With reference to Fig. 2.4, one can define the two rays in terms of the standard line equation $y = mx + c$ after passing through the thin lens by substituting $m = u_3$ from Eq. (2.68) and defining each as entering the thin lens at h_1, h_2 respectively to find,

$$y_1 = \left(u - \frac{h_1}{f}\right) x + h_1 \tag{2.69}$$

$$y_2 = \left(u - \frac{h_2}{f}\right) x + h_2. \tag{2.70}$$

When equating Eq. (2.69) and Eq. (2.70) to find their intersection with respect

Stellenbosch University http://scholar.sun.ac.za

to the x-axis, denoted by the symbol $x = x_1$ and simplifying we find,

$$x_1 = f. \tag{2.71}$$

One can now find the position where they intersect with respect to the y-axis, denoted by the symbol d, by substitution of Eq. (2.71) into Eq. (2.69) or Eq. (2.70) to find

$$d = uf \tag{2.72}$$

where, from Fig. 2.4

$$\begin{aligned} d &= \text{The position above the optical axis} \\ u &= \text{The gradient of the ray before the lens} \\ f &= \text{The focal length of the lens.} \end{aligned}$$

This neatly implies that in the first order approximation of a thin lens, there is a linear one to one relationship between the focus position (x_1, d) and the angles of incoming plane waves. It further implies these points to lie on a plane at $x = x_1 = f$. If we further take into consideration phase addition caused by the path length of rays in the first order approximation of a thin lens we can show that the resultant output at the focal plane of the thin lens is a Fourier transform, see Appendix A.3, Eq. (A.28). The resultant function found is

$$f(u) = K_{\mathrm{A}} \int_{-\infty}^{\infty} f(y) e^{j\frac{2\pi}{\lambda} yu} dy \tag{2.73}$$

Even though this is an approximation it indicates ideal behaviour, therefore one can conceptually view a lens as such bearing in mind it will not perform perfectly like this. The difference between the first order approximation and the actual situation is known as aberrations. In Section 2.4 we take a more critical look at aberrations in the Fourier optical regime.

2.4 Aberrations and Fourier optics

A wave front error could be calculated for each point on the focal plane. It is known that a perfect optical system would transform light from each point at the focal plane into a plane wave. One can use ray tracing to determine the difference

Stellenbosch University http://scholar.sun.ac.za

between the ideal Optical Path Length (OPL) and the resultant OPL from the optical system as is illustrated in Fig. 2.5.

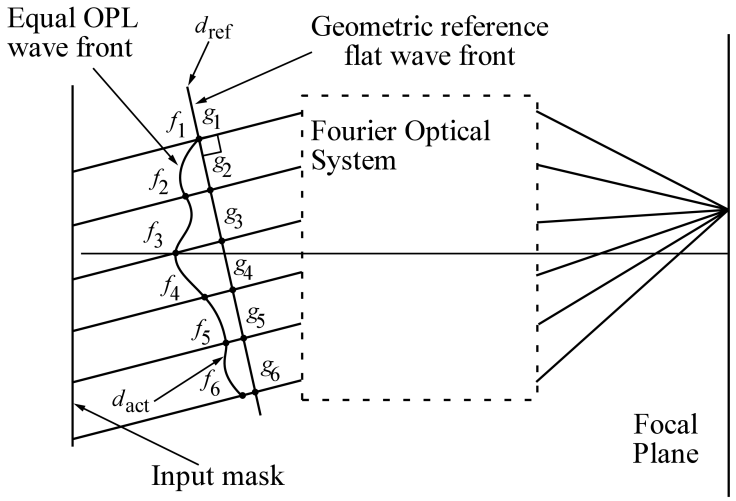

Figure 2.5: Wave front error calculation of an Fourier optical system.

The wavefront error for each point could therefore be described by the the following equation

$$d_{err} = d_{act} - d_{ref} \tag{2.74}$$

where

$$\begin{aligned} d_{err} &= \text{The calculated wave front error} \\ d_{ref} &= \text{The OPL to the geometric reference flat} \\ d_{act} &= \text{The OPL to the actual wavefront.} \end{aligned}$$

When looking at Fourier optical systems such as the general one illustrated in Fig. 2.5, one has to think in terms of how such a system transforms the input mask according to angle at the Fourier optical plane. In this view the wave front error is translated to an angular error and it becomes apparent that even for seemingly large wave front errors, in the order of 5λ, the angular error is still negligibly small. Wave front curvature further results in a slight weighting effect as rays are always perpendicular to the wave front. This weighting is due a spreading of the position from where rays originate at the aperture, but once again the effect is small if the wave front error is small. The resultant effect is loss of pattern definition the same as with imaging.

Stellenbosch University http://scholar.sun.ac.za

2.5 Diffraction theory

Thus far we have shown how the ideal lens performs a Fourier transform, we also discussed briefly how deviation from the ideal could be viewed and how it affects the end result. Diffraction theory completes the picture in the sense that it explains what happens before the aperture and why one is able to view the aperture as a source in itself despite it only being illuminated by a source.

In this section we will give a brief historical view of the development of diffraction theory which follows loosely from Goodman [2][15]. We will then take a look at the mathematical formulation of diffraction theory, the angular spectrum and a more formal approach to the lens as a Fourier optical system.

In simple terms, light not propagating according to rectilinear lines as predicted by reflection or refraction is viewed as diffraction. The existence of diffraction phenomena was first observed experimentally by Grimaldi in 1665. In the experiment Grimaldi placed a light source in front of a screen. The corpuscular theory of light at the time predicted a sharply defined shadow, but the experiment showed a shadow which was not sharply defined.

In 1678 Christian Huygens produced a theory which partially explained the diffraction phenomenon. He theorised that one could construct the wave front at any position by taking the envelope of an infinite number off sources placed on the known wave front as is illustrated in Fig. 2.6.

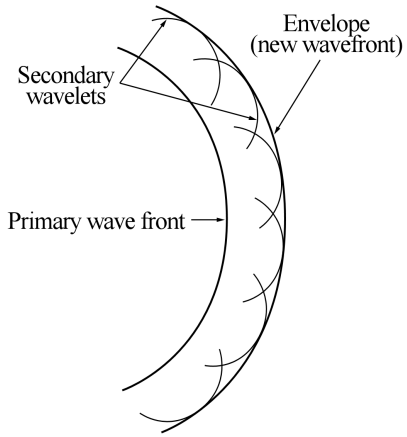

Figure 2.6: Construction of the Huygens envelope from Goodman [2]

In 1818 Augustin Jean Fresnel expanded on the theory of Huygens by taking the phase contribution into account thereby taking interference into account and making some arbitrary assumptions about the initial phases of the secondary

[15]Goodman [2] on page 30

Stellenbosch University http://scholar.sun.ac.za

sources. The theory of Huygens and Fresnel was later proven mathematically by Gustav Kirchoff in 1882. Kirchoff made some assumptions in his mathematical formulation which were proven inconsistent, respectively, by Poincaré in 1892 and Sommerfeld in 1894.

It has to be noted that both the Huygens-Fresnel and Rayleigh-Sommerfeld diffraction theories treat light as a scalar phenomenon thereby neglecting the coupling of the electric and magnetic fields through Maxwell's equations. It has been shown that results from experiments are accurate if the scalar conditions are met, see Section 2.2.1.

2.5.1 Mathematical theory

The mathematical derivations from Goodman [2][16] gives the reader insight into the analysis of diffraction phenomena and serves as a basis for Fourier optical theory with application to light and optics.

Green's theorem is central in the derivation of both the Fresnel-Kirchhoff diffraction formula and the Rayleigh-Sommerfeld diffraction formula. The different solutions resulting from a different choice of Green's functions for each.

From Goodman [2][17], Green's theorem in general states: *Let $U_c(P)$ and $G_c(P)$ be any two complex-valued functions of position, and let S be a closed surface surrounding a volume V. If U_c, G_c and their first and second partial derivatives are single valued and continuous within and on S, then we have:*

$$\iiint_V \left(G_c \nabla^2 U_c - U_c \nabla^2 G_c\right) dv = \iint_S \left(G_c \frac{\partial U_c}{\partial n} - U_c \frac{\partial G_c}{\partial n}\right) ds \qquad (2.75)$$

where $\frac{\partial}{\partial n}$ signifies a partial derivative in the outward normal direction at each point on S.

In the context of this thesis we have,

$$\begin{aligned} U_c &= \text{A complex disturbance at an observation point in space} \\ G_c &= \text{An arbitrary choice of Green's function} \\ V &= \text{Denotes the volume of integration} \\ S &= \text{Denotes a surface enclosing the volume of integration.} \end{aligned}$$

[16] Goodman [2] on page 33
[17] Goodman [2] on page 34

Stellenbosch University http://scholar.sun.ac.za

2.5.1.1 The integral theorem of Helmholtz and Kirchhoff

The integral theorem of Helmholtz and Kirchhoff describes the disturbance at an observation point in terms of the boundary conditions for a chosen Green's function and is an important step in further derivations.

Goodman [2][18] shows how to derive an expression for the observed disturbance at a point P_0. With reference to Fig. 2.7, one can define U_c as the disturbance at an observation point P_0. Application of Green's theorem and choosing a Green's function G_c at an arbitrary point P_1 one finds

$$G_c(P_1) = \frac{\exp(jkr_{01})}{r_{01}} \tag{2.76}$$

where

G_c = the chosen Green's function

r_{01} = the length of the vector $\bar{\mathbf{r}}_{01}$ between the points P_1 and P_0.

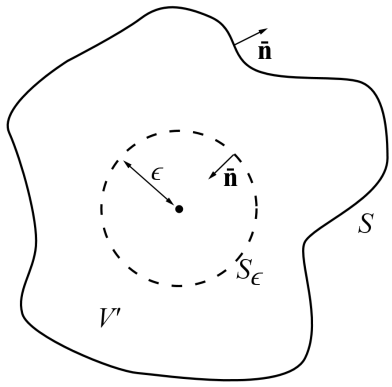

Figure 2.7: Cross section through closed volume of integration. Surfaces indicated by S and S_ϵ, from Goodman [2]

Due to the continuity requirement with respect to the volume of integration, the geometry is divided as shown in Fig. 2.7. The discontinuity at P_0 is excluded by enclosing it in a sphere of radius ϵ. Mathematically this results in a new volume of integration given by

$$S_a = S + S_\epsilon \tag{2.77}$$

[18] Goodman [2] on page 33

Stellenbosch University http://scholar.sun.ac.za

where, from Fig. 2.7,

$$\begin{aligned} S_a &= \text{The newly defined total volume} \\ S &= \text{The new definition of the volume without } S_\epsilon \\ S_\epsilon &= \text{The definition of the excluded volume.} \end{aligned}$$

An expanding spherical wave G_c satisfies the Helmholtz equation (2.21). Noting that the disturbance U_c must also satisfy the Helmholtz equation (2.21) one has

$$\left(\nabla^2 + k^2\right) U_c = 0 \tag{2.78}$$

$$\left(\nabla^2 + k^2\right) G_c = 0. \tag{2.79}$$

If one multiplies Eq. (2.78) by G_c and Eq. (2.79) by U_c and subtract the result one finds

$$G_c \nabla U_c^2 - U_c \nabla G_c^2 = 0. \tag{2.80}$$

Eq. (2.80) can now be substituted into Eq. (2.75) for the surface area as defined in Eq. (2.77) to give

$$-\iint\limits_{S\epsilon} \left(G_c \frac{\partial U_c}{\partial n} - U_c \frac{\partial G_c}{\partial n}\right) ds = \iint\limits_{S} \left(G_c \frac{\partial U_c}{\partial n} - U_c \frac{\partial G_c}{\partial n}\right) ds. \tag{2.81}$$

Now one can find a solution to the left hand side of Eq. (2.81) by solving for the limit where ϵ approaches zero as

$$\iint\limits_{S\epsilon} \left(G_c \frac{\partial U_c}{\partial n} - U_c \frac{\partial G_c}{\partial n}\right) ds = -4\pi U_c\left(P_0\right) \tag{2.82}$$

where

$$P_0 = \text{The observation point.}$$

If one substitutes Eq. (2.82) into Eq. (2.81) and rearrange one finds

$$U_c\left(P_0\right) = \frac{1}{4\pi} \iint\limits_{S} \left(\frac{\partial U_c}{\partial n} G_c - U_c \frac{\partial G_c}{\partial n}\right) ds. \tag{2.83}$$

Stellenbosch University http://scholar.sun.ac.za

The result given in Eq. (2.83) is known as the integral theorem of Helmholtz and Kirchhoff and is used in the further development of diffraction theory as it expresses any arbitrary point P_0 in terms of the boundary values of a wave on any closed surface surrounding said wave.

2.5.1.2 Fresnel-Kirchhoff and Rayleigh-Sommerfeld diffraction

Diffraction integrals such as the Fresnel-Kirchhoff and Rayleigh-Sommerfeld could be derived by solving Eq. (2.83) for the geometry given in Fig. 2.8, also referred to as the z half space as space is split where $x = 0$ and $y = 0$ in the plane of an aperture. In Fig. 2.8 the integral solution Eq. (2.83) is split into two surfaces, a spherical dome which is connected to a plane parallel to the surface of the aperture. Thus Eq. (2.83) becomes

$$U_c(P_0) = \frac{1}{4\pi} \iint_{S_1+S_2} \left(\frac{\partial U_c}{\partial n} G_c - U_c \frac{\partial G_c}{\partial n} \right) ds. \tag{2.84}$$

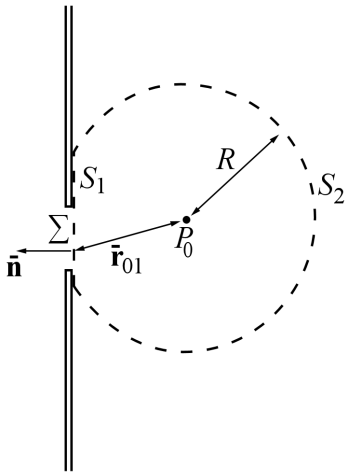

Figure 2.8: Diffraction geometry with diffracting aperture, from Goodman [2]

Let's define G_c as

$$G_c = \frac{\exp(jkr_{01})}{r_{01}}. \tag{2.85}$$

On the surface S_2 the chosen Green's function, as given in Eq. (2.85), is given

Stellenbosch University http://scholar.sun.ac.za

by

$$G_c = \frac{\exp(jkR)}{R}. \tag{2.86}$$

If one takes the normal derivative where the angle between the normal on the surface S_2 and the vector $\bar{\mathbf{r}}_{01}$ is zero, one has

$$\frac{\partial G_c}{\partial n} = \left(jk - \frac{1}{R}\right)\frac{\exp(jkR)}{R} \cong jkG_c \tag{2.87}$$

where the latter approximation holds for sufficiently large R. One can rewrite the integral over S_2 as

$$\frac{1}{4\pi}\iint_{S_2}\left[\frac{\partial U_c}{\partial n}G_c - U_c(jkG_c)\right]ds = \int_{\Omega} G_c\left(\frac{\partial U_c}{\partial n} - jkU_c\right)R^2 d\omega. \tag{2.88}$$

If one looks at Eq. (2.88) it can be seen that the quantity $|RG_c|$ is uniformly bounded on S_2

$$|RG_c| = |\exp(jkR)| = 1.$$

Therefore if

$$\lim_{R\to\infty} R\left(\frac{\partial U_c}{\partial n} - jkU_c\right) = 0 \tag{2.89}$$

then the integral in Eq. (2.88) of the surface S_2 will contribute zero to Eq. (2.84) which means only the surface S_1 contributes to the observation point at P_0. Now Eq. (2.84) can be simplified to

$$U_c(P_0) = \frac{1}{4\pi}\iint_{S_1}\left(\frac{\partial U_c}{\partial n}G_c - U_c\frac{\partial G_c}{\partial n}\right)ds. \tag{2.90}$$

The relation given in Eq. (2.89) is known as the Sommerfeld radiation condition. If we consider that the aperture will be illuminated by a linear combination of spherical disturbances we can be confident that the requirement given by Eq. (2.89) will be satisfied.

The resultant equation, given as Eq. (2.90), means one only needs to integrate over the surface S_1 and this is central to both Fresnel-Kirchhoff and Rayleigh-Sommerfeld diffraction theories.

Stellenbosch University http://scholar.sun.ac.za

Fresnel-Kirchhoff diffraction

With reference to Fig. 2.8, the aperture is opaque except for the open area. Kirchhoff made the following assumptions with respect to the aperture and screen:

- The field across the surface Σ and its derivative are the same as they would be if no aperture were present.
- On the portion of the surface S_1 which lies in the shadow behind the aperture the contribution of the field and its derivative is zero.

These two assumptions allows one to neglect the effect of the boundaries of the aperture and it further simplifies the integral over the surface S_1 such that it needs only be applied over the opening in the aperture denoted by Σ on Fig. 2.8. Thus Eq. (2.90) simplifies to

$$U_c(P_0) = \frac{1}{4\pi}\iint_{\Sigma}\left(\frac{\partial U_c}{\partial n}G_c - U_c\frac{\partial G_c}{\partial n}\right)ds. \tag{2.91}$$

If one takes the normal derivative for the disturbance G_c as given in Eq. (2.85) at a point P_1 inside the opening as illustrated in Fig. 2.9 then the derivative could be written as

$$\frac{\partial G_c(P_1)}{\partial n} = \cos(\bar{\mathbf{n}}, \bar{\mathbf{r}}_{01})\left(jk - \frac{1}{r_{01}}\right)\frac{\exp(jkr_{01})}{r_{01}}. \tag{2.92}$$

If one further assumes r_{01} to be many wavelengths the following condition holds $k \gg \frac{1}{r_{01}}$ and Eq. (2.92) could be approximated by

$$\frac{\partial G_c(P_1)}{\partial n} \cong jk\cos(\bar{\mathbf{n}}, \bar{\mathbf{r}}_{01})\frac{\exp(jkr_{01})}{r_{01}}. \tag{2.93}$$

Substituting Eq. (2.93) into Eq. (2.91) one finds

$$U_c(P_0) = \frac{1}{4\pi}\iint_{\Sigma}\frac{\exp(jkr_{01})}{r_{01}}\left[\frac{\partial U_c}{\partial n} - jkU_c\cos(\bar{\mathbf{n}}, \bar{\mathbf{r}}_{01})\right]ds. \tag{2.94}$$

Now consider Fig. 2.9, if one defines

$$U_c(P_1) = \frac{A\exp(jkr_{21})}{r_{21}} \tag{2.95}$$

Stellenbosch University http://scholar.sun.ac.za

and take the derivative in a similar fashion to the disturbance G_c at a point in the opening of the aperture, P_1, again making the assertion that $k \gg \frac{1}{r_{21}}$ then one finds

$$\frac{\partial U_c(P_1)}{\partial n} \cong jk\cos(\bar{\mathbf{n}}, \bar{\mathbf{r}}_{21})\frac{\exp(jkr_{21})}{r_{21}}. \tag{2.96}$$

Substituting Eq. (2.95) and Eq. (2.96) into Eq. (2.94) one finds

$$U_c(P_0) = \frac{A}{j\lambda}\iint_{\Sigma}\frac{\exp[jk(r_{21}+r_{01})]}{r_{01}r_{21}}\left[\frac{\cos(\bar{\mathbf{n}}, \bar{\mathbf{r}}_{01}) - \cos(\bar{\mathbf{n}}, \bar{\mathbf{r}}_{21})}{2}\right]ds. \tag{2.97}$$

The result relates the observable disturbance at point P_0 to the source disturbance at P_2 as the sum of the secondary sources in the opening of the aperture. The resultant relation given by Eq. (2.97) is known as the Fresnel-Kirchhoff diffraction equation. It is interesting to note that Eq. (2.97) is symmetric, ie. the source could be the sink and the sink the source.

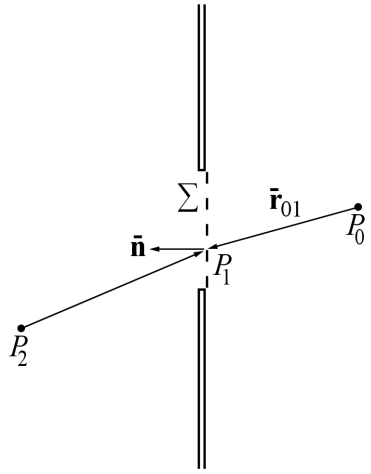

Figure 2.9: Point source illumination of a plane screen, from Goodman [2]

One can rewrite Eq. (2.97) in a simplified form. Let's define

$$U_{ca} = \frac{1}{j\lambda}\left[\frac{A\exp(jkr_{21})}{r_{21}}\right]\left[\frac{\cos(\bar{\mathbf{n}}, \bar{\mathbf{r}}_{01}) - \cos(\bar{\mathbf{n}}, \bar{\mathbf{r}}_{21})}{2}\right]. \tag{2.98}$$

Now one can rewrite (2.97) as

$$U_c(P_0) = \iint_{\Sigma} U_{ca}(P_1)\frac{\exp(jkr_{01})}{r_{01}}ds. \tag{2.99}$$

Stellenbosch University http://scholar.sun.ac.za

With reference to Eq. (2.98) $\frac{\cos(\bar{\mathbf{n}},\bar{\mathbf{r}}_{01})-\cos(\bar{\mathbf{n}},\bar{\mathbf{r}}_{21})}{2}$ is the obliquity factor.

It is interesting to note that the choice of Green's function to arrive at the Fresnel-Kirchhoff diffraction formula Eq. (2.97) leads to the assumption that on the surface of the aperture excluding the opening the disturbance U_c and it's derivative $\frac{\partial U_c}{\partial n}$ is both zero, but this implies that the function must be zero everywhere. This is a mathematical inconsistency. The Rayleigh-Sommerfeld choice of Green's function removes this inconsistency and following the same logic it can be shown that a combination of two similar choices of Green's functions as used by Rayleigh-Sommerfeld will give a result equivalent to the Fresnel Kirchoff solution.

Rayleigh-Sommerfeld diffraction

The difference between the Fresnel-Kirchhoff and the Rayleigh-Sommerfeld diffraction theories lies therein that the second assumption made in the derivation of Fresnel-Kirchhoff's diffraction theory, namely that both the function and it's derivative must be zero on the boundary directly behind the aperture, is eliminated by the choice of a Green's function such that this is affected.

Given a geometry as illustrated in Fig. 2.10 and considering again the function in Eq. (2.90), then for a given Green's function

$$G_{c\phi\text{-}}(P_1) = \frac{\exp(jkr_{01})}{r_{01}} - \frac{\exp(jk\widetilde{r}_{01})}{\widetilde{r}_{01}} \tag{2.100}$$

if the derivative is taken one finds

$$\frac{\partial G_{c\phi\text{-}}}{\partial n} = \cos(\bar{\mathbf{n}},\bar{\mathbf{r}}_{01})\left(jk-\frac{1}{r_{01}}\right)\frac{\exp(jkr_{01})}{r_{01}} - \cos(\bar{\mathbf{n}},\widetilde{\bar{\mathbf{r}}}_{01})\left(jk-\frac{1}{\widetilde{r}_{01}}\right)\frac{\exp(jk\widetilde{r}_{01})}{\widetilde{r}_{01}}. \tag{2.101}$$

Recognising that $\widetilde{P}_0$ is a reflection of P_0 one can write

$$r_{01} = \widetilde{r}_{01} \tag{2.102}$$

$$\cos(\bar{\mathbf{n}},\bar{\mathbf{r}}_{01}) = -\cos(\bar{\mathbf{n}},\widetilde{\bar{\mathbf{r}}}_{01}). \tag{2.103}$$

Substituting Eq. (2.102) and Eq. (2.103) into Eq. (2.100) and Eq. (2.101) one finds

$$G_{c\phi\text{-}} = 0 \tag{2.104}$$

Stellenbosch University http://scholar.sun.ac.za

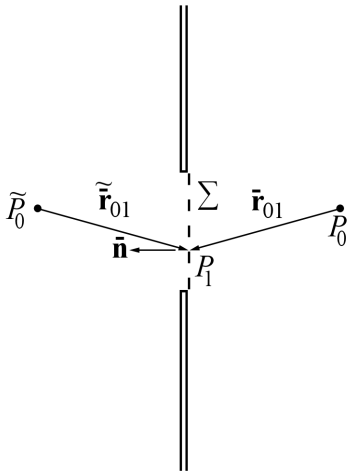

Figure 2.10: Rayleigh-Sommerfeld formulation of diffraction. Note that the points $\widetilde{P}_0$ is a reflection of point P_0. Goodman [2]

and

$$\frac{\partial G_{c\phi\text{-}}}{\partial n} = 2\cos(\bar{\mathbf{n}}, \bar{\mathbf{r}}_{01})\left(jk - \frac{1}{r_{01}}\right)\frac{\exp(jkr_{01})}{r_{01}}. \tag{2.105}$$

Substituting Eq. (2.104) and Eq. (2.105) into Eq. (2.90) by noting that $G_c = G_{c\phi-}$ and $\frac{\partial G_c}{\partial n} = \frac{\partial G_{c\phi\text{-}}}{\partial n}$ one finds

$$U_c(P_0) = \frac{1}{2\pi}\iint_{S_1} U_c(P_1)\frac{\exp(jkr_{01})}{r_{01}}\cos(\bar{\mathbf{n}}, \bar{\mathbf{r}}_{01})\left(jk - \frac{1}{r_{01}}\right)ds. \tag{2.106}$$

Once again noting that $k \gg \frac{1}{r_{01}}$ and noting that the boundary conditions on the surface S_1 need only be applied to U_c one can rewrite Eq. (2.106) as

$$U_c(P_0) = \frac{1}{j\lambda}\iint_{\Sigma} U_c(P_1)\frac{\exp(jkr_{01})}{r_{01}}\cos(\bar{\mathbf{n}}, \bar{\mathbf{r}}_{01})ds. \tag{2.107}$$

Now one can describe $U_c(P_1)$ in terms of a point source disturbance at P_2 as

$$U_c(P_1) = \frac{A\exp(jkr_{21})}{r_{21}} \tag{2.108}$$

and substitute Eq. (2.108) into Eq. (2.106) to find

$$U_c(P_0) = \frac{A}{j\lambda}\iint_{\Sigma} \frac{\exp(jk\left[r_{01} + r_{21}\right])}{r_{01}r_{21}}\cos(\bar{\mathbf{n}}, \bar{\mathbf{r}}_{01})ds. \tag{2.109}$$

Stellenbosch University http://scholar.sun.ac.za

The resultant equation given by Eq. (2.109) is known as the Rayleigh-Sommerfeld diffraction theorem. One can rewrite Eq. (2.109) in a simplified form by defining

$$\begin{aligned} U_{ca} &= U_c(P_1)\cos(\bar{\mathbf{n}}, \bar{\mathbf{r}}_{01}) \\ &= \frac{A\exp(jkr_{21})}{r_{21}}\cos(\bar{\mathbf{n}}, \bar{\mathbf{r}}_{01}) \end{aligned} \tag{2.110}$$

and substitute Eq. (2.110) into Eq. (2.109) to find

$$U_c(P_0) = \frac{1}{j\lambda}\iint_{\Sigma} U_{ca}(P_1)\frac{\exp(jkr_{01})}{r_{01}}ds. \tag{2.111}$$

With reference to Eq. (2.110), $\cos(\bar{\mathbf{n}}, \bar{\mathbf{r}}_{01})$ is the obliquity factor.

Another solution for the Rayleigh-Sommerfeld diffraction formulation could be calculated by taking the Green's function at P_1 to be the sum of two in phase wave functions mirrored across the $z = 0$ plane, see Appendix A.2. The resulting solution is then given by

$$U_c(P_0) = -\frac{A}{j\lambda}\iint_{\Sigma} \frac{\exp(jk\,[r_{01} + r_{21}])}{r_{01}r_{21}}\cos(\bar{\mathbf{n}}, \bar{\mathbf{r}}_{21})ds. \tag{2.112}$$

If one looks at the results for Fresnel-Kirchhoff diffraction with reference to Eq. (2.98), Eq. (2.99) and Rayleigh-Sommerfeld diffraction with reference to Eq. (2.110), Eq. (2.111) it can be seen that these equations only differ in their obliquity factors.

It is interesting to note that if one were to apply the linearity principle and take the disturbance at P_0 to be due to two point sources a and b placed a small distance ϵ apart centred about P_2 with their respective intensities half and one further asserts that for the one source we take the in phase solution of the Green's function Eq. (2.112) and for the other source we take the out of phase solution of the Green's function Eq. (2.109), then the resultant disturbance must be the sum of the two as illustrated in Fig. 2.11. The resultant equation is,

$$\begin{aligned} U_c(P_0) = \frac{1}{2}\frac{A}{j\lambda}\iint_{\Sigma} \frac{\exp(jk\,[r_{01} + r_{21a}])}{r_{01}r_{21a}}\cos(\bar{\mathbf{n}}, \bar{\mathbf{r}}_{01})ds \\ -\frac{1}{2}\frac{A}{j\lambda}\iint_{\Sigma} \frac{\exp(jk\,[r_{01} + r_{21b}])}{r_{01}r_{21b}}\cos(\bar{\mathbf{n}}, \bar{\mathbf{r}}_{21b})ds. \end{aligned} \tag{2.113}$$

Stellenbosch University http://scholar.sun.ac.za

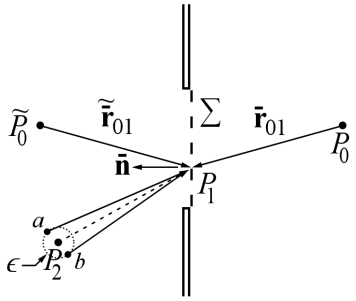

Figure 2.11: Rayleigh-Sommerfeld formulation of diffraction with two sources of half intensity centred about point P_2. Note that the points $\widetilde{P}_0$ is a reflection of point P_0

Now letting ϵ approach zero one finds

$$\lim_{\epsilon \to 0} r_{21\mathrm{b}} = r_{21\mathrm{a}} = r_{21}. \tag{2.114}$$

Substitution of Eq. (2.114) into Eq. (2.113) and simplifying yields

$$\lim_{\epsilon \to 0} U_{\mathrm{c}}(P_0) = \frac{A}{j\lambda} \iint_{\Sigma} \frac{\exp(jk\,[r_{01} + r_{21}])}{r_{01} r_{21}} \left[\frac{\cos(\bar{\mathbf{n}}, \bar{\mathbf{r}}_{01}) - \cos(\bar{\mathbf{n}}, \bar{\mathbf{r}}_{21})}{2} \right] ds \tag{2.115}$$

which is the same as the result of Fresnel-Kirchhoff diffraction solution as given by Eq. (2.97).

2.5.2 The angular spectrum

From Fourier theory it is known that one can break any signal into it's spectral components by taking it's Fourier transform. The following follows from Goodman [2][19].

In a Cartesian co-ordinate system if one has a known plane wave disturbance at the plane $z = 0$ then one can take the Fourier transform by substitution of the known function $U_{\mathrm{c}}(x, y, 0)$ into the following equation,

$$A_{0\mathrm{c}}(f_{\mathrm{X}}, f_{\mathrm{Y}}) = \iint_{-\infty}^{\infty} U_{\mathrm{c}}(x, y, 0) \exp\left[-j2\pi(f_{\mathrm{X}} x + f_{\mathrm{Y}} y)\right] dxdy \tag{2.116}$$

[19] Goodman [2] on page 49

Stellenbosch University http://scholar.sun.ac.za

where

$$\begin{aligned} U_c(x,y,0) &= \text{The wave function at the } z=0 \text{ plane} \\ A_{0c} &= \text{The angular spectrum at the input mask} \\ (f_X, f_Y) &= \text{Spectral co-ordinate} \\ (x,y) &= \text{Spatial co-ordinate.} \end{aligned}$$

If one has the spectrum of a function then one can reconstruct the original input function with the inverse Fourier transform by substitution of the spectrum A_{0c} into the following equation,

$$U_c(x,y,0) = \iint_{-\infty}^{\infty} A_{0c}(f_X, f_Y) \exp\left[j2\pi(f_X x + f_Y y)\right] df_X df_Y. \tag{2.117}$$

By noting that the general equation for the propagation of a plane wave with direction cosines (α, β, γ) is [20]

$$B_c(x,y,z) = \exp\left[j\frac{2\pi}{\lambda}(\alpha x + \beta y + \gamma z)\right] \tag{2.118}$$

with the direction cosines defined as

$$\begin{aligned} \alpha &= \lambda f_X \\ \beta &= \lambda f_Y \\ \gamma &= \sqrt{1-(\lambda f_X)^2 - (\lambda f_Y)^2} \end{aligned} \tag{2.119}$$

one can rewrite Eq. (2.116) as

$$A_{0c}\left(\frac{\alpha}{\lambda}, \frac{\beta}{\lambda}\right) = \iint_{-\infty}^{\infty} U_c(x,y,0) \exp\left[-j2\pi\left(\frac{\alpha}{\lambda}x + \frac{\beta}{\lambda}y\right)\right] dxdy. \tag{2.120}$$

The resultant equation, given as Eq. (2.120), is referred to as the *angular spectrum*.

Let's look at the angular spectrum at a distance z from the origin. Rewriting

[20] See Section A.4 for additional information about the given definition of the plane wave and interpretation of the direction cosines (α, β, γ).

Stellenbosch University http://scholar.sun.ac.za

the relation, given by Eq. (2.117), by taking the distance z into account one finds

$$U_c(x,y,z) = \iint_{-\infty}^{\infty} A_c\left(\frac{\alpha}{\lambda},\frac{\beta}{\lambda},z\right)\exp\left[j2\pi(\frac{\alpha}{\lambda}x+\frac{\beta}{\lambda}y)\right]d\frac{\alpha}{\lambda}d\frac{\beta}{\lambda}. \quad (2.121)$$

From Goodman [2][21] we see that by substituting the inverse Fourier transform, given by Eq. (2.121), into the Helmholtz equation, given by Eq. (2.21), one can find an arbitrary solution for $A_c\left(\frac{\alpha}{\lambda},\frac{\beta}{\lambda},z\right)$ given as

$$A_c\left(\frac{\alpha}{\lambda},\frac{\beta}{\lambda},z\right) = A_{0c}\left(\frac{\alpha}{\lambda},\frac{\beta}{\lambda}\right)\exp\left(j\frac{2\pi}{\lambda}z\sqrt{1-\alpha^2-\beta^2}\right). \quad (2.122)$$

If one substitutes Eq. (2.122) into the inverse Fourier transform given by Eq. (2.121) one finds the complete solution for angular spectral propagation given by

$$U_c(x,y,z) = \iint_{-\infty}^{\infty} A_{0c}\left(\frac{\alpha}{\lambda},\frac{\beta}{\lambda}\right)\exp\left(j\frac{2\pi}{\lambda}z\sqrt{1-\alpha^2-\beta^2}\right) \exp\left[j2\pi(\frac{\alpha}{\lambda}x+\frac{\beta}{\lambda}y)\right]d\frac{\alpha}{\lambda}d\frac{\beta}{\lambda}. \quad (2.123)$$

The transfer function due to propagation in the z direction thus being

$$H_c\left(\frac{\alpha}{\lambda},\frac{\beta}{\lambda}\right) = \exp\left(j\frac{2\pi}{\lambda}z\sqrt{1-\alpha^2-\beta^2}\right). \quad (2.124)$$

It is of interest that under certain conditions the angular spectrum could be imaged at an image plane and the light from this image plane could be collected and refocused to form the original image again. This allows us to easily do simple types of exclusion filtering in the plane where the angular spectrum is imaged.

2.5.3 The Fresnel and Fraunhofer regions

Certain approximations can be made which hold under defined conditions, these approximations make it possible to numerically calculate solutions to diffraction problems with more ease. The following section follows loosely from Goodman [2][22].

[21] Goodman [2] on page 50
[22] Goodman [2] on page 57

Stellenbosch University http://scholar.sun.ac.za

When viewing the diffraction formulas of either Fresnel-Kirchhoff, given by Eq. (2.97), or Rayleigh-Sommerfeld, given by Eq. (2.112), for the case of a near planar wave incident upon the origin of the z half space and observing the resultant field a distance away from the source one can approximate the obliquity factors, $\cos(\bar{\mathbf{n}}, \bar{\mathbf{r}}_{01})$ and $\frac{\cos(\bar{\mathbf{n}},\bar{\mathbf{r}}_{01})-\cos(\bar{\mathbf{n}},\bar{\mathbf{r}}_{21})}{2}$, of both equations to be approximately equal to one. According to Goodman [2][23] this approximation is accurate to within 5 % for angles smaller than 18°. The obliquity factors being the only difference between the two functions an approximation which applies to both Eq. (2.97) and Eq. (2.112) can be written as

$$U_c(P_0) = \frac{A}{j\lambda} \iint_{\Sigma} \frac{\exp(jk\,[r_{01} + r_{21}])}{r_{01} r_{21}} ds. \tag{2.125}$$

The initial assertion was that the incident light is near planar, thus one can split these functions into a source function and observed function for Eq. (2.125) as follows

$$U_c(P_0) = \frac{A}{j\lambda} \iint_{\Sigma} \frac{\exp(jkr_{01})}{r_{01}} \frac{\exp(jkr_{21})}{r_{21}} ds. \tag{2.126}$$

If the source is a near planar wave one can view the geometry as illustrated in Fig. 2.12.

With respect to the geometry illustrated in Fig. 2.12 one can rewrite Eq. (2.126) as

$$U_c(x_0, y_0) = \frac{A}{j\lambda} \iint_{\Sigma} U_c(x_1, y_1) \frac{\exp(jkr_{01})}{r_{01}} dx_1 dy_1 \tag{2.127}$$

with r_{01} defined as

$$r_{01} = \sqrt{z^2 + (x_0 - x_1)^2 + (y_0 - y_1)^2}. \tag{2.128}$$

One can further define, keeping in mind the simplification to the obliquity factor, the transfer function

$$h_c(x_0, y_0; x_1, y_1) \cong \frac{1}{j\lambda} \frac{\exp(jkr_{01})}{r_{01}}. \tag{2.129}$$

[23] Goodman [2] on page 58

Stellenbosch University http://scholar.sun.ac.za

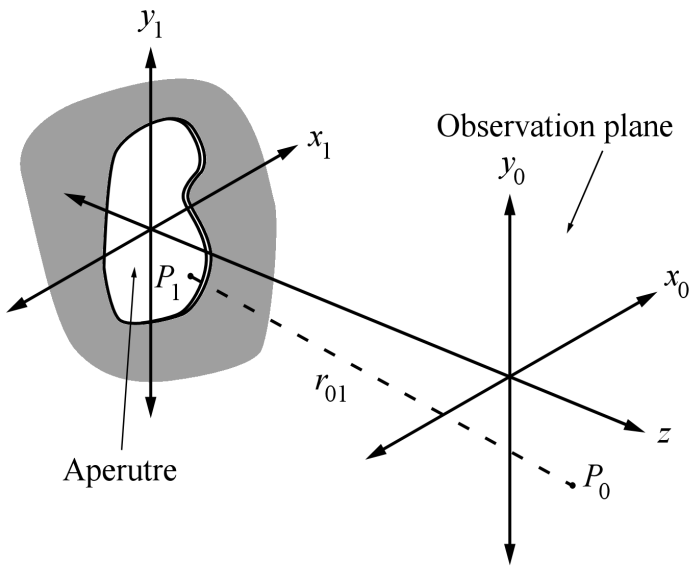

Figure 2.12: Diffraction geometry for a approximately planar wave incident on the aperture from Goodman [2]

Now simplifying Eq. (2.129) under the small angle approximation, thus $r_{01} \cong z$ one finds

$$h_c(x_0, y_0; x_1, y_1) \cong \frac{1}{j\lambda z} \exp(jkr_{01}). \tag{2.130}$$

With these simplifications one can rewrite Eq. (2.127) as

$$U_c(x_0, y_0) = \iint_{\Sigma} h_c(x_0, y_0; x_1, y_1) U_c(x_1, y_1) dx_1 dy_1. \tag{2.131}$$

The Fresnel and Fraunhoffer approximations are used to simplify the transfer function, h_c, and will be explained in the following section.

2.5.3.1 The Fresnel approximation

The Fresnel approximation is made by taking into account the binomial expansion of the square root

$$\sqrt{1+b} = 1 + \frac{1}{2}b - \frac{1}{8}b^2 + \cdots \qquad |b| < 1. \tag{2.132}$$

Stellenbosch University http://scholar.sun.ac.za

Rewriting r_{01} given in Eq. (2.128) as

$$r_{01} = z\sqrt{1+\left(\frac{x_0-x_1}{z}\right)^2+\left(\frac{y_0-y_1}{z}\right)^2} \tag{2.133}$$

one can use Eq. (2.132) to approximate Eq. (2.133), by taking only the linear component into account, as

$$r_{01} \cong z\left[1+\frac{1}{2}\left(\frac{x_0-x_1}{z}\right)^2+\frac{1}{2}\left(\frac{y_0-y_1}{z}\right)^2\right]. \tag{2.134}$$

In the case when z is large enough for the approximation given in Eq. (2.134) to be accurate, the observer is said to be in the region of Fresnel diffraction which is defined as

$$z^3 \gg \frac{\pi}{4\lambda}\left[(x_0-x_1)^2+(y_0-y_1)^2\right]^2_{\max}. \tag{2.135}$$

If one looks at the validity condition for the Fresnel approximation given in Eq. (2.135), it can be seen that for small values of z the region where the observation would be valid is small. The requirement given in Eq. (2.135) as stated for the validity of the Fresnel approximation does not need to be applied as strictly. The approximation is applied to a superposition integral of a complex exponential function. As such it is only required that the phase contribution due to the higher order terms to be negligibly small. By noting that the wave number k is very large and subsequently the quantity $\frac{k}{2z}$ would be very large for small values of z where the condition given by Eq. (2.135) would fail, the quadratic phase factor contribution due to the approximation would oscillate rapidly and thus the primary contribution would arise from points near $(x_1 = x_0, y_1 = y_0)$ where phases are not rapidly changing. Accepting the validity of this approximation one can express the superposition integral as

$$U_c(x_0,y_0) = \frac{\exp(jkz)}{j\lambda z} \iint_{-\infty}^{\infty} U_c(x_1,y_1)\exp\left\{j\frac{k}{2z}\left[(x_0-x_1)^2-(y_0-y_1)^2\right]\right\}dx_1dy_1 \tag{2.136}$$

Stellenbosch University http://scholar.sun.ac.za

or alternatively expanding the quadratic terms one has

$$U_c(x_0,y_0) = \frac{\exp(jkz)}{j\lambda z}\exp\left[j\frac{k}{2z}({x_0}^2+{y_0}^2)\right]\iint_{-\infty}^{\infty} U_c(x_1,y_1) \exp\left[j\frac{k}{2z}({x_1}^2+{y_1}^2)\right]\exp\left[-j\frac{2\pi}{\lambda z}(x_0x_1+y_0y_1)\right]dx_1dy_1. \quad (2.137)$$

The Fresnel approximation is applicable from an observation plane which is within a few wavelengths from the aperture to infinity.

2.5.3.2 The Fraunhofer approximation

The Fraunhofer approximation is made for large values of z such that the following condition holds,

$$z \gg \frac{k({x_1}^2+{y_1}^2)_{\max}}{2}. \quad (2.138)$$

When this condition is satisfied the quadratic phase factor could be approximated by one, and the superposition integral becomes

$$U_c(x_0,y_0) = \exp(jkz)\exp\left[j\frac{k}{2z}({x_0}^2+{y_0}^2)\right] \iint_{-\infty}^{\infty} U_c(x_1,y_1)\exp\left[-j\frac{2\pi}{\lambda z}(x_0x_1+y_0y_1)\right]dx_1dy_1. \quad (2.139)$$

The requirement as stated by Eq. (2.138) can be imposing, for example if one has a 2.5 cm aperture the requirement for z would be $z \gg 1600$ meters for plane wave illumination of the aperture.

2.5.4 Fourier transformation by lenses

From Goodman [2][24] one can see that the paraxial approximations are used in order to describe the phase modification introduced by a lens. In the following development the index of refraction before and after the lens is taken as $n_a = 1$. The development starts by describing the phase delay of a wave front passing

[24] Goodman [2] on page 80

Stellenbosch University http://scholar.sun.ac.za

through a lens as

$$\phi(x,y) = kn \triangle (x,y) + k[\triangle_0 - \triangle (x,y)]. \tag{2.140}$$

One can express Eq. (2.140) as a multiplicative phase transformation as follows

$$t_{\mathrm{lc}}(x,y) = \exp[jk \triangle_0] \exp[jk(n-1) \triangle (x,y)]. \tag{2.141}$$

The phase transformation equation given by Eq. (2.141) allows one to write an expression for the field immediately behind the lens as

$$U'_{\mathrm{c}}(x,y) = t_{\mathrm{lc}}(x,y) U_{\mathrm{lc}}(x,y). \tag{2.142}$$

Now deriving an equation describing the thickness of the lens by making the paraxial approximation one finds

$$\triangle (x,y) = \triangle_0 - \frac{x^2+y^2}{2}\left(\frac{1}{R_1} - \frac{1}{R_2}\right). \tag{2.143}$$

Through the paraxial approximation the focal length can be derived as is done for Eq. (2.67) and thus the focal length can be defined as, again note that $n_{\mathrm{a}} = 1$,

$$\frac{1}{f} = (n-1)\left(\frac{1}{R_1} - \frac{1}{R_2}\right). \tag{2.144}$$

Substitution of Eq. (2.143) and Eq. (2.144) into the multiplicative phase transformation equation, given as Eq. (2.141), one finds a simplified expression for the phase transformation affected by a thin lens as

$$t_{\mathrm{lc}}(x,y) = \exp[jkn \triangle_0] \exp\left[-j\frac{k}{2f}(x^2+y^2)\right]. \tag{2.145}$$

With this background information it is possible to derive expressions for the case where an object is placed before a lens, against a lens and after a lens as illustrated in Fig. 2.13, Fig. 2.14 and Fig. 2.15.

One can now write the expressions by application of the Fresnel superposition integral, given as Eq. (2.137), to the phase transformation equation, given as Eq. (2.145), to find an expression for each case.

Stellenbosch University http://scholar.sun.ac.za

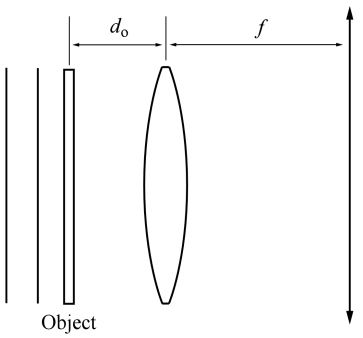

Figure 2.13: Object placed before the lens, from Goodman [2]

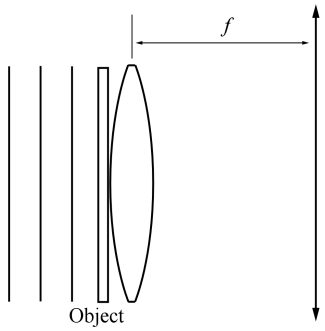

Figure 2.14: Object placed against the lens, from Goodman [2]

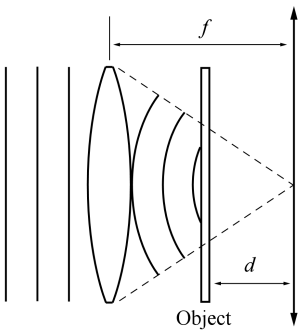

Figure 2.15: Object placed after the lens, from Goodman [2]

By noting that it is field intensity that is observed at the focal plane one can neglect any phase which is not part of the superposition integral as it does not have an effect on the measured intensity. The following equations from Goodman [2][25] therefore omit the constant phase factor in the phase transformation equation, given by Eq. (2.145), in the subsequent derivation.

When the object is placed in front of the lens deep within the Fresnel diffraction region one can approximate the aperture for which light travelling in the same direction would be added together at an image point at the focal plane, the effect of light not being included in the superposition integral due to its travelling direction and it's point of origin being such that it misses the lens aperture. $P(x, y)$ is the pupil function which is the projection of the lens aperture onto the object plane centred about the co-ordinates $(x_o = -\frac{d_o}{f}x_f, y_o = -\frac{d_o}{f}y_f)$ as is illustrated in Fig. 2.16. This effect is known as vignetting.

With reference to Fig. 2.13 the equation for a field at the focal plane for a thin

[25] Goodman [2] starting from page 83

Stellenbosch University http://scholar.sun.ac.za

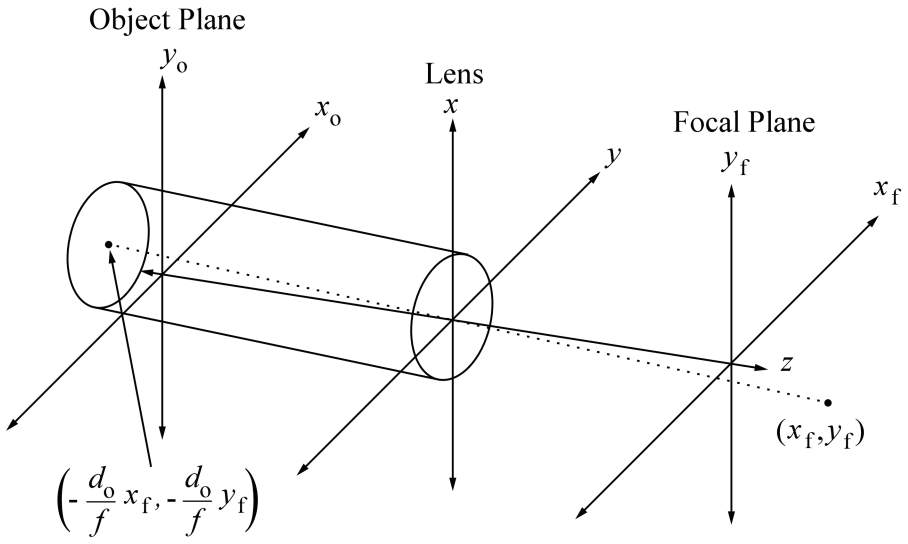

Figure 2.16: Vignetting of the object, from Goodman [2]

lens with the object placed in front of the lens is given as

$$U_{fc}(x_f, y_f) = \frac{A \exp\left[j\frac{k}{2f}\left(1 - \frac{d_o}{f}\right)(x_f{}^2 + y_f{}^2)\right]}{j\lambda f}$$
$$\iint_{-\infty}^{\infty} t_{oc}(x,y) P\left(x_o + \frac{d_o}{f}x_f, y_o + \frac{d_o}{f}y_f\right) \exp\left[-j\frac{2\pi}{\lambda f}(x_o x_f + y_o y_f)\right] dx_o dy_o \quad (2.146)$$

where

$$\begin{aligned} t_{oc} &= \text{The input mask function} \\ P(x,y) &= \text{The pupil function.} \end{aligned}$$

With reference to Fig. 2.14 the equation for a field at the focal plane for a thin lens with the object placed against the lens is given as

$$U_{fc}(x_f, y_f) = \frac{A \exp\left[j\frac{k}{2f}(x_f{}^2 + y_f{}^2)\right]}{j\lambda f} \iint_{-\infty}^{\infty} t_{oc}(x_o, y_o) \exp\left[-j\frac{2\pi}{\lambda f}(x_o x_f + y_o y_f)\right] dx_o dy_o. \quad (2.147)$$

If the object is placed behind the lens as illustrated in Fig. 2.15 the pupil func-

Stellenbosch University http://scholar.sun.ac.za

tion is again approximated geometrically by projecting the lens aperture with a cone of rays towards the focal point on the optical axis. If the object is completely within this cone of rays the pupil function could be neglected. With reference to Fig. 2.15 the equation for a field at the focal plane for a thin lens with the object placed after the lens is given as

$$U_{\mathrm{fc}}(x_{\mathrm{f}}, y_{\mathrm{f}}) = \frac{A \exp\left[j\frac{k}{2f}({x_{\mathrm{f}}}^2 + {y_{\mathrm{f}}}^2)\right]}{j\lambda d} \frac{f}{d} \iint_{-\infty}^{\infty} t_{\mathrm{oc}}(x, y) P\left(x_{\mathrm{o}}\frac{f}{d}, y_{\mathrm{o}}\frac{f}{d}\right) \exp\left[-j\frac{2\pi}{\lambda d}(x_{\mathrm{o}}x_{\mathrm{f}} + y_{\mathrm{o}}y_{\mathrm{f}})\right] dx_{\mathrm{o}}dy_{\mathrm{o}}. \quad (2.148)$$

2.6 Simplification of theory for specific application

If we take into consideration our Fourier optical application then we note that we will be using a sensor to detect the resultant light intensity at the observation plane, the intensity is given by

$$I(x_{\mathrm{f}}, y_{\mathrm{f}}) = |U_{\mathrm{c}}(x_{\mathrm{f}}, y_{\mathrm{f}})|^2, \quad (2.149)$$

with the resultant effect that we can neglect all phase contributions which do not form part of the superposition integral. If we further note that we are interested only in the relative intensity of the output field then we can replace the amplitude scaling factor with a single constant. As for the purposes of this thesis we rewrite the Fresnel approximation, given in Eq. (2.137), as

$$U_{\mathrm{c}}(x_{\mathrm{f}}, y_{\mathrm{f}}) = K \iint_{-\infty}^{\infty} U_{\mathrm{c}}(x_{\mathrm{o}}, y_{\mathrm{o}}) \exp\left[j\frac{k}{2z}({x_1}^2 + {y_1}^2)\right] \exp\left[-j\frac{2\pi}{\lambda z}(x_0x_1 + y_0y_1)\right] dx_1dy_1. \quad (2.150)$$

If we rewrite the lens equations given as Eq. (2.146), Eq. (2.147) and Eq. (2.148) with the simplifications we can make due to measuring the intensity and being only interested in relative intensities, we can simplify these to:

Stellenbosch University http://scholar.sun.ac.za

1. For the object placed before the lens as in Fig. 2.13,

$$U_{\mathrm{fc}}(x_{\mathrm{f}}, y_{\mathrm{f}}) = K_1 \iint_{-\infty}^{\infty} t_{\mathrm{oc}}(x,y) P\left(x_{\mathrm{o}} + \frac{d_{\mathrm{o}}}{f} x_{\mathrm{f}}, y_{\mathrm{o}} + \frac{d_{\mathrm{o}}}{f} y_{\mathrm{f}}\right) \exp\left[-j\frac{2\pi}{\lambda f}(x_{\mathrm{o}}x_{\mathrm{f}} + y_{\mathrm{o}}y_{\mathrm{f}})\right] dx_{\mathrm{o}} dy_{\mathrm{o}} \tag{2.151}$$

2. For the object placed against the lens as in Fig. 2.14,

$$U_{\mathrm{fc}}(x_{\mathrm{f}}, y_{\mathrm{f}}) = K_2 \iint_{-\infty}^{\infty} t_{\mathrm{oc}}(x_{\mathrm{o}}, y_{\mathrm{o}}) \exp\left[-j\frac{2\pi}{\lambda f}(x_{\mathrm{o}}x_{\mathrm{f}} + y_{\mathrm{o}}y_{\mathrm{f}})\right] dx_{\mathrm{o}} dy_{\mathrm{o}} \tag{2.152}$$

3. For the object placed after the lens as in Fig. 2.15,

$$U_{\mathrm{fc}}(x_{\mathrm{f}}, y_{\mathrm{f}}) = K_3 \iint_{-\infty}^{\infty} t_{\mathrm{oc}}(x,y) P\left(x_o \frac{f}{d}, y_o \frac{f}{d}\right) \exp\left[-j\frac{2\pi}{\lambda d}(x_{\mathrm{o}}x_{\mathrm{f}} + y_{\mathrm{o}}y_{\mathrm{f}})\right] dx_{\mathrm{o}} dy_{\mathrm{o}} \tag{2.153}$$

Another consequence of our specific application allows us to simplify the Fresnel-Kirchhoff and Rayleigh-Sommerfeld diffraction formulas, given by Eq. (2.97) and Eq. (2.109) respectively as explained below.

With reference to Fig. 2.12, if we consider a Fourier optical system with a near planar wave front at the input mask with the resultant obstruction such that the small angle approximation holds then we can approximate the obliquity factors as unity. We further note that we can describe the input mask Σ as a function which is defined over the aperture as $t_{\mathrm{c}}(P_1)$. The resultant equation found is

$$U_{\mathrm{c}}(P_0) \quad = \quad K_{\mathrm{b}} \iint_{-\infty}^{\infty} \frac{t_{\mathrm{c}}(P_1)}{r_{01}} \exp(jkr_{01}) ds. \tag{2.154}$$

In Eq. (2.154) the optical path length r_{01} acts mainly as a phase modifier and to a negligible extent as an amplitude modifier. This implies that we only need to take into account the interference effect due to the difference in path length between all points at the input plane to determine the resultant amplitude at a point at the observation plane. This principle is still valid if a lens is inserted between the aperture and the observation plane, with the added requirement of

Stellenbosch University http://scholar.sun.ac.za

having the ability to determine the relevant optical path lengths. This allows us to use ray tracing to determine the location where plane waves would interfere after passing through a lens which in turn could be used to determine the position of maxima and minima of resultant diffraction patterns caused by an aperture.

Stellenbosch University http://scholar.sun.ac.za

3

The measurement of animal hair fibre

In this chapter we look at the properties of animal hair fibre with the main focus on wool, we will briefly discuss experimental methods to measure fibre diameter that had been tried, give a brief overview of the classification of wool in a trade context, give an overview of devices currently in use and finally discuss in more detail previous attempts to build devices based on the diffraction principle.

3.1 Animal hair fibre

In this section background information is given on animal hair fibres. Animal hair fibres is a large subject area. We will focus on information which is relevant to the proposed measurement device. In terms of the device under development, we are interested in those properties of animal hair fibres which could affect the measurement of mean diameter of said fibres. We will focus on the following properties, the range of diameters for which the device must be operable, the shape of the fibres and their transparency related properties with the main focus specifically on wool fibres as the device is intended for use in the wool industry, but could easily be used to measure other types of animal hair fibres.

As the main focus will be on wool let's take a brief look at the definition of the term wool. The definition of the term wool varies in the literature. Dic [18] defines wool as: *"the outer coat of sheep, yaks, etc, which consists of short curly hairs"* and Dic [19] defines wool as: *"the fine, soft, curly hair that forms the fleece of sheep and certain other animals, characterized by minute, overlapping surface scales that give it its felting property"*. D'Arcy [20][1] makes the following statement in reference to the hair of mammals, *"In a general sense they are all hair fibres, but those grown by sheep are referred to as 'wool' "*.

These statements overlap in their definition of wool but none can be viewed as absolutely clear, correct and definitive. The word woolly is derived from the

[1] D'Arcy [20] on page 69

Stellenbosch University http://scholar.sun.ac.za

word wool and can be used as an adjective to imply fuzzy, unclear or disorganised separately or combined, see Dic [21]. It is only fitting then that in itself the definition of wool is woolly. For the purposes of this thesis we use the term wool defined as that hair fibre which is grown by sheep.

3.1.1 Mean fibre diameter

It is intuitive that the characteristics of a type or sample of animal hair fibre determines for which application it is most suited. The most prominent characteristic of hair fibre is mean diameter as it determines both the feel and strength of the resultant product produced from said fibre.

The importance of mean fibre diameter is acknowledged throughout the literature. Hill [22] states *"In animal husbandry no one can hold to attain more than a fair success with sheep if he is not able to distinguish degrees of fineness with accuracy"*, Burns [23] states *"Diameter, This was one of the first characters of wool to be measured"*, Fairbanks [24] states *"The diameter of the wool fibre has commanded the interest and attention of wool technicians for many years"* and Stobart *et al.* [25] states that *"fibre diameter is recognized as the most important dimensional character of raw wool"*. Clearly mean diameter is a very important attribute of wool. Looking further in the literature the reason becomes clear, Dunlop and McMahon [26] states *"Fibre diameter is recognized as the most important physical attribute of raw apparel wool in terms of the fabric into which it may be processed"* and McNicholas and Curtis [27] states *"The average diameter of wool is a dominant dimensional characteristic of the material immediately affecting its value for manufacturing purposes"*. Thus, fibre diameter determines the application and price of wool.

3.1.2 The diameter range of animal hair fibre

In general the diameter of wool for textile purposes ranges roughly between 20 µm up to 40 µm, see Simpson *et al.* [28][2]. These results are supported in a report on the trial of wool measurement systems by Baxter [29]. In this trial samples from four countries were measured and the mean fibre diameter ranged between $16 - 36$ µm. In another study a comparative test between two instruments were done on the entire South-African clip and wools were measured ranging between $16 - 31$ µm, see Heath *et al.* [30].

[2]Simpson *et al.* [28] on page 80

Stellenbosch University http://scholar.sun.ac.za

The minimum and maximum fibre diameters are important design parameters for any system intended to measure fibre diameter. Let's look in more detail at the upper and lower limits of fibre diameter.

3.1.2.1 Minimum fibre diameter

Towards the specialised end of the market we find super fine wool, cashmere hair fibre, musk-ox qiviut hair fibre and vicuña hair fibre. Let's take a brief look at each of these in terms of fibre diameter.

- Superfine wool: It is reported in ASW [31] that the winner of the Loro Piana World Cup Challenge in 2009 produced 96 kg of wool with mean diameter of 11.5 µm. In a report on a comparative study between measurement results of the OFDA and Laserscan instrument Baxter [32] discusses the lower limit of wool fibre diameter. Baxter [32] reported that fibres of 5 µm had been reported to have been measured. It was not certain if these measurements were valid. In order to gain certainty on this matter, Baxter [33] did a study where two independent samples of super fine wool were tested with the OFDA2000 system and showed fibres measured with diameter in the 5 µm range. These samples were then sent to two independent laboratories who validated these measurements using an electron microscope and confirmed the existence of 5 µm fibres.

- Cashmere fibre: The cashmere fibre is shorn from a type of goat and the fibre is very fine, see von Bergen [34]. In an article by Tonin *et al.* [35] methods to identify fibres from protected species of goat had been investigated. Cashmere was studied in comparison with two other types of rare goat fibres. In this study by Tonin *et al.* [35], the mean diameter of cashmere was observed to be 13.9 µm with a standard deviation of 2.8 µm.

- Musk-Ox fibre: Musk-Ox are found in Canada and Greenland and produce a very fine fibre during winter time known as qiviut, see von Bergen [36]. In a sample measured by von Bergen [36] he reports the mean width of the middle part of the fine musk-ox fibres to be 15.28 µm and in a more recent article with a bigger sampling base of musk-ox fibres Rowell *et al.* [37] measured the mean fibre thickness for the qiviut hairs of the musk-ox to be between 16.5 µm and 18.2 µm with a standard deviation of $\pm$ 5 µm.

Stellenbosch University http://scholar.sun.ac.za

- Vicuña fibre: The Vicuña is a very rare wild camelid found in the Andes in Peru, Ecuador and Bolivia, see von Bergen [38]. A sample was measured to determine it's fineness and was found to be 13.55 μm, see von Bergen [38].

From the above discussion it is clear that the verified minimum fibre diameter is 5 μm, this limit is very rarely encountered and certainly never as a the mean diameter, thus we can conclude that a more practical lower limit, for mean fibre diameter, in the specialist fine fibre market would be 10 μm based on the 11.5 μm result by ASW [31]. If one were to consider only the normal production market one could set the minimum limit at 15 μm based on the studies by Baxter [29] and Heath *et al.* [30].

3.1.2.2 Maximum fibre diameter

Fibres used in clothing textiles are limited in maximum diameter by the fibres ability to cause a prickle sensation on the skin. Boos *et al.* [39] reports that the cause of the prickle sensation is due to the ability of fibres with sufficient girth to activate the nerve ends of the skin. Boos *et al.* [39] further states that studies have shown that wool and acrylic fibres with diameters greater than 30 μm can cause discomfort in knitted goods.

Wool and fibres used for carpets, however, are not limited in this respect and the average diameter for carpet wools is roughly 40 μm, see D'Arcy [20][3].

The above discussion seems to indicate an upper limit of 40 μm, yet measurement devices such as the OFDA, see Baxter and Brims [40], have a measurement range of $5 - 125$ μm and the laserscan device has an operating range of $5 - 150$ μm according to Glass [41].

3.1.3 The physical properties of animal hair fibres

The basic structure for all hair fibres are the same consisting of an external cuticle layer and an internal core of splinter like corticle cells, see D'Arcy [20][4]. The detailed chemical composition of wool and other animal hair fibres is beyond the scope of this thesis.

Wool is a fibre consisting of up to 90 % keratin. Keratins can be found in skin, nails, claws, hair, horn, feathers and scales, see Cardamone *et al.* [42].

[3] D'Arcy [20] on page 53
[4] D'Arcy [20] on page 69

Stellenbosch University http://scholar.sun.ac.za

The corticle cells of wool are divided between the paracortex and the orthocortex and this is thought to cause the natural curvature of wool known as crimp, see Simpson *et al.* [28][5].

The cuticular scales in wool fibres are more highly developed in comparison with hair fibre from other mammals and the scales all point in the same direction giving the wool it's felting capacity, see D'Arcy [20][6].

The cross sectional shape of wool fibres are varied, illustrated in Fig. 3.1. The cross section of merino fibres are mostly slightly elliptical, however the cross sectional shape of wool fibres can be round, elliptical, bean shaped, ovoid and other shapes exhibiting concavities, see Sommerville [43].

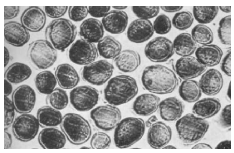

(a) Fine fineness wool magnified x500

(b) Medium fineness wool magnified x500

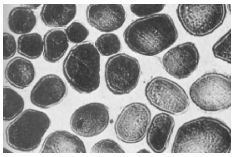

(c) Coarse fineness wool magnified x500

Figure 3.1: Cross section view of wool with different fineness from von Bergen and Krauss [3]

Along the length of the fibre the scales give them a serrated appearance which is more prominent in wool fibres than in other animal hair.

Fig. 3.2(a) shows the jagged structure of wool fibres. In Fig. 3.2(b) oil and dirt particles are clearly visible on the greasy wool sample.

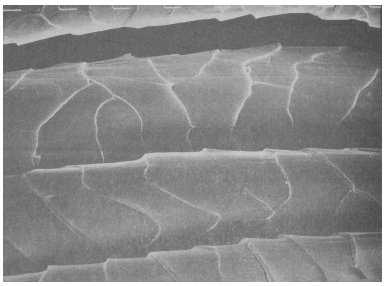

(a) Clean fibre at x2700 magnification

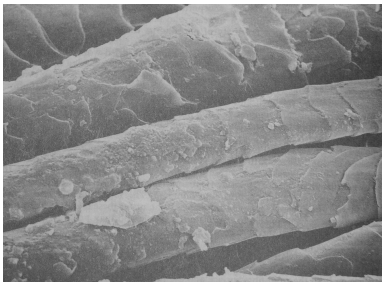

(b) Greasy fibre at x1700 magnification

Figure 3.2: Electron micrographs of fibres from Perich *et al.* [4]

3.1.4 Scattering and diffractive properties of animal hair fibres

Lundberg [44] measured and documented the light scattering properties of large fibres for light at normal incidence. In his experiment he used gold wire, nylon,

[5]Simpson *et al.* [28] on page 70
[6]D'Arcy [20] on page 79

Stellenbosch University http://scholar.sun.ac.za

Dacron and glass. Lundberg [44] found scattering of the gold wire to be in good agreement with predictions by the Fraunhofer diffraction equation. He did however not find good agreement for the dielectric fibres and speculated that it could be due to the geometry or a varying refractive index or possibly both. Animal hair fibre do not behave like dielectric fibres as was found by Lynch and Thomas [45]. The authors investigated the optical diffraction pattern of phosphor bronze wire, wool, hair, jute and filaments of nylon, terylene and glass and concluded that the hair, wool and jute fibres are optically uniform and that their diffraction profiles result from their geometrical shape. This conclusion by Lynch and Thomas [45] indicated that the diameter of wool and animal fibres could be determined by diffraction methods and reawakened research into devices operating on these principles.

3.2 The statistics of wool fibre measurement

Fibre diameter is classified in terms of it's statistical mean and its standard deviation. Measurement accuracy is determined by the 95 % Confidence Limit (CL) and is used to evaluate the performance of a measurement device.

Some devices determine the mean and the standard deviation by taking a fixed number of samples and analysing the data, while others determine the mean empirically as an output parameter. In this thesis we will only look at basic statistic background in order to have insight into wool measurement.

3.2.1 The mean and the variance of a sample

The mean and variance of a sample are basic statistical properties for a random variable X. In the case of instruments which takes N discrete samples the mean can be determined by

$$\bar{X} = \frac{1}{N}\sum_{i=1}^{N} x_i \tag{3.1}$$

and the variance by,

$$\sigma^2 = \frac{1}{N}\sum_{i=1}^{N} {x_i}^2 - \bar{X}^2 \tag{3.2}$$

Stellenbosch University http://scholar.sun.ac.za

where

$$\begin{aligned} \bar{X} &= \text{The mean of the sample} \\ N &= \text{The number of samples} \\ x_i &= \text{The } i\text{'th sample in the sample set} \\ i &= \text{An index} \\ \sigma^2 &= \text{The variance.} \end{aligned}$$

3.2.2 The confidence limit

Wool measurement devices must be accurate. The 95 % CL is an indication of measurement accuracy as it gives us a sampling interval within which there is a 95 % chance that another measurement of the same number of samples will fall.

If the variance and the number of samples taken in order to obtain a mean for a sample is known then one can simply use the relation from Appendix A.5, (A.40),

$$\sigma_{\text{mean}} = \frac{\sigma}{\sqrt{N}} \tag{3.3}$$

where

$$\begin{aligned} \sigma_{\text{mean}} &= \text{Average standard deviation} \\ \sigma &= \text{Standard deviation} \end{aligned}$$

to find the variance and Standard Deviation (SD) of the mean.

The central limit theorem is applied to calculate confidence intervals, from Peebles [46][7] we have

$$W_{\text{N}} = \frac{1}{\sqrt{N}\,\sigma} \sum_{i=1}^{N} (x_i - \bar{x}) \tag{3.4}$$

where

$$\bar{x} = \text{The true mean which we do not know.}$$

Substituting Eq. (3.1) and Eq. (3.3) into Eq. (3.4) one can define a new random

[7] Peebles [46] on page 125

Stellenbosch University http://scholar.sun.ac.za

variable W

$$W = \frac{\bar{X} - \bar{x}}{\sigma_{\text{mean}}}. \tag{3.5}$$

From the normal distribution one can solve for w,

$$0.95 = P(-w \leq W \leq w) \tag{3.6}$$

to find

$$0.95 = P(-1.96 \leq W \leq 1.96). \tag{3.7}$$

Substituting Eq. (3.5) into Eq. (3.7) and simplifying one finds the 95 % Confidence Interval as

$$0.95 = P(\bar{X} - 1.96\,\sigma_{\text{mean}} \leq W \leq \bar{X} + 1.96\,\sigma_{\text{mean}}). \tag{3.8}$$

If one assumes the random variable W to have a normal distribution, which is a valid assumption through the Central Limit Theorem, one can find an expression for the 95 % CL as

$$\text{CL}_{95\%} = \pm 1.96\,\sigma_{\text{mean}}\,. \tag{3.9}$$

3.3 Fibre diameter measurement in the past

Over the years different methods have been used in the laboratory to measure fibre diameter. The following is a list of said methods and the date when they had been reported as an indication of a time line.

- The microscope: It is reported in the literature that Daubenton measured the diameter of wool fibres as early as 1777 using a microscope see Burns [23], Burns [47] and Buchanan and Bolin [48]. The microscope was later used in many different setups most notably of these the projection microscope, which would project a sample onto a screen from where measurements are made.
- The principle of diffraction: McNicholas and Curtis [27] reports that Thomas Young measured fibre diameter as early as 1824 using diffraction with a device he called the eriometer.

Stellenbosch University http://scholar.sun.ac.za

- The micrometer calliper: In 1924 Koehler [49] studied the differences between measurements made by microscope and measurements made by micrometer calliper and found that the micrometer calliper proved to be an accurate instrument for the measurement of wool fibres.

- Gravimetry: From 1932 as reported by Sommerville [50], gravimetry had been used to class wool by weighing a specific number of fibres of specific length and expressing the mean fibre fineness as the weight of a standard length of fibre. In later years the relationship between mass, volume and density was used to determine mean fibre diameter of a sample of known quantity, weight and length of fibre, see Sommerville [50].

- Porosity: Devices based on this principle measures the mean diameter of wool fibres by utilising the relationship which exists between the flow and pressure of air as it flows through a specific mass and volume of wool fibres, see Sommerville [51]. Studies to utilise this principle had started in 1940, see Sommerville [5].

- Sedimentomitry: The rate of settlement of particles in a fluid can be used to calculate the Stokes Diameter of the particles. This value is then used to calculate the actual diameter of the wool fibres. The first work using this principle was done in 1948, see Sommerville [52].

- Harmonics: In 1952 Buchanan and Bolin [48] investigated a device which made use of harmonic wave principles to measure mean fibre diameter. A fibre of known length and density would be tensioned to a known tension in front of a sound source of variable frequency. The frequency would be varied until a standing wave is observed on the fibre, enabling one to calculate the fibre diameter, see Sommerville [53].

- Photometry: The term photometry is an umbrella term which is used whenever measured modification of light intensity is used as an indicator to quantify some arbitrary effect. A device was developed in 1957 which operated as follows: A light source illuminates a sensor which measures the intensity of the light. If a fibre is inserted in the beam a change in intensity is measured which is proportional to the area of the obstructed light, see Sommerville [9].

- Conductomitry: Change in conductivity of a conductive liquid is proportional to the displacement by immersed wool fibres. The volume of displacement is thus determined and if the length of fibre is known the diame-

Stellenbosch University http://scholar.sun.ac.za

ter can be calculated. Experiments was done using this principle from 1962 to 1969, see Sommerville [54].

- Radioactive isotopes: The possible use of radioactive isotopes to measure wool fibre diameter was identified in 1963. Wool is placed inside a radioactive solvent. The radio active solvent covers the surface area of the wool. The wool is then removed and dissolved in another solution which now contains an amount of radioactive solvent proportional to the surface area of the wool. If the volume of the wool is known the mean diameter can be determined, see Sommerville [55].

- Image analysis: Starting in 1970 work was done to automate the projection microscope. As computer processing power increased and computers became more readily available, image processing by computer became plausible.

The devices developed after 1970 have been accepted and accredited and are still in use today even though some are being phased out. These devices will be dealt with in Section 3.5.

3.4 The classification of wool

In the early days, around the 1930's, people were trained in wool discrimination. They were employed by wool buyers and sellers. No objective measurement technique was available which was rapid and economical enough to serve the market, see McNicholas and Curtis [27].

These wool discriminators could by sight estimate the mean fibre diameter of wool. This ability was looked at in a rather matter of fact fashion as illustrated by the following quote from Hill [22] *"For any one who has good average vision, judging the fineness of wool is no more difficult than judging the size of trees. Both are a matter of practice and based on comparisons with known standards of size"*.

From 1922 teaching and training methods to develop this ability was under active development. The article by Hill [22] suggested an improved training system whereby a student could be taught how to class wool wherein he states *"I have found that it takes the average student less than one-half an hour to measure 100 fibres. An hour a day for three or four months can be profitably spent in this kind of work if the student wants to specialize in the fineness of wool"*. Hill [22] suggested a training system where students would use micrometer callipers to practice their ability to

Stellenbosch University http://scholar.sun.ac.za

estimate wool fibre thickness. In 1927 Burns [56] expanded on this training to allow among other things students to develop the ability to estimate the mean fibre diameter of a sample of wool to within five tenths of a ten-thousandth of an inch, which is roughly within 1.27 µm. Simpson *et al.* [28][8] states *"For fine wool products, where wool mean fibre diameter is a critical parameter, these assessment experts were capable of discriminating readily between 18, 20 and 22 micron wools, and more often than not their subjective assessments correlated with laboratory measurements to within a fraction of a micron"*.

Fantastic as this may seem the subjective nature of this classification system would always be undesirable. In some cases such as breeding programmes aimed at increasing the fineness of wool, the need for better accuracy was especially important as is evident from this quote by Hardy [57] *"In a carefully organized breeding program such inaccuracies in eye judgment are a great handicap to progress. One mistake may introduce, into a flock, variations which will require several generations to correct"*.

The wool discriminators of old did not only include an estimate of mean fibre diameter but also style which their clients believed to be a superior indication of wool quality, Simpson *et al.* [28][9]. In an article dated 1933, Wilson [58] stated *"Units of expression applied to individual fibres are excellent as far as they go, but they do not yield sufficient information"*. Wilson [58] speculated that this could be the reason for the apathy of manufacturers towards research in the field of wool production.

There were several hurdles to overcome before objective measurement systems would replace the subjective measurement system. The biggest of which had been, how to interpret data from measurements into useful information and developing systems which could reliably and rapidly extract such data. The IWTO (International Wool Trade Organisation) worked toward this end. During this time development was slow and it was not until around 1970 that the shift towards objective measurement occurred. Simpson *et al.* [28][10] states *"This is an enormous transformation that has mainly been affected since 1970, after which time the means for improved testing and their ratification by IWTO have come to dominate wool marketing"*.

The IWTO works towards standardisation of wool measurement and classification techniques. In order to achieve this each property of wool to be measured and quantified has to be done according to guidelines provided by the IWTO

[8] Simpson *et al.* [28] on page 6
[9] Simpson *et al.* [28] on page 6
[10] Simpson *et al.* [28] on page 6

Stellenbosch University http://scholar.sun.ac.za

on machines accredited with IWTO approval in order for the classification to be IWTO accredited. Further the IWTO co-ordinates the continuous testing and evaluation of all accredited test methods by means of round trials, see Marler and Harig [12]. In these round trials the same samples are used to compare the different measurement systems, as such measurement and sample preparation techniques are constantly under active development.

The IWTO publishes the IWTO SPECIFICATIONS referred to by the IWTO as the "Red Book". The IWTO states that *"IWTO Specifications include all test methods and draft test methods developed within the Committees of IWTO for the measurement of wool fibre, yarn and fabric properties"* see IWT [59]. The IWTO also publishes the IWTO ARBITRATION AGREEMENT referred to by the IWTO as the "Blue Book". The IWTO states that *"The Blue Book is the basis for the conditions under which most of the world wool trade conducts its business"* see IWT [59].

3.5 Current wool measurement devices

From the list of available IWTO test specifications one can see that there exists a wide variety of test specifications documenting the procedures and conditions according to which tests must be performed in order for results to be certifiable.

At the date of writing this thesis no draft test methods were available for the measurement of mean fibre diameter and the distribution of mean fibre diameter, thus no new instruments were in the process of being evaluated. The following is a list of available IWTO test specifications to measure and classify fibres in terms of mean fibre diameter and fibre diameter distribution.

- Method of Test for the Determination of the Mean Diameter of Wool Fibres in Combed Sliver using the Airflow Apparatus, see IWTO [60].
- Determination by the Airflow Method of the Mean Fibre Diameter of Core Samples of Raw Wool, see IWTO [61].
- Method of Determining Fibre Diameter Distribution Parameters and Percentage of Medullated Fibres in Wool and other Animal Fibres by the Projection Microscope, see IWTO [62].
- Measurement of the Mean and Distribution of Fibre Diameter Using the Sirolan-Laserscan Fibre Diameter Analyser, see IWTO [63].
- Measurement of the Mean and Distribution of Fibre Diameter of Wool using an Optical Fibre Diameter Analyser (OFDA), see IWTO [64].

Stellenbosch University http://scholar.sun.ac.za

- Determination Of Fibre Length, Length Distribution, Mean Fibre Diameter And Fibre Diameter Distribution Of Wool Top & Slivers By The Ofda4000, see IWTO [65].

From the list of available test methods it is apparent that the following devices are accredited by the IWTO to classify wool:

- The projection microscope
- The airflow device
- The laserscan device
- The Optical Fibre Diameter Analyser (OFDA) range of devices

The difference in measurement accuracy stated as the 95 % CL is very small between these devices as listed in Table 3.1.

Table 3.1: 95 % CL for the accredited devices from Marler and Harig [12]

Mean fibre diameter	Method	95 % CL
20 µm	Airflow	±0.03 µm
	Laserscan	±0.05 µm
	OFDA	±0.06 µm
	Projection Microscope	±0.09 µm
35 µm	Airflow	±0.08 µm
	Laserscan	±0.14 µm
	OFDA	±0.15 µm
	Projection Microscope	±0.16 µm

In the following sections we will look at the principle of operation of each device listed in more detail.

3.5.1 The projection microscope

The projection microscope as the name implies uses optics to enlarge and project a sample onto a screen with a magnification factor of 500. This method can be used to obtain the mean fibre diameter as well as the distribution of mean fibre diameter. The projected image is analysed by a trained operator who takes measurements by hand. This method of measurement is considered to be a direct

Stellenbosch University http://scholar.sun.ac.za

measurement of fibre diameter, as it is a measure of the actual fibre image and not the effect of the fibre on some tangible stimulus. Accordingly the projection microscope is regarded as the reference method by the IWTO, see Sommerville [66].

3.5.1.1 Projection microscope methodology

A sample is prepared by cutting fibres into lengths not shorter than 800 µm and placing them on a slide. The slide is then viewed in transmission mode by projecting the sample onto a screen, see Sommerville [66]. The ideal scale of the projected image is said to be 500 : 1. The large magnification means the operator needs to take care in focusing the projected image for each measurement. Direct measurements of the transverse diameter of the fibres are made and scaled down from the projected image. Each measurement is classified into one of forty or more class intervals separated by 2 µm boundaries. The mean and standard deviation of the mean can thus be determined, see Sommerville [66].

3.5.1.2 The projection microscope in overview

The hand measurement required by this device can be tedious and the big magnification can cause focusing difficulties. In order to have reliable measurements the measurement procedure requires two operators to measure at least 300 snippets each, see Sommerville [66].

The time consuming nature of this method makes it impractical for large scale fibre classification, as such it is only used in order to verify new measurement systems as a reference test.

3.5.2 The airflow device

The airflow device measures the pressure drop across a known mass of fibres packed in a chamber. D'Arcy [20][11] describes it like this *"When a current of air is passed through a mass of fibres packed in a chamber with perforated ends the ratio of airflow to differential pressure is primarily determined by the total surface area of the fibres"*.

The first detailed report of measurement of wool using the flow of air was by Cassie [67] in 1942. Since then a lot of work was done to bring theory and practice together. A test standard specification by the IWTO for the WIRA (Wool Industries Research Association) airflow device was released in 1960. This prepared

[11] D'Arcy [20] on page 189

Stellenbosch University http://scholar.sun.ac.za

the ground work for the device which has since become the de facto standard for wool classification, see Sommerville [5]. It is only in recent years that alternative technologies started to overtake the airflow apparatus along with the rise in market awareness of variation of mean fibre diameter.

In the following section we will first look at the theory behind the airflow device and then at the implemented device in order to give the reader a good conceptual grasp of the airflow system for wool fibre measurement. We will not go into minute details as the subject area is beyond the scope of this thesis.

3.5.2.1 The airflow device from a theoretical perspective

The theory of the flow of air through a porous bed containing wool fibres is extrapolated from Poiseuille's law which describes the flow of fluids through capillaries, see Sommerville [5].

In this model the porous bed consists of a fixed volume through which air can flow freely. How such a system could be realised will be looked at in Section 3.5.2.2.

The derivation follows from Sommerville [5]. Given the equation for flow through a porous bed of fibres,

$$Q = K_{\mathrm{b}} \frac{A_{\mathrm{c}}}{L_{\mathrm{c}}} \frac{\varepsilon^3}{(1-\varepsilon)^2} \Delta P d^2 \tag{3.10}$$

where

$$\begin{aligned} Q &= \text{the flow rate of air} \\ K_{\mathrm{b}} &= \text{an experimentally determined constant} \\ A_{\mathrm{c}} &= \text{the area of the porous bed} \\ L_{\mathrm{c}} &= \text{the depth of the porous bed} \\ \varepsilon &= \text{the porosity of the fibres inside a porous bed} \\ \Delta P &= \text{the pressure difference across the porous bed with fibres} \\ d &= \text{the mean diameter of the wool} \end{aligned}$$

with porosity defined as

$$\varepsilon = \frac{V_{\mathrm{c}} - V_{\mathrm{m}}}{V_{\mathrm{c}}} \tag{3.11}$$

Stellenbosch University http://scholar.sun.ac.za

where

V_c = the volume of the porous bed
V_m = the volume of the fibres contained in the porous bed.

If one recognises that

$$V_m = \frac{m}{\rho} \tag{3.12}$$

where

m = the mass of an object consisting of a substance, in this case wool
ρ = the density of a substance, in this case wool

then by substituting Eq. (3.12) into Eq. (3.11), Eq. (3.11) could be rewritten as

$$\varepsilon = 1 - \frac{m}{\rho V_c}. \tag{3.13}$$

Looking at Eq. (3.13) one can see that the porosity of wool could be held at a constant value by compressing a known mass of wool fibres into a fixed volume.

It can now be seen that the variables A_c, L_c and ε could be maintained constant simply by deciding on fixed dimensions for the chamber wherein the fibre plug will be placed and a practical weight for the fibre plug which would fix the porosity given by Eq. (3.13) and therefore Eq. (3.10) could be rewritten as

$$Q = K_c \Delta P d^2 \tag{3.14}$$

where

K_c = an experimentally determined constant which includes the contribution of A_c, L_c and ε .

From Eq. (3.14) it can be seen that the mean diameter of wool could be determined by fixing the flow of air through a porous bed containing fibres and measuring the drop in pressure across the bed, or by keeping the pressure constant across a porous bed containing wool fibres and measuring the flow of air through the bed.

The results for the model in described by Eq. (3.10) do not take into account the variation of diameter of the fibres. Anderson and Warburton [68] demon-

Stellenbosch University http://scholar.sun.ac.za

strated the relationship given by Eq. (3.15) by taking the effect of variation of diameter along and between fibres into account by defining

$$d = \overline{d}\left(1 + C^2\right) \tag{3.15}$$

where

$$\begin{aligned} \overline{d} &= \text{true mean fibre diameter} \\ C &= \text{the fractional coefficient of variation in } \overline{d}. \end{aligned}$$

In terms of Eq. (3.15), since the coefficient of variation is unknown, the device is calibrated with an assumed value for C.

3.5.2.2 The functioning of the airflow device

The device is assembled as illustrated in Fig. 3.3. A vacuum pump is connected to a flow control valve *(2)*. The flow control valve *(2)* is connected to the end of a flow meter *(5)*. The other end of the flow meter *(5)* is connected to one end of a constant volume chamber *(1)*. The other end of the constant volume chamber *(1)* is connected to the top end of a fluid reservoir *(4)*. The bottom end of the fluid reservoir *(4)* is connected to a manometer *(6)*. All the parts are connected by pipes and tubes *(7, 8, 9, 10, 3)*.

The functioning of the device is as follows. The vacuum pump creates a vacuum in front of the flow control valve *(2)*. The device is operated by slowly opening the flow control valve *(2)*. This will cause air to flow through the top opening *(12)* of the constant volume chamber *(1)* and through the porous bed *(13)* through the system towards the vacuum pump. The flow of air is created by a vacuum inside the constant volume chamber *(1)*. The pressure inside the constant volume chamber *(1)* causes the level of the manometer *(6)* to drop in relation to the vacuum. The flow control valve *(2)* is opened until the liquid level in the manometer *(6)* corresponds to a predetermined fixed point *(z)*. The height of the rotameter *(11)* in the flow meter *(5)* is then measured as *(y)* and used to determine the mean diameter of the wool fibres in the porous bed with constant volume *(13)*.

3.5.2.3 The airflow device in overview

This is an indirect method for measurement of wool fibre diameter and the device has to be calibrated against a sample with known fibre diameter. The intrinsic dependence on the surface area of the fibres means this device is not suitable for

Stellenbosch University http://scholar.sun.ac.za

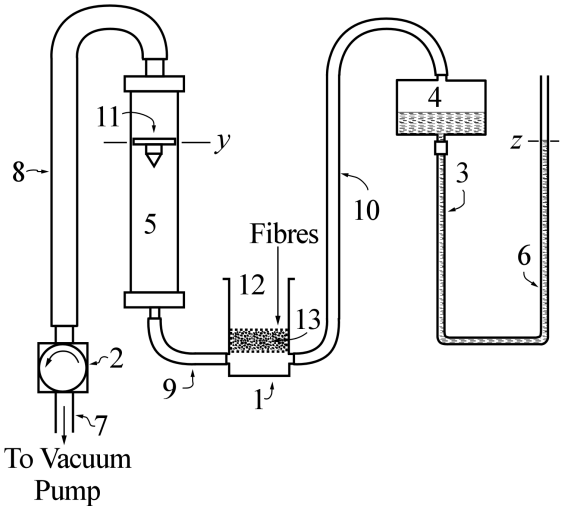

Figure 3.3: Schematic of the WIRA airflow device from Sommerville [5]

all wool types such as medullated fibres, see Sommerville [9], as the hollow centre of said fibres increases the surface area of the fibres altering the measurements.

The device assumes a fixed value for the coefficient of variation for diameter and this can lead to inaccurate measurements in the case where the actual coefficient of variation for the diameter is markedly different from the assumed coefficient of variation of diameter. These errors are small, but even so could be commercially significant.

The industry has become very aware of the benefits of a measurement of the variation in fibre diameter. The inability of the airflow device to measure the distribution of fibre diameter is the biggest drawback of this device.

3.5.3 The laserscan device

The laserscan device measures the amount of light occluded by a fibre, through scattering, when it passes through a beam of light, see Lynch and Michie [7].

The laserscan is the primary means of classification of wool in Australia today. The original patent, from which the modern day laserscan device was derived, was lodged by Lynch and Michie [6] in 1973 and accepted in 1976. The CSIRO (Commonwealth Scientific and Research Organization) developed and constructed the device based on the patent by Lynch and Michie [6]. The device as built by the CSIRO is referred to as the Fibre Fineness Distribution Analyser (FFDA) or alternatively as the Fibre Distribution Analyser (FDA), see Sommerville [9].

Stellenbosch University http://scholar.sun.ac.za

Development on the device continued in order to resolve issues with it's performance. By 1989 most problems have been identified which led to the development of an improved device, the Sirolan™Laserscan, see Sommerville [9]. Evaluation of the device commenced and in 1995 the IWTO published a test specification for the device, see Sommerville and Teasdale [69]. With most of the technical issues solved, the improved device was patented in 1996 by Cantrall *et al.* [8].

We will first look at the theoretical model on which the functioning of the laser scan device is based, then at the original device by Lynch and Michie [6] and finally at the modern day laserscan device as patented by Cantrall *et al.* [8].

3.5.3.1 The theory behind the laserscan device

The theory of diameter prediction by the occlusion of light is based on the following model. If one assumes a parallel beam of equal irradiance and a perfect projected shadow of the fibre on the sensing area, then the relationship between the area of the shadow of a fibre of specific width and the diameter of the beam can be expressed by

$$A = \frac{D^2}{2}\left[\sin^{-1}\left(\frac{d}{D}\right) + \frac{d}{D}\sqrt{1-\frac{d^2}{D^2}}\right] \tag{3.16}$$

where

$$\begin{aligned} A &= \text{the area of the beam which is occluded by the fibre snippet} \\ D &= \text{the diameter of the beam} \\ d &= \text{the diameter of the fibre snippet} \end{aligned}$$

as illustrated in Fig. 3.4, see Lynch and Michie [7].

If $d < D/6$ then Eq. (3.16) is almost linear according to Lynch and Michie [7].

This is a very simplified model ignoring the complex nature of electromagnetic waves. According to Glass [41], a detailed look into the problem would require one to solve Maxwell's equations.

Fortunately the scattering object is large in comparison to the wavelength of the scattered light thus the scalar conditions are satisfied and diffraction is the dominant phenomenon. As such the deviation from the theoretic model can be predicted by diffraction theory.

From the patent by Cantrall *et al.* [8] one finds the physical dimensions for the device which did not change markedly from the first device. As such the pinhole

Stellenbosch University http://scholar.sun.ac.za

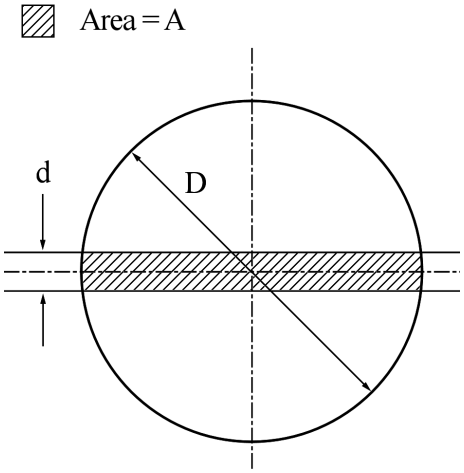

Figure 3.4: An infinite rectangle crossing a circle with it's centerline through the centre of the circle, the width of the rectangle is much exaggerated for clarity

is located within the Fresnel region of diffraction of the laser source and is followed by the flow cell which is located in the resultant Fresnel diffraction pattern again within the Fresnel region. The detector is again within the Fresnel region of the resultant beam passing through the flow cell. Thus the measured diffraction pattern on the sensor is due to a double Fresnel diffracted input as described by Glass [41]. This makes theoretical calculations difficult, but in principle it would be possible to determine a calibration curve with a set of samples of predetermined diameter to calibrate the device empirically, see Sommerville [9].

Glass [41] studied the theoretical effect of fibre curvature in the range of 160 µm to 600 µm on the measurement of fibre snippets with the laserscan device. The findings by Glass [41] predict measurement errors for extremely curved fibres with the laserscan device. Glass [41] did however report that in a typical wool sample the occurrence of such extremely curved fibres are sufficiently small to be neglected.

3.5.3.2 The Fibre Fineness Distribution Analyser

Lynch and Michie [6] describes their invention as follows: *"This invention concerns the measurement of diameter of fibrous material, for example wool, by an optical shadowing technique"*.

In Fig. 3.5 the FFDA device as patented by Lynch and Michie [6] is illustrated. The FFDA device measures fibre snippets by submerging said fibre snippets *(2)* in a liquid, the fibre snippets *(2)* are then carried by the liquid in suspension through a conduit *(8)* with two transparent walls *(6)* forming a flow cell *(3)*. A light beam source *(11)* is setup such that the light beam *(10)* penetrates the flow cell *(3)* and

Stellenbosch University http://scholar.sun.ac.za

terminates on a split electric sensor *(14, 15)* on the other side of the flow cell *(3)*. Electrodes along the sides of the flow cell *(7)* and parallel to the beam could be used to align and elongate the fibres *(2)* such that they perpendicularly cross the light beam. The amount of shadow cast by the fibre snippet *(2)* is then measured as the difference in light beam intensity, which is related to the shadow of the fibre snippet *(2)*, by an electro-optical sensor *(12)*. The electro-optical sensor is split into two sections *(14, 15)* which is used to discriminate between correct and incorrect measurements by monitoring the difference in measured signal between the sensors. The measured signal by the electro-optical sensor *(12)* is used to calculate the diameter of the fibre snippet *(2)*.

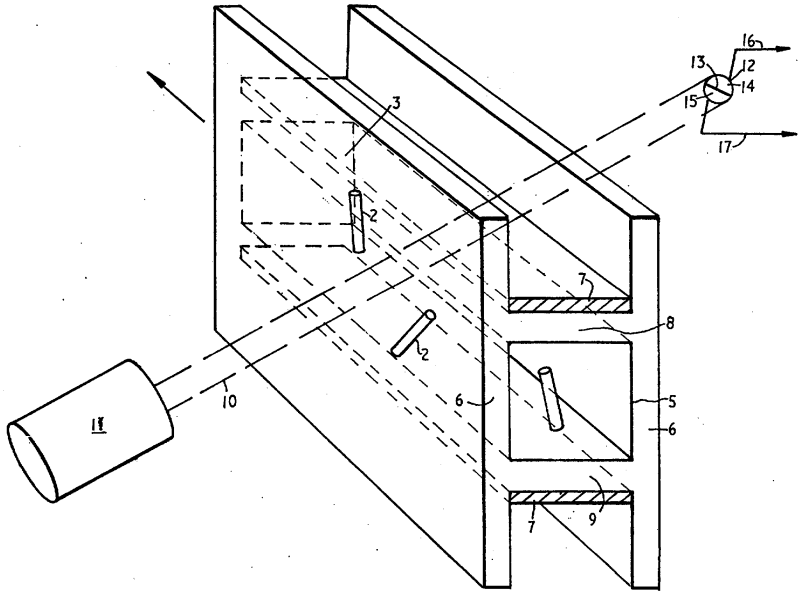

Figure 3.5: The schematic of the FFDA device from Lynch and Michie [6]

Lynch and Michie [6] acknowledged the need for the device to be able to detect if a measurement is acceptable. The following situations where a measurement would be unacceptable were identified.

- A fibre snippet could partially cross the beam with the end of the fibre snippet present in the beam, see Fig. 3.6, or a piece of dirt could cross the beam, see Fig. 3.7.
- More than one fibre snippet could cross the beam as illustrated in Fig. 3.8.

The proposed system of discrimination between partial fibre crossings of the

Stellenbosch University http://scholar.sun.ac.za

beam, see Fig. 3.6, was to use a split electronic detector, indicated in Fig. 3.6, Fig. 3.7, Fig. 3.8 by zones A and B. If the measured difference in signal by the two halves of the split electronic detector were less than 10 % the measurement would be accepted as correct. In the same way the split detector would also be able to invalidate the measurement of a dirt particle crossing the beam, see Fig. 3.7.

In the event of more than one fibre crossing the beam, see Fig. 3.8, Lynch and Michie [6] suggested that if the solution of fibres in the carrier fluid was dilute enough the probability of more than one fibre crossing the beam would be negligible.

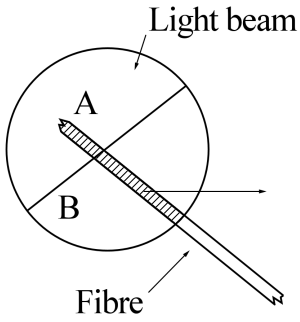

Figure 3.6: A fibre passing the beam partially. Zones A and B indicates the corresponding zones on the electronic sensor, from Lynch and Michie [7]

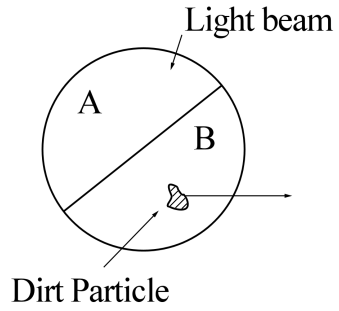

Figure 3.7: A piece of dirt moving past the light beam. Zones A and B indicates the corresponding zones on the electronic sensor, from Lynch and Michie [7]

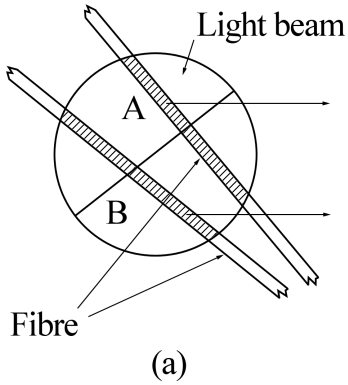

Figure 3.8: Two fibres moving past the light beam. Zones A and B indicates the corresponding zones on the electronic sensor, from Lynch and Michie [7]

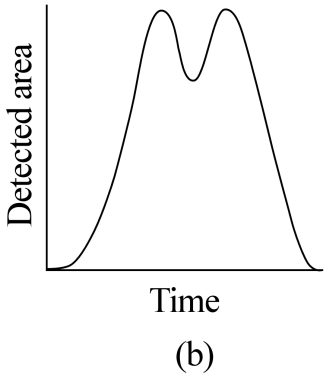

Figure 3.9: The detectable double peak of the detected area in time as the fibres in (a) moves past the sensor, from Lynch and Michie [7]

Thus far we have looked at the FFDA as described in the patent by Lynch and Michie [6]. The patent was written in such a way as to be unambiguous in principle yet ambiguous in implementation. As such the patent does not contain

Stellenbosch University http://scholar.sun.ac.za

specific detail with regard to the elements that are used to realise the device.

Without going into the precise detail of the device, let's look at some key aspects related to its implementation. As mentioned earlier the practical implementation of the device was done by the CSIRO. In Fig. 3.10 the basic setup of the device is illustrated. The light source is a laser beam with diameter 1 mm. The laser source beam is incident on a circular 200 μm pin hole. The resultant beam is circularly symmetric and slowly diverging. A part of the beam is split off by a beam splitter to monitor and control the intensity of the beam. The transmitted beam then passes through the flow cell where the beam diameter is approximately 300 μm and terminates on the split electronic photo sensing device. The photo sensing device is placed in the far field of the laser beam such that only the central lobe of the resultant diffraction pattern caused by the pinhole, is incident on the sensor.

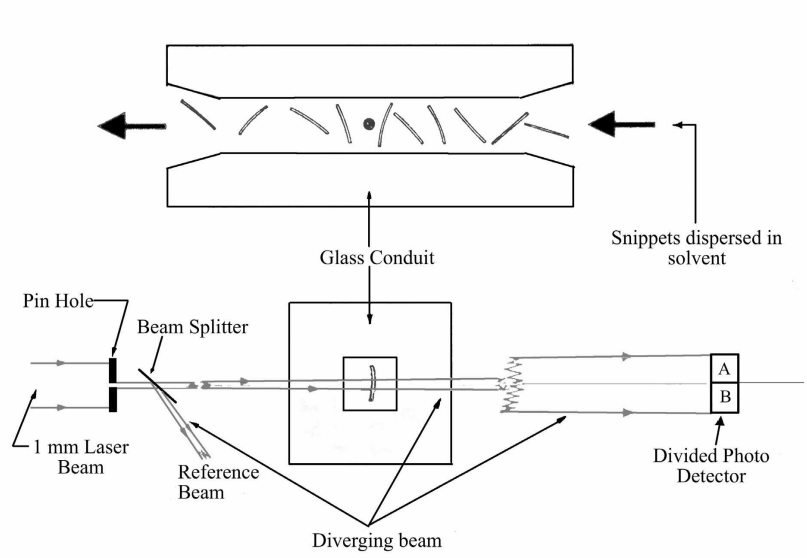

Figure 3.10: The schematic of the FFDA device as implemented by the CSIRO from Lynch and Michie [7]

From 1983 to 1989 the FFDA device was under development and scrutiny. During this period several modifications were made to the device. There were many practical problems that needed to be solved. These were related to the transporting liquid, the orientation of the fibre when the beam is intersected, the effectiveness of discriminating between valid and invalid fibre measurements, the stability of the electro-optics, sample preparation and calibration methods for the device, see Sommerville [9].

During this phase of development two issues in particular lead to the revision of the original device, see Sommerville [9].

Stellenbosch University http://scholar.sun.ac.za

- It was found that the split electro-optic sensor system for rejecting readings was not accurate enough.

  If a fibre varies more than 30 % in diameter in less than the beam diameter this would give an unequal reading on the split electro-optic sensor and result in the measurement being rejected despite being correct. It was found that fibres that had not completely crossed the light beam had been accepted instead of being rejected, see Sommerville [9]. If fibre snippets did not cross the beam in its entirety, such as when it is parallel to the flow of the fluid when moving through the beam off centre, an erroneous measurement would result.

- It was found that in practice the probability of occurrence of two fibres crossing the laser beam at the same time was significant.

  Originally in the early years of the development of the device a system that would monitor the measured signal for multiple peaks was devised, see Fig. 3.9, however it was found to be of insufficient accuracy as this system would not be able to invalidate a measurement if the fibres were very close or in contact when crossing the laser beam, see Sommerville [9].

The resulting patent by Cantrall *et al.* [8] along with the practical solution of all the practical problems encountered during the development phase of the device lead to the modern day laserscan device.

3.5.3.3 The modern day laserscan device

Years of research and development with regard to the occlusion of a laser beam by fibres in order to determine the diameter of said fibres lead to the patent by Cantrall *et al.* [8]. The patent by Cantrall *et al.* [8] consists of two possible device setups to measure the diameter of a sample of fibre snippets with a common system to determine the correctness of the fibre measurement signal. These device setups consist of an improved FFDA and a system which in essence does the same as the FFDA but achieves this with the use of fibre-optics. In the following sections we will look at the improved FFDA and the fibre-optics based FFDA.

The improved FFDA

The following is a description of the device with reference to Fig. 3.11 based on the patent by Cantrall *et al.* [8]. The device can be broken into three functional

Stellenbosch University http://scholar.sun.ac.za

parts. One part to determine the diameter of a fibre snippet, a part to monitor beam intensity and a part to do measurement validation.

The detection of diameter by the device is affected as follows. A He-Ne laser *(101)* illuminates a pinhole *(102)*. The expanding beam with it's diameter modified, exiting the pinhole *(102)* is split by a beam splitter *(103)*. The transmitted beam passes through a flow cell *(105)* where the beam can interact with a fibre snippet submerged in a slurry flowing through the flow cell *(105)*. The beam is then split by another beam splitter *(104)*. The transmitted beam is terminated on a detector *(118)* which is connected to a processor *(110)*. The processor *(110)* monitoring the light intensity of the source is electrically connected to the computer *(115)*. The processor *(110)* calculates the diameter of snippets interacting with the beam in the flow cell *(105)* according to the attenuation measured by the detector *(118)* and the value is sent to the computer *(115)* to be validated and stored.

Fluctuations of the beam intensity is taken into account as follows. The intensity of the split off beam by the beam splitter *(103)* is measured by a reference detector *(109)*. This intensity is fed back to the processor *(110)* which uses the measurement to adapt readings made by the optical detector *(118)* accordingly.

Measurement correctness is affected as follows. The split off beam by beam splitter *(104)* is imaged by a microscope objective *(106)* onto the face plane *(107)* of an optical fibre bundle *(108)* which is connected to a photo diode detector *(112)*. The photo diode detector is connected electrically to processor/timer *(113)*. The processor/timer *(113)* is connected to both the computer *(115)* and the processor *(110)*. The signals from the optical fibre bundle *(108)* is processed by the processor/timer *(113)* to determine if the measurement detected by the optical detector *(118)* is correct.

Data communication and feedback signals are affected by electrical lines *(111, 114, 116, 117, 119, 120)*.

The measurement correctness discriminator operates in the following way with reference to Fig. 3.12. The material crossing the laser beam is imaged onto an fibre optic bundle. The fibre optic bundle is divided into segments each of which is connected to a sensor in such a way that electronics are able to detect when a wool snippet crosses the axis of the beam as well as the relative position of the wool snippet with respect to the outside radius of the beam. In doing so this device is able to detect if a wool snippet intersects the beam entirely, if dirt intersects the beam and it is able to detect whether or not multiple wool snippets intersects the beam, see Sommerville [9].

Stellenbosch University http://scholar.sun.ac.za

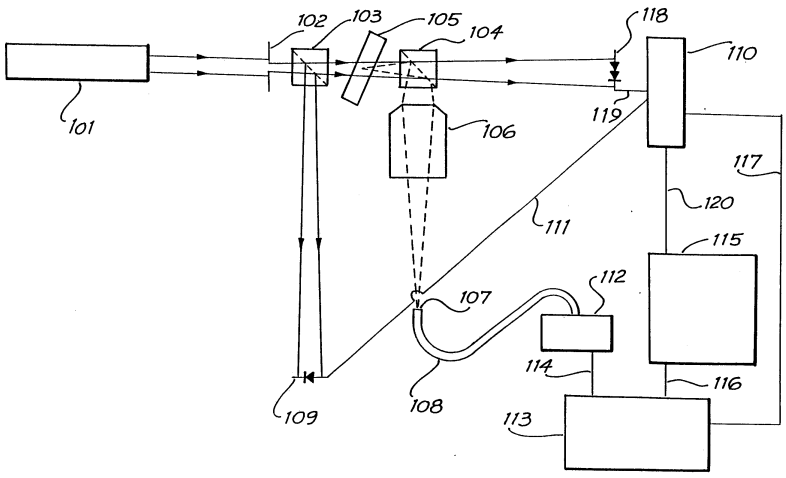

Figure 3.11: The schematic of the laserscan device from Cantrall *et al.* [8]

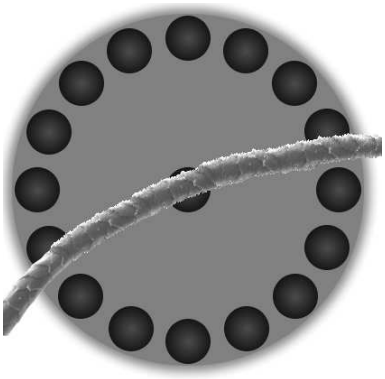

Figure 3.12: Conceptual illustration of the fibre optic discriminator from Sommerville [9]

The fibre-optic based FFDA

The fibre-optic based FFDA operates as follows with reference to Fig. 3.13 and the patent by Cantrall *et al.* [8]. As the device is functionally the same but is implemented using fibre optics, the device can be divided into four functional parts. One part to determine the diameter of a fibre snippet, a part to monitor beam intensity, a part to do measurement validation and a part to do calibration.

Measurement of a fibre snippet is affected as follows. A laser diode *(201)* is used as the source and injects light into the core of a single mode fibre *(202)* which is connected to a single mode coupler *(209)* with three ports. One port *(205)* is connected to a single mode fibre *(207)*. The light exiting from this fibre *(207)* is collimated by a collimating lens *(219)*. The light emerging from the collimating lens *(219)* is incident on a flow cell *(220)* where the laser light could interact with

Stellenbosch University http://scholar.sun.ac.za

a fibre snippet. The light emerging from the flow cell *(220)* is incident on a partial mirror *(221)* which reflects light back through the flow cell *(220)* and some of this light is injected into the fibre end *(208)* by the collimating lens *(219)*. The returning light is measured by a photo diode *(216)* and this signal is processed by a computer *(218)* to determine the mean diameter of the snippet.

The laser diode source intensity is controlled as follows. Some of the light from the laser diode *(201)* is fed back to a photo diode *(211)*. The photo diode *(211)* is connected to a processor *(213)* which uses the signal and holds the power output of the source laser diode *(201)* constant.

Measurement validity is affected as follows. Some of the light which interacted with a fibre snippet in the flow cell *(220)* is transmitted by the partial mirror *(221)*. This light is focused by a lens *(222)* onto the end plane *(223)* of a fibre optic bundle *(224)* forming a diffraction pattern caused by the fibre in the flow cell *(220)*. The fibre optic bundle is connected to a neural network *(225)*. The neural network *(225)* discriminates between correct and incorrect measurements. The neural network *(225)* is connected to the computer *(218)* where the measurement is marked accordingly.

A calibration curve for the device is determined as follows. The computer *(218)* signals the mechanical stage (228) to translate a sample carrier *(229)* through the beam. The sample on the sample carrier *(229)* consists of typically wires with known diameters in the range of 5 μm to 200 μm and as each moves through the beam the calibration curve is determined.

A single mode coupler *(209)* is used to split and redirect portions of the light to the different parts of the setup via single mode fibres *(202, 207, 210, 215)* connected to ports *(203, 204, 205, 206)*. Electrical communication, feedback and controll is affected via electrical lines *(212, 214, 217, 226, 227)*.

3.5.3.4 The laserscan device in overview

After the initial development of the device by Lynch and Michie [6] the device was plagued by anomalies in measurement according to Sommerville [9]. These were finally resolved and after refinement of the device it was adopted as the primary testing method for Australian wools, see Sommerville [9].

The device is sensitive to temperature and due to the temperature control equipment that it needs to operate it is physically bulky. As such it is only suited for laboratory purposes.

Stellenbosch University http://scholar.sun.ac.za

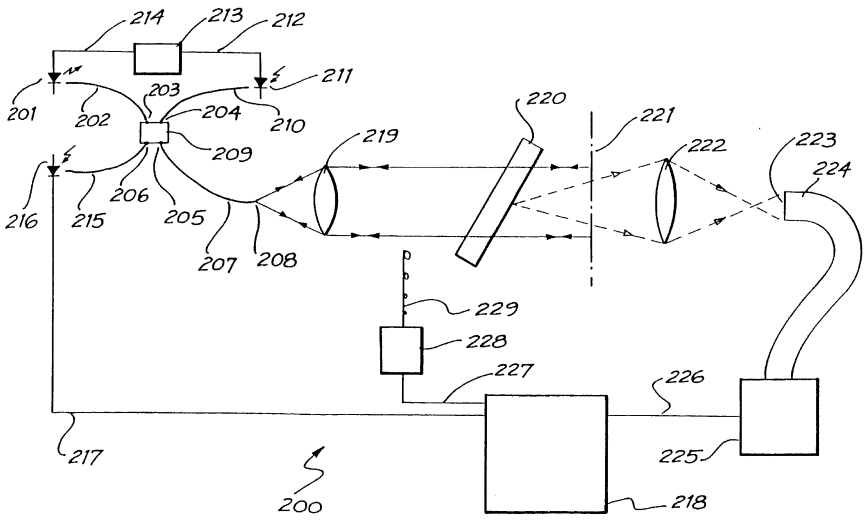

Figure 3.13: The schematic of the fibre optic implementation of the laserscan device from Cantrall *et al.* [8]

The laserscan device provides both the mean and the standard deviation of a sample of wool. The latter putting it ahead of the airflow device for classification.

3.5.4 Optical fibre diameter analyser (OFDA)

The OFDA range of systems are automated versions of the projection microscope. As processing power became more readily available, direct image analysis by computer became possible. Baxter *et al.* [70] described the design and development of the OFDA device.

In 1991 a draft test method was submitted based on the OFDA device. After round trials were conducted it was accepted as a TME (Test Method under Evaluation) by the IWTO. It was, however, not accepted as standard draft test method due to the difference in measured standard deviation in comparison with the projection microscope. Development and inter-laboratory testing of the device continued and in 1995 the OFDA 100 received an IWTO test specification IWTO-47, see Sommerville [71].

The initial device was called the OFDA 100, it's follower up the OFDA 2000 and the latest edition to the range of devices is the OFDA 4000 device, each subsequent device with technical improvements and a longer list of measurable wool attributes, see Sommerville [71], Baxter [72] and Baxter and Brims [73].

Stellenbosch University http://scholar.sun.ac.za

3.5.4.1 The functioning of the OFDA range of devices

These devices uses an optical imaging sensing device which is mounted on a microscope and connected to a computer. The computer has software which enables it to analyse the image from the imaging sensor. A mechanical translation stage is responsible for the movement of a sample of wool mounted between plates on the translation stage, such that multiple measurements of the sample could be made by image acquisition and processing, see Sommerville [71].

3.5.4.2 An overview of the OFDA range of systems

The devices in the OFDA range are able to measure a long list of wool attributes including mean fibre diameter and the distribution of the mean. As the device consists of a microscope with mechanical translation stage connected to a computer, the size of the device shrank along with the computer. The device is not as sensitive to it's external environment in comparison to it's counterpart the Laserscan, but it is dust sensitive. The increased robustness makes it suitable for on site testing in a small mobile laboratory.

3.6 History of devices based on the diffraction principle

The diffraction principle of light shows potential as a fast method to determine the mean diameter of wool and animal hair fibres. Several methods have been used in the past utilising the diffraction principle all failing due to the eye of the operator forming an integral part of the instrument causing difficulties with some operators, see McNicholas and Curtis [27], Matthew [10], Boshoff and Kruger [11] and David and Connell [74]. We hope to solve this problem with modern technology by replacing the eye of the operator with an electronic sensing device.

Matthew [10] and McNicholas and Curtis [27] reports that Thomas Young invented and built the eriometer in 1824 which could measure fibre diameter by utilising the diffraction principle. Young called his instrument the 'eriometer' based on the ancient Greek for wool being 'erio', see Wik [75].

The devices by Matthew [10], McNicholas and Curtis [27] and Boshoff and Kruger [11] were based on the original eriometer by Young. All three of these devices use the eye as an integral part of the instrument. This introduces an element of subjectivity to these devices and difficulty of operation with some operators.

Stellenbosch University http://scholar.sun.ac.za

The difference between these early devices are as follows. The devices by Matthew [10] and McNicholas and Curtis [27] were based on a rectangular light source and a parallel arrangement of fibres whereas the device by Boshoff and Kruger [11], called the Mikronmeter, was based on a circular light source and a random arrangement of the fibres in the sample. In the following sections we describe the eriometer based devices and the Mikronmeter in more detail.

3.6.1 The functioning of the eriometer

Several devices have been based on the eriometer which was devised by Young in 1824. Matthew [10] describes the basic principle of the eriometer device as follows. The device would consist of a slit source of white light which is viewed through an aperture some distance away. A sample of parallel fibres is placed across the aperture parallel to the slit. When the source is viewed with the eye, the fibres cause a diffraction pattern extending parallel to the length of the slit and perpendicularly away from the slit. Through diffraction theory a relation between the fibre width and the spacing of the diffraction pattern exists.

The basic geometry of these devices is illustrated in Fig. 3.14. The angle θ_n is the angle at which the diffraction minima are observed, with n denoting the order of the maximum or minimum. The position where they are observed in the shadow of the source screen is denoted by S_n.

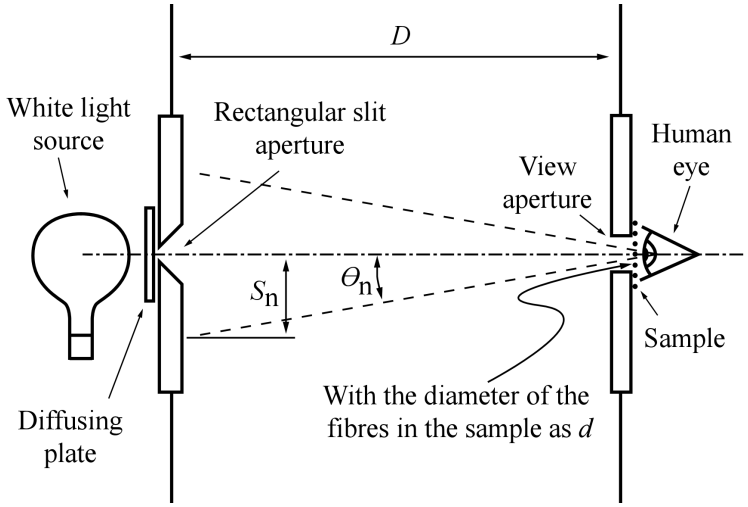

Figure 3.14: A conceptual schematic of the eriometer.

From the geometry of Fig. 3.14 one can see that the lens of the eye performs an optical Fourier transform with the input transparency or object placed approximately against the lens. As the eye is sensitive only to light intensity we can use the simplified form of the equation for an optical Fourier transform with the in-

Stellenbosch University http://scholar.sun.ac.za

put against the lens as given by Eq. (2.152). If the input function is an infinitely long obstruction of width d then from Fourier theory it is known that one can view the function as an infinitely long slit of width d noting that the zero order component of the transform will have a very high intensity corresponding to the total integration area. In optics this inversion of an input mask is referred to as Babinets principle.

Let's assume for now that all the elements extend infinitely along the length coordinate such that one can write Eq. (2.152) as

$$f(x_f) = K_2 \int_{-\frac{d}{2}}^{\frac{d}{2}} f(x_o) \exp\left(-j\frac{2\pi}{\lambda f} x_o x_f\right) dx_o \tag{3.17}$$

where

$$\begin{aligned} d &= \text{The width of the infinitely long slit} \\ f &= \text{The focal distance of the optical system} \\ \lambda &= \text{The average wavelength} \\ x_o &= \text{The coordinate in the plane of the fibres} \\ x_f &= \text{The coordinate in the image plane of the eye} \\ K_2 &= \text{Arbitrary constant.} \end{aligned}$$

If $f(x_o)$ is a plane wave with fixed amplitude then the solution is

$$f(x_f) = dK_2 A \operatorname{sinc}\left(\frac{2\pi}{\lambda f}\frac{d}{2} x_f\right) \tag{3.18}$$

where

$$A = \text{The amplitude.}$$

Eq. (3.18) is applied to the geometry as illustrated in Fig. 3.15.

Now solving for the position of the zero's or the maxima of the function $f(x_f)$ is possible. The position of the maxima can be found by differentiating the function and finding the position of the zero's. As such one has

$$x_{fn}|_{zero} = \frac{n\lambda f}{d} \tag{3.19}$$

$$x_{fn}|_{max} = \frac{(n+0.43)\lambda f}{d} \tag{3.20}$$

Stellenbosch University http://scholar.sun.ac.za

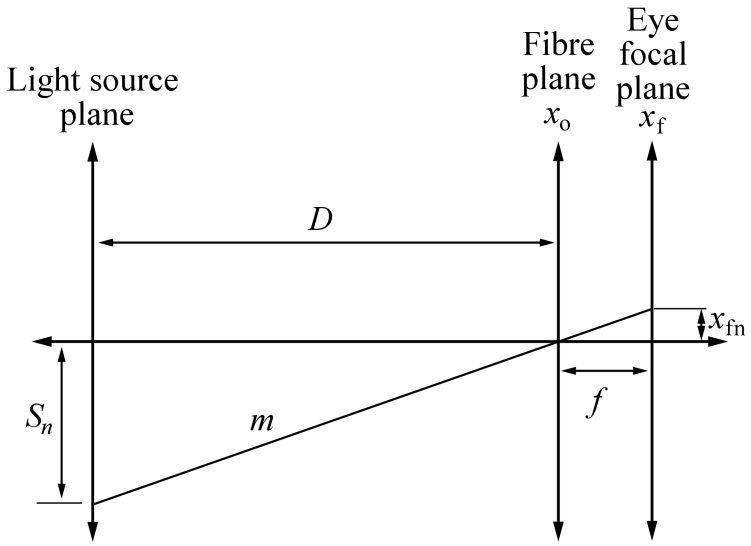

Figure 3.15: The geometry of the eriometer.

where

$$x_{\mathrm{fn}}|_{\mathrm{zero}} = \text{The location of the n'th zero}$$
$$x_{\mathrm{fn}}|_{\mathrm{max}} = \text{The location of the n'th maxima.}$$

With reference to Fig. 3.15, if one projects the principle ray back towards the light source plane, then it is known that the gradient of such a ray in the thin lens approximation is simply $m = \frac{x_{\mathrm{fn}}}{f} = \frac{n\lambda}{d}$. Now the coordinate in the plane of the light source is $S_{\mathrm{n}} = mD = \frac{n\lambda D}{d}$. Thus one can substitute this result into Eq. (3.19) and Eq. (3.20) to find the position of the projected zero's and maxima in the plane of the source as,

$$S_{\mathrm{n}}|_{\mathrm{zero}} = \frac{Dn\lambda}{d} \tag{3.21}$$
$$S_{\mathrm{n}}|_{\mathrm{max}} = \frac{(n+0.43)D\lambda}{d}. \tag{3.22}$$

where

$$S_{\mathrm{n}}|_{\mathrm{zero}} = \text{The location of the n'th projected zero}$$
$$S_{\mathrm{n}}|_{\mathrm{max}} = \text{The location of the n'th projected maximum.}$$

In all these instruments the sample consists of more than a single fibre. From Fourier theory it is known that as long as the distance between the fibres is greater than the fibre diameter the additional fibres would serve only to increase the in-

Stellenbosch University http://scholar.sun.ac.za

tensity of the pattern.

In the instruments based on a slit light source, the view aperture and the human eye are dimensionally limited, yet the ratio of length to width is such that these limits are small enough to ignore and the system input sample could be seen as infinite along the length but finite in width, thus the initial approximation to arrive at Eq. (3.17) is valid.

If a sample is inserted at the view aperture then the observed diffraction pattern by the eye is seen as a projection onto the plane of the light source. The spacing between the zero's and the maxima can then be determined and used in conjunction with Eq. (3.21) and Eq. (3.22) to determine the mean diameter of the sample.

The different systems vary only in the mechanical way that the parameter S_n is determined. As the eye is sensitive to light intensity, the zero's are observed as the positions where the intensity is a minimum and the maxima are observed as positions where the intensity is a maximum. Ewles [76] used a fixed reference point on the plane of the source slit which is then aligned with the first projected maximum or minimum by varying the distance between the source and the eye. Matthew [10] used a split slit light source and then aligned the first maximum or minimum of the projected diffraction pattern of one source with the other. In order to achieve this he used a micrometer screw to translate the slit sources relative to each other, the resultant diffraction pattern is illustrated by Fig. 3.16. Very similarly McNicholas and Curtis [27] used a micrometer screw to translate the edges of the slit relative to the stationary slit until they align with the maximum of the projected diffraction pattern on the source plane.

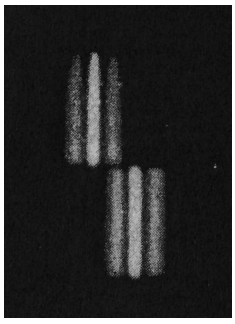

Figure 3.16: The diffraction pattern observed by the split source system, from Matthew [10]

These devices functioned fairly well, but were operator sensitive and limited in sample size by the effective aperture of the eye. Variation of fibre diameter would cause a spreading of the projected diffraction pattern and made accurate

Stellenbosch University http://scholar.sun.ac.za

measurements generally more difficult.

3.6.2 The Mikronmeter

The Mikronmeter by Boshoff and Kruger [11] is in essence based on the eriometer by Young, only it allows for any orientation of the fibres. The resultant diffraction pattern being the sum of the individual contributions from each fibre tends to form a circular disc projected on the source plane.

The basic construction of the Mikronmeter is illustrated in Fig. 3.17. With reference to Fig. 3.17, on the source plane which is a blackened Perspex disc *(F)* a ring is made in the opaque material such that a ring of light is visible on the plane *(F)* at the light source. A sample is placed in the sample holder *(D)* and the inner tube *(E)* and outer tube *(C)* can be slid to change the distance between the eye at the sample holder *(D)* and the source plane *(F)* where the diffraction rings are projected. The diffraction rings are then positioned such that the first minimum of the diffraction pattern and the light ring on the Perspex disc *(F)* coincide. The mean diameter of the fibres could then be read from the scale *(J)* by noting the position of the pointer *(B)*.

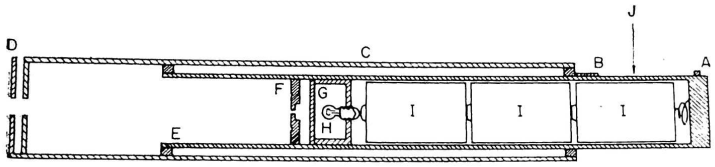

Figure 3.17: Cross-sectional view of mikronmeter from Boshoff and Kruger [11] with: A - micro-switch; B - pointer; C - outer tube; D - sample holder; E - inner tube; F - blackened perspex disc; G - diffusing window; H - light bulb; I - batteries; J - scale

The initial testing of the Mikronmeter was positive, indicating a 95 % confidence limit of $\pm$ 0.9 µm even though Boshoff and Kruger [11] found that some operators had difficulty operating the device. In a more extensive trial of the instrument, David and Connell [74] confirmed that it was not uncommon for an operator to be unable to use the device satisfactorily and further found the 95 % confidence limit from their trials to be $\pm$ 2 µm. The poor accuracy and difficulties some operators experienced with the device is said to be the reason why the device never gained ground in the market, despite being the only hand held device capable of on-farm measurement, see Sommerville [51].

Stellenbosch University http://scholar.sun.ac.za

4

Design considerations

The system designed during this project is based on the same principle as the Mikronmeter which uses a sample of randomly oriented fibres. A key factor in the randomly orientated fibre sample is the amount of useful data contained in such a sample. The sample size and density determines the statistical number of measurements that can be made. The number of measurements in turn determines the deviation of the mean and the 95 % Confidence Limit, see Section 3.2.

One can intuitively see that a sample which is completely covered with fibres contains no discernable fibre diameter information whereas an empty sample also contains none. We are interested in what happens in between these extreme conditions. As such we will analyse sample density in order to find the relation between sample density and the obtainable diameter data from such a sample.

If the importance of sample density is understood we move on to the initial design and selection of components.

4.1 Sample density analysis

Let's refer to a *sample area* as a two dimensional flat area onto which fibres are perfectly projected. It is intuitive that *sample density*, which refers to the percentage of the sample area covered by fibres, is a key contributing factor to the number of samples which statistically could be measured on such a sample area. If more fibres are introduced to a sample at random positions and orientations the sample density increases. As sample density increases so too does the amount of fibre crossings. It is intuitive that fibre width information cannot be extracted from these crossings, as such we want to understand the relationship between sample density and extractable fibre thickness information.

The simplest way to do this is to view the sample in terms of area. Let's subdivide the sample into the following areas, the total fibre area, the measurable fibre

Stellenbosch University http://scholar.sun.ac.za

area and the non-measurable fibre area. The *total fibre area* can be defined as the area of a sample which is occluded by fibres, which when normalised to the total area gives us the sample density. In order to define the *measurable fibre area* of a sample, let's first look at the measurable fibre area of a single fibre. It is intuitive that the measurable area of a fibre refers to those parts of a fibre which can be measured perpendicularly across, See Fig. 4.1. The same rule applies to a sample where there are multiple fibres, in which case we have to additionally omit the areas where fibres cross. Normalising the measurable fibre area with respect to the total area gives us the *measurable density* of the sample. The *non-measurable fibre* area refers to the areas where the fibres cannot be measured perpendicularly across and is the difference between the total fibre area and the measurable fibre area, which when normalised with respect to the total area is referred to as the *non-measurable density* of a sample. Let's refer collectively to the three density parameters as the *measurability properties*.

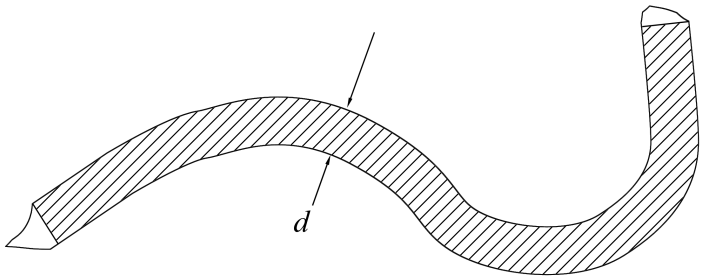

Figure 4.1: Fibre shape with the measurable fibre area etched

It is our goal to determine the general relationship between sample size and density and how that affects the measurability properties of a sample and further to find a reference on which to calculations could be based.

4.1.1 Defining the model for the analysis

In order to define a model to do the analysis we need to approximate fibres such that we can generate approximate sample areas on a computer. Let's first look at a strand of wool in terms of it's diameter and shape, see Section 3.1.3.

1. One can expect to see a surface pattern on the fibre surface causing a small variation in thickness along the fibre.

2. A fibre varies slightly in thickness from root to tip.

Stellenbosch University http://scholar.sun.ac.za

3. The cross sectional shape of a fibre can be circular, elliptical or even bean shaped. If such a fibre is twisted along it's axis it's observed diameter will vary.

4. Fibres have curvature along their length.

5. Fibres within a sample vary in diameter.

To implement a model with the properties above would be very time consuming and slow in computation when generating such complex sample areas. Certain approximations can be made in order to simplify the model with negligible impact on the resultant measurability properties but major impact on development and computational time. The approximations below can be made due to the averaging process which naturally occurs when working with areas.

1. The variation in thickness due to the surface pattern is small and the fibre can be taken as smooth if it is understood that the new diameter of the smooth surface is the mean diameter.

2. The variation from root to tip is small enough to neglect if one considers that it will only effect the mean thickness.

3. The shape of the cross section is near circular enough to ignore the variation which a twist in such a fibre will introduce.

4. The diameter of the average fibre curl is many orders of magnitude larger than the fibre diameter and is therefore negligible. If one takes a fibre as straight this would not have an effect on the measurability properties, yet the fibre count for a fixed fibre density would differ as it would take more straight fibres to cover the same area compared to the number of curved fibres needed to cover the same area of a sample. Thus one can approximate fibres as straight if it is understood that the number of fibres is not a literal quantity.

5. The variation between fibres is small enough to be ignored if it is understood that this effect is combined into the mean.

From these assumptions one can define a *simplified sample area* as a set of randomly orientated and positioned rectangular shapes with fixed width crossing a square bounded area with fixed height, see Fig. 4.2. Such a rectangular shape is

Stellenbosch University http://scholar.sun.ac.za

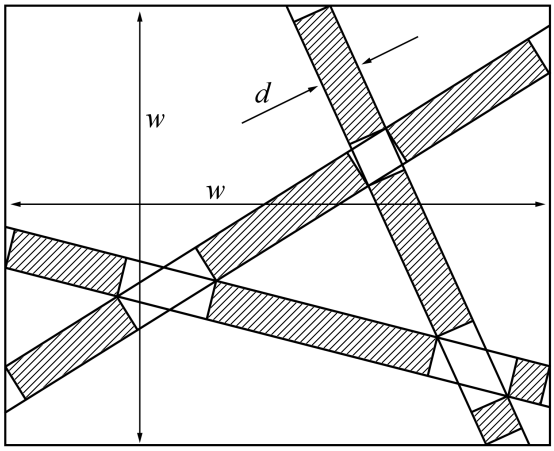

Figure 4.2: A sample area consisting of fibre shapes of width d bounded inside a bounding area of width and height w, with the perpendicularly measurable area hashed

representative of a fibre, thus for the purpose of this analysis let's refer to such a rectangular shape crossing the bounding area as a *fibre shape*.

If one places many fibre shapes onto a sample area, such a simplified sample area can be approximated on the computer as matrix referred to as a *matrix sample*. In such a matrix sample a fibre shape is not smooth but pixelated and is referred to as a *matrix fibre shape*.

One can generate matrix samples such that perpendicularly measurable area's have a value of one, crossings have a value of bigger than one and the rest has a zero value. This would make it possible to determine the measurability properties of the matrix sample. In order to find the sample density of a matrix sample one needs only count all the cells with a value bigger than zero and divide by the total number of cells. Similarly the measurable density could be extracted from a matrix sample by counting the number of cells equal to one and dividing by the total number of cells. The non-measurable density could be found by calculating the difference between the sample density and the measurable density or could be extracted from the matrix sample by counting the number of cells with a value greater than one and dividing by the total number of cells. As such the relationship between these areas, if two of the areas are known, is given by

$$D_{\mathrm{t}} = D_{\mathrm{m}} + D_{\mathrm{n}} \tag{4.1}$$

Stellenbosch University http://scholar.sun.ac.za

where

$$\begin{aligned} D_{\mathrm{t}} &= \text{Total fibre area.} \\ D_{\mathrm{m}} &= \text{Total measurable fibre area.} \\ D_{\mathrm{n}} &= \text{Total non-measurable fibre area.} \end{aligned}$$

If matrices are used to approximate sample areas one needs to consider the implications of the discrete nature of a matrix due to the finite number of cells therein. This causes the sample area to become pixelated, see Fig. 4.3. To minimize the pixelation one can increase the size of the matrix. The bigger the matrix, the more computer memory and computation time is required thus, the increase in matrix size is subject to hardware and computational ability of the computer used.

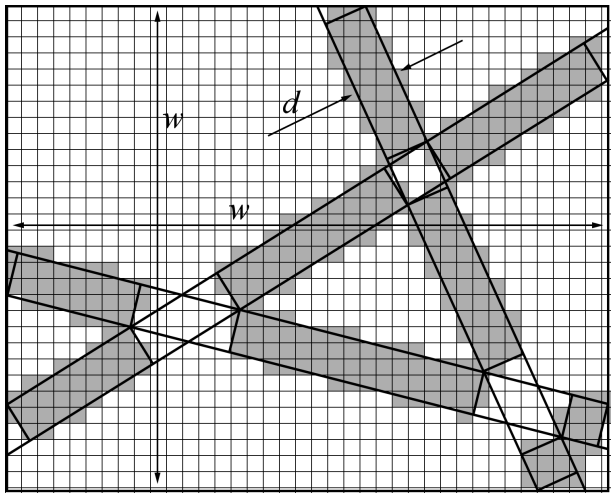

Figure 4.3: Pixilation effect

4.1.2 Generating a matrix sample

Generation of a matrix sample would require that one places the matrix on a Cartesian co-ordinate system with its indices whole numbers, referred to as the *matrix bounded area*. In order to generate a matrix sample one needs to place matrix fibre shapes on a matrix bounded area. Each matrix fibre shape can be completely characterized in terms of it's centre position co-ordinate (x, y), it's orientation θ and it's width d. Let's refer to a matrix fibre shape with random position and orientation as a *random matrix fibre shape*. The length of the random matrix fibre shape is negligible because it is a constant value chosen to be large enough such that the matrix fibre shape will always reach across the matrix bounded area.

Stellenbosch University http://scholar.sun.ac.za

A matrix sample can be characterized by the number of random matrix fibre shapes it contains as n, the width of the random matrix fibre shapes d, and the width of the matrix bounded area w. Thus every matrix sample is a function of n, d and w and contains information related to it's measurability properties in the value of it's cells.

4.1.2.1 Generating matrix fibre shapes

In order to generate matrix samples one needs to generate a set of random matrix fibre shapes each of which is then processed in order to be divided into segments which correspond to each individual matrix fibre shapes measurability properties.

A matrix fibre shape has a centre line which determines it position and orientation referred to as the *fibre centre line*. On the fibre centre line perpendicular line sections of fixed length d are placed each centred on the fibre centre line, let's refer to these line sections as *linelets*. A continuous fibre shape of width d would then consist of an infinite number of linelets with length d spaced an infinitely small distance apart.

One needs to ensure that any matrix fibre shape incorporated into a matrix sample crosses the entire matrix sample regardless of its position and orientation, thus the centre line is placed within the matrix bounded area with a length greater than the diagonal length of the matrix bounded area in order to ensure it crosses the entire matrix bounded area.

If one projects a fibre shape onto a matrix the number of cells is finite, thus only a finite number of linelets, spaced such that the distance between the linelets does not allow any cell within the matrix fibre shape to be omitted, are needed. Each linelet is used to calculate the co-ordinates of the matrix cells which it crosses within the matrix bound area, referred to as the *linelet co-ordinates*. The *fibre shape co-ordinates* is then defined as the sum of the linelet co-ordinates.

In order to generate a random matrix fibre shape of width d, a random position co-ordinate must be generated within the matrix bound area and a random orientation between zero and π. Linelets of length d are then used to calculate the fibre shape co-ordinates. The fibre shape co-ordinates can be used to create a matrix with the cells corresponding to the co-ordinates given a value of one and the rest of the cells a value of zero.

If one has a matrix sample one can determine the measurability properties of each element in the set of random matrix shapes by creating a new matrix sam-

Stellenbosch University http://scholar.sun.ac.za

ple which consists of all the random matrix fibre shapes except the one under scrutiny, referred to as the *exception matrix*. Let's call the random matrix fibre under scrutiny the *test fibre matrix* and the set of linelets which comprises the test fibre matrix as the *test linelets*. One can compare the test fibre matrix to the exception matrix by using the test linelet co-ordinates of the test fibre matrix to separate it into it's measurability properties. This is done by checking each of the test linelet co-ordinates of a test linelet to see if any of the corresponding co-ordinates in the exception matrix has a value greater than zero. If it does this indicates the linelet overlaps with another random matrix fibre shape. Depending on the result a corresponding value of one for no overlap or two for overlap is assigned to all cells in the test linelet co-ordinate set. This is done for all test linelets making up the test fibre matrix. After repeating the process for all elements in the set of random matrix fibre shapes the resultant set of test fibre matrices are added together to give the random matrix sample separated into it's measurability properties. See Fig. 4.4.

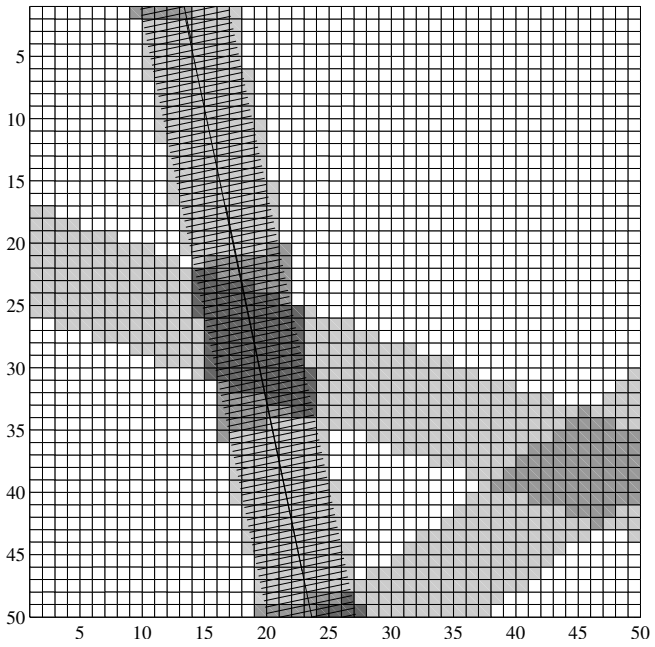

Figure 4.4: Matrix sample with matrix fibre shapes used to illustrate how linelets are used to find the measurable and non-measurable areas of a matrix fibre shape

4.1.2.2 Finding matrix co-ordinates for a line

In order to calculate the matrix indices one can create a function which calculates the co-ordinates of a line centred at some random co-ordinate at some random

Stellenbosch University http://scholar.sun.ac.za

orientation. This line must be sufficiently long to cross the matrix bounded area. The function returns the co-ordinates of steps along this line starting at the centre and stepping outwards up to a specified value. These steps are calculated along either the x or y axis depending on which axis the line has the smallest gradient difference with, referred to here as the *nearest axis*. This ensures that at least every step size cell falls within a matrix cell co-ordinate. If for example a step size of 2 is chosen then one knows the returned selection of cell co-ordinates will be spaced two cells apart along the nearest axis. If a step size of 1 is chosen one knows all cells will be adjoining and a chosen step size of 0.5 would return co-ordinates always perpendicularly adjoining, see Fig. 4.5. Once these co-ordinates are obtained one can use the same function and generate co-ordinates perpendicularly to the centre line to calculate the linelets. In order to be sure no matrix co-ordinates are missed we chose a step size of 0.5 to ensure a solid matrix fibre shape, see Fig. 4.4.

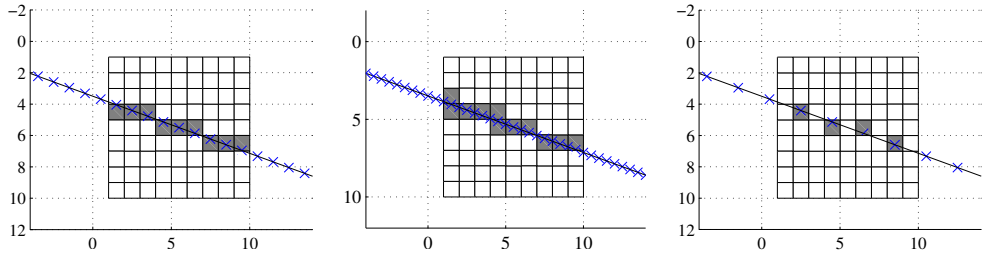

(a) 1 pixel spacing (b) 0.5 pixel spacing (c) 2 pixel spacing

Figure 4.5: Matrix lines with different step sizes

4.1.3 Analysis of random matrix samples

Using the techniques described above one is able to generate random matrix samples as illustrated in Fig. 4.6. Every random matrix sample can be reduced to it's measurability properties by normalising the respective areas, see Fig. 4.6(b) and 4.6(c), with respect to the total area.

As such one can generate a set of random matrix samples such that each subsequent random matrix sample has more random fibre shapes. One can then plot the measurability properties of the resultant random matrix sample set as illustrated in Fig. 4.7. Due to the random method used to generate the matrix sample areas one expects the measurability properties to have some variance.

One can deduce from Fig. 4.7 that results can be described by the following

Stellenbosch University http://scholar.sun.ac.za

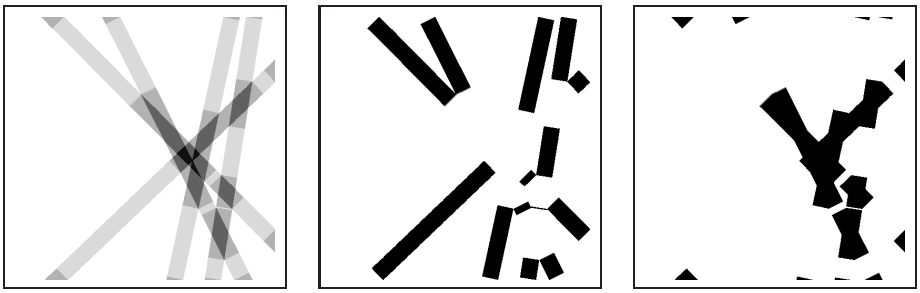

(a) Total area (b) Measurable area (c) Non-measurable area

Figure 4.6: Example of a random matrix sample, 500 pixels wide with fibre sample's 30 pixels in width, split into it's respective measurability areas

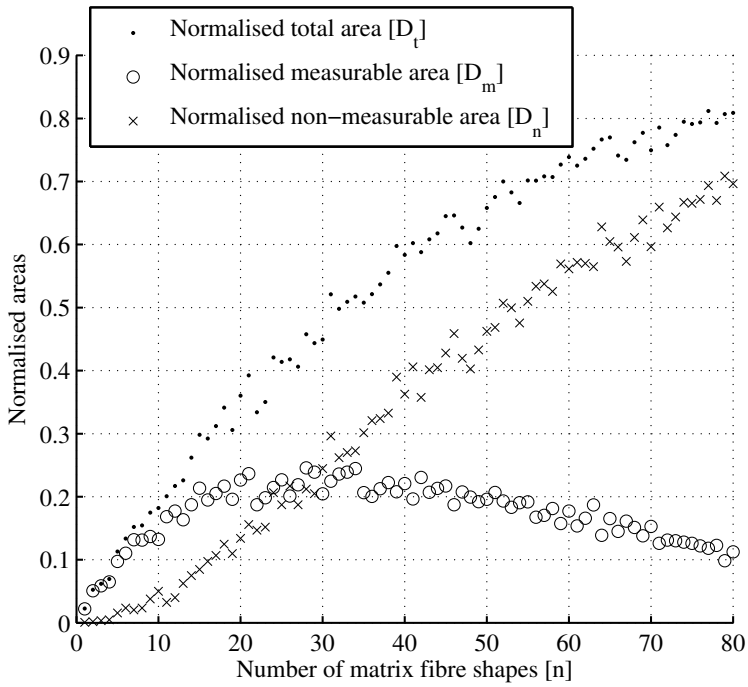

Figure 4.7: Example of measurability properties calculated for a set of random matrix samples by increasing the number of matrix fibre shapes

family of functions,

$$D_t = 1 - \exp(-k_1 x) \tag{4.2}$$

$$D_m = x \exp(-k_2 x). \tag{4.3}$$

It is intuitive that

$$x \propto \frac{nd}{w} \tag{4.4}$$

Stellenbosch University http://scholar.sun.ac.za

where

$$\begin{aligned} n &= \text{Number of matrix fibre shapes} \\ d &= \text{The thickness of the matrix fibre shapes} \\ w &= \text{The width of the matrix sample area.} \end{aligned}$$

Now one can substitute Eq. (4.4) into Eq. (4.3) and by noting that due to pixelation the actual value of d will vary as $d + \Delta d$ one finds,

$$D_{\mathrm{t}} = 1 - \exp\left[-k_1 \frac{n(d+\Delta d)}{w}\right] \tag{4.5}$$

$$D_{\mathrm{m}} = \frac{n(d+\Delta d)}{w} \exp\left[-k_2 \frac{n(d+\Delta d)}{w}\right]. \tag{4.6}$$

This allows us to find a relation for k_1 by fitting Eq. (4.5) to a number of data sets with arbitrary chosen width and fibre shape thickness. Due to the variance we take the mean of multiple samples for each point on the resultant measurability property graphs. Table 4.1 shows the data sets chosen and the resultant values for k_1 and Δd.

Table 4.1: Resultant fits from data sets for the total area of a matrix sample.

Width	Fibre shape thickness	Points averaged	k_1	Δd
300	10	25	1	0.6
500	10	25	1	0.6
850	15	15	1	0.3
1000	30	15	1	0

The same method is used to find k_2 and again Δd. The results are listed in Table 4.2.

Table 4.2: Resultant fits from data sets for the measurable area of a matrix sample.

Width	Fibre shape thickness	Points averaged	k_2	Δd
300	10	25	$\ln(0.2)$	0.6
500	10	25	$\ln(0.2)$	0.6
850	15	15	$\ln(0.2)$	0.3
1000	30	15	$\ln(0.2)$	0

Stellenbosch University http://scholar.sun.ac.za

Using this method we find k_1 to be unity and k_2 to be $\ln(0.2)$, thus we only need to adapt Δd for each of our arbitrary data sets. For each result the error value was within 1 %. An example of the resultant fit is illustrated in Fig. 4.8

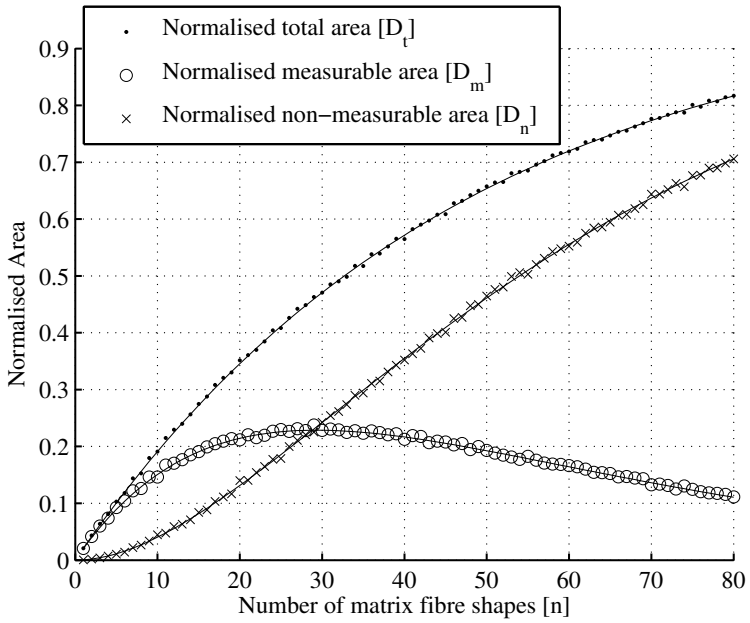

Figure 4.8: Example of the calculated fit for the measurability properties indicated by the solid lines. The sample size is 500, the fibre shape thickness is 10 and the mean of 25 random matrix samples is used to calculate each point on the graph.

From the tables, Table 4.1 and Table 4.2, it is apparent that the constants k_1 and k_2 do not vary with n, d and w, thus we can substitute the values into (4.6) to find,

$$\begin{aligned} D_{\mathrm{t}} &= 1 - \exp\left[-\frac{n(d+\Delta d)}{w}\right] \\ D_{\mathrm{m}} &= \frac{n(d+\Delta d)}{w}\exp\left[-\ln(0.2)\frac{n(d+\Delta d)}{w}\right]. \end{aligned} \tag{4.7}$$

Further it is intuitive that any random sample, which is not approximated by a matrix, must be linearly scalable. This implies that one can adapt the measurability property equations given by Eq. (4.7) by substituting all d values with kd and all w values with kw such that k is a scaling factor. Further it is intuitive that the matrix approximation will become non pixelated if the matrix sample area is taken as infinite such as is the case when the scaling factor approaches infinity.

Stellenbosch University http://scholar.sun.ac.za

One can substitute the scaling functions into Eq. (4.7) and solve for $k \to \infty$ to find

$$\begin{aligned} D_{\mathrm{t}} &= \lim_{k\to\infty} 1 - \exp\left(-\frac{nd}{w}\right) \\ D_{\mathrm{m}} &= \lim_{k\to\infty} \frac{nd}{w} 0.2^{-\frac{nd}{w}} \\ D_{\mathrm{n}} &= D_{\mathrm{t}} - D_{\mathrm{m}}. \end{aligned} \tag{4.8}$$

The resultant equations, given by Eq. (4.8), are continuous and are no longer bound to the matrix environment. We are therefore able to use these equations to make predictions about the properties of simplified sample areas. As simplified sample areas are an approximation for wool covering a square aperture we are able to gain insight into the relation between sample density and the measurability properties of a sample.

4.1.4 Discussion of sample size analysis

The equations estimating the measurability properties given by Eq. (4.8) have useful implications. The zero order transmitted light after passing through a sample placed in the path of the light will be attenuated in intensity proportional to the obstructed area of the sample which is related to the sample density. Thus the light intensity before and after a random sample of fibres could be used to estimate the measurability properties of the sample. In the model the beam intensity profile is not considered, intuitively we assume the main effect of the beam intensity profile would be to affect the effective sample area.

From the equations describing the measurability properties given by Eq. (4.8), it is seen that a constant point exists where the measurable area is equal to the non-measurable area referred to as the 50 % point. The value for a relative variable $x = \frac{nd}{w}$ at the point of optimal measurability can be found from the measurability property equations given by Eq. (4.8) by reading from a graphical plot the x value where $D_{\mathrm{m}} = D_{\mathrm{n}}$. The expected value of the area density at this position could then be found from the relation $D_{\mathrm{t}} = D_{\mathrm{n}} + D_{\mathrm{m}}$.

If one normalises the measurable sample density and non-measurable sample density equations with respect to the sample density for a relative $x = \frac{nd}{w}$ the

Stellenbosch University http://scholar.sun.ac.za

measurable area and the non-measurable area of the fibre shapes are found as

$$\begin{aligned} D_{\text{sm}} &= \frac{x\,0.2^x}{1-\exp(-x)} \\ D_{\text{sn}} &= 1 - \frac{x\,0.2^x}{1-\exp(-x)} \end{aligned} \tag{4.9}$$

where

D_{sm} = The normalised measurable area of the fibre shapes

D_{sn} = The normalised non-measurable area of the fibre shapes.

If one plots the resultant equations given by Eq. (4.9) the 50 % point where the measurable and non-measurable normalised fibre shape areas intersect can clearly be seen, see Fig. 4.9. The 50 % point occurs where $x = 0.6108$ which will be refered to as $x_{50\%}$.

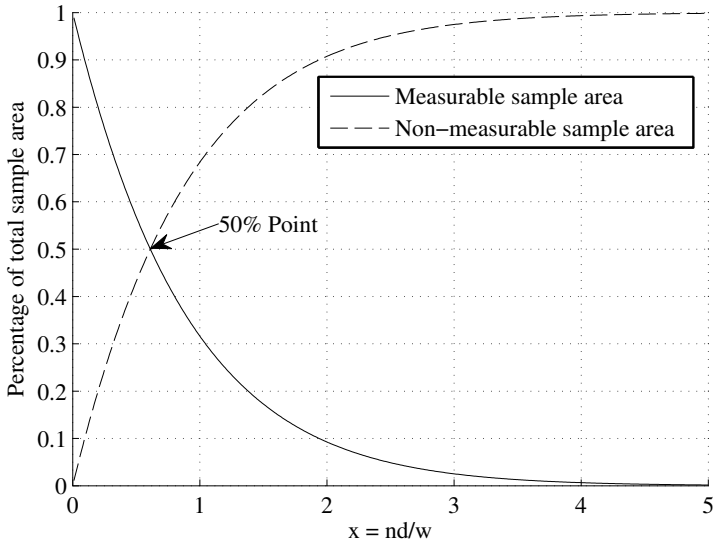

Figure 4.9: The percentage of sample area which is measurable and non-measurable plotted against a relative $x = \frac{nd}{w}$.

As stated earlier the measurability properties of a sample could be obtained by measuring the attenuation of the zero order before and after a sample is placed in the path of the beam. At the 50 % point the beam will be attenuated by a factor of $D_{\text{t}}(x_{50\%}) = 0.46$ and the sample's measurability will be optimised under the assumed condition of an equal random distribution of fibres across the sample area.

As noted earlier the number of fibres n is a count of straight fibre shapes which

Stellenbosch University http://scholar.sun.ac.za

will yield a different result to curved fibre shapes. It does, however, give us a relative indication of the number of fibre shapes which could be contained in a sample of a given size. An equivalent relative number of fibre shapes at the 50 % point could be derived from the relative equation $x = \frac{nd}{w}$ as,

$$n_{50\%} = \frac{x_{50\%} w}{d} \tag{4.10}$$

where

$$\begin{aligned} x_{50\%} &= \text{A constant value where } D_{\text{m}} = D_{\text{n}} \\ n_{50\%} &= \text{The equivalent relative number of fibres at } x = x_{50\%}. \end{aligned}$$

By noting that w is the square root of the area for a square sample shape and that the properties are related to area, one can write Eq. (4.10) more generally as

$$n_{50\%} = \frac{x_{50\%} \sqrt{A}}{d} \tag{4.11}$$

where

$$A = \text{The area of the sample.}$$

In practice the measurement method primarily determines the number of samples taken. For example in the OFDA range of devices, the cross section of fibres is measured at random positions. It is possible that the same fibre is measured multiple times. One can take the average of this occurrence and obtain a constant with which to multiply the relative number of samples. In an ideal Fourier optical system all information regarding the sample could be retrieved and one would have a different constant with which to multiply the relative number of samples. As such a system could be evaluated to find it's measurement efficiency.

4.2 The optical system

During the design the of the optical system the sample size has to be maximised for a fixed maximum pattern size. The pattern size is determined by the dimensions of the Charge Coupled Device (CCD) based camera. The sample is located at the sample plane and the Fourier optical pattern is located at the observation plane. The relationship between the sample plane and the observation plane is determined by the Fourier optical properties of lenses, specifically the relation-

Stellenbosch University http://scholar.sun.ac.za

ship between the dimensions of the input sample at the input plane and the dimensions of the Fourier optical pattern at the output plane.

The basic Fourier optical system is illustrated in Fig. 4.10. The complete source consists of a primary source, a beam expander and a pinhole filter. The sampling space is where the fibre sample is inserted and the Fourier optical system which is represented by a single lens performs the Fourier optical transformation which is detected at the Fourier plane.

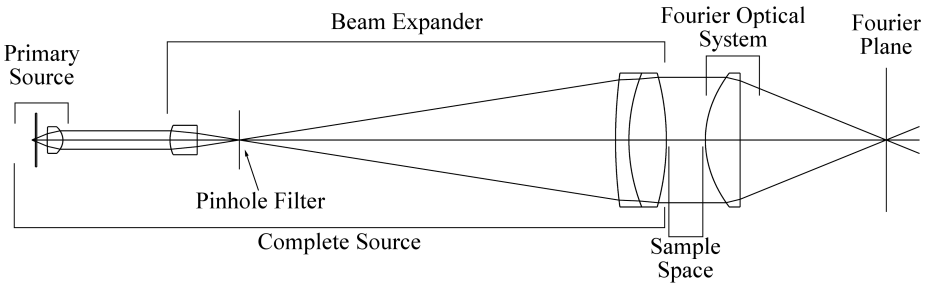

Figure 4.10: Schematic view of the basic optical system.

The size of the Fourier pattern is inversely proportional to the wavelength and the focal length of the lens. The active area of a CCD camera is generally small with respect to the size required for a Fourier optical pattern. Therefore a lens with a short focal length is required. One can further decrease the size of the potential Fourier optical pattern by using as long a wavelength of light as is possible while still meeting the scalar conditions. One is also limited by the availability of equipment capable of functioning at the chosen wavelength.

One needs to keep in mind that the output dimensions are inversely proportional to the input dimensions as a result of the optical Fourier transform and thus a CCD camera with high resolution is preferred for maximum discrimination ability.

The source is related to the sample area by the requirement that it must be able to fully illuminate the sample area. A further constraint is that it must do so with a nearly flat wave front.

With all these constraints we had to select components while keeping in mind they must be such that they could form part of other experiments in the future. This is primarily a financial consideration due to the expensive nature of optical components.

The prototype developed is considered the first device in a design cycle. On the basic level it remained to be proven that an optical Fourier setup could be made to work within the very limiting design parameters.

Stellenbosch University http://scholar.sun.ac.za

A light source with a similar wavelength to that of a HeNe laser was chosen as there are many HeNe lasers available should one need to verify some aspect of the proposed device requiring a high precision beam with near ideal properties. As such the chosen wavelength is $\pm$ 632 nm. The chosen wavelength satisfies all design conditions, it is a long wavelength, within the visible range and there are Laser Diodes available with good quality beams in this range. The laser diode selected was the Hitachi HL6343G/44G with a typical output wavelength of 635 nm, low beam ellipticity with the aspect ratio given as typically 1.2 and an optical output power of 10 mW. Driving current is given as $0 - 35$ mA with a maximum of 45 mA.

A CCD camera was selected with good sensitivity at the chosen wavelength, reasonably high resolution, a large sensor area and overall good scientific performance as the device would later form part of other setups. The device selected was the Pixelink PL-A741 CCD camera.

As the dimensions of the sensor area is known one can calculate the focal length needed such that the optical diffraction pattern that results from the minimum diameter fibre will fit onto the sensor area of the CCD camera. The data sheet of the CCD camera supplies it's dimensions as 8.576 mm by 6.912 mm.

With the minimum diameter of fibre and the dimensions of the sensor area of the CCD camera known, one can calculate a focal length for the Fourier optical system. It is known that the positions of the minima of the Fourier optical pattern is equivalent for a disc and a random sample of wool if the diameter of the disc is the same as the mean diameter of the wool. Thus from Appendix A.7 we can use Eq. (A.64) with $r_o = r_s$, simplify and rewrite with f as the subject to find,

$$f = \frac{r_s d}{n\lambda} \tag{4.12}$$

where

f = Focal length
d = The diameter of the disc
n = Number of intensity minima starting from the origin
r_s = The co-ordinate on the sensor area at a distance from the origin.

From the discussion in Section 3.1.2 it is known that a mean fibre diameter of 10 µm is very rare, thus one can take this as the lower limit. If one position the resultant Fourier optical pattern in the centre of the sensor area of the CCD

Stellenbosch University http://scholar.sun.ac.za

camera then r_s is 3.46 mm. If one wants to observe the entire first lobe of the resultant Fourier optical pattern on the sensor area of the CCD camera then one must choose n as 2. This is quite a strict requirement as we only need to be able to detect the first zero, thus n could be anything between 1.1 and 2. The value 1.1 is chosen to be arbitrarily larger than 1 as a value of 1 would mean the first zero would be right on the edge of the active area of the CCD which could complicate detection. For the purposes of the design we chose n as between 1.1 and 2. The minimum and maximum focal lengths are calculated as,

$$\begin{aligned} f_{\text{min}} &= \frac{3.456 \times 10^{-3} \cdot 10 \times 10^{-6}}{2 \cdot 635 \times 10^{-9}} \\ &= 27.24 \times 10^{-3} \end{aligned}$$

$$\begin{aligned} f_{\text{max}} &= \frac{3.456 \times 10^{-3} \cdot 10 \times 10^{-6}}{1.1 \cdot 635 \times 10^{-9}} \\ &= 49.53 \times 10^{-3}. \end{aligned}$$

We find that the required focal distance f of our optical system must be less than 27.2 mm or less than 49.5 mm.

The primary lens was chosen such that it could perform the Fourier optical transform by itself as one could always add additional lenses to decrease or increase the focal length of the final optical system. Lenses come in standard sizes of 0.5 ″, 1 ″ and 2 ″. The shorter the focal distance of a standard spherical lens, the bigger and the larger the aberrations become as the lens needs to be thicker with surfaces with small radii of curvature to accomplish the short focal length. Thus the sample area which one would like to be as large as possible is limited by the possible size of the lens due to aberrations. Fortunately special spherical lenses are available with reduced aberrations and short focal lengths. The chosen lens is the Precision Asphere 47731 (from the 2006 catalogue of Edmund Optics) and have a focal length of 31.25 mm and a diameter of 25.2 mm.

For the chosen lens if we assume the area at the sampling space to be scaled by a scaling factor of 0.6 due to the effect on the effective area by the shape of the intensity of the beam then we can calculate the relative number of fibre shapes, with Eq. (4.11), for the sampling space at the 50 % point for 30 µm fibres as,

$$\begin{aligned} n_{50\%} &= \frac{0.61 \cdot \sqrt{0.6 \cdot (12.5 \times 10^{-3})^2 \cdot \pi}}{30 \times 10^{-6}} \\ &= 349. \end{aligned}$$

Stellenbosch University http://scholar.sun.ac.za

The resultant number of 349 equivalent fibre shapes gives us a relative indication of number of samples for a measurement and is certainly a large enough number if one considers that 300 measurements must be taken per sample when measurements are made with the projection microscope.

In order to illuminate the sample area one needs to collimate, filter and expand the light from the source. The collimated beam must be expanded and spatially filtered. As a spatial filter consists of focusing a beam through a pinhole, one is able to combine the spatial filter and the beam expander. As such the beam expander consists of two convex lenses, the first focuses light through a pinhole and the second then collimates the expanded beam. The required beam diameter at the sample determine the lens parameters of the beam expander.

The specification of the laser diode lists a possible beam divergence of up to 25°, thus one can calculate the maximum possible required numerical aperture of the collimating lens as,

$$\begin{aligned} \text{NA} &= n_{\text{air}} \sin\theta \\ &= 1 \cdot \sin(25°) \\ &= 0.42\,. \end{aligned}$$

A collimating lens with a numerical aperture of 0.55 and effective diameter of 4.95 mm with an anti-reflection coating in the near infrared spectral range was chosen. A parameter file for the lens was obtained in the format of the software OSLO from the retailer of the lens. From the software we can find a more accurate estimate for the Effective Focal Length (EFL) of the lens as the lens was originally designed at a wavelength of 720 nm. The software reports the EFL of the lens to be 4.47 mm when used with a wavelength of 635 nm.

One can calculate the beam diameter for the light collimated by the collimating lens from the known beam divergence of the laser diode. One can use Eq. (A.50) from Appendix A.6 to calculate the beam diameter and when considering that the beam will be spatially filtered we approximate M^2 as one to find,

$$\begin{aligned} d_{\text{i-min}} &= 2 \cdot \frac{4.47 \times 10^{-3}}{1} \tan(17°) \\ &= 2.73 \times 10^{-3} \end{aligned}$$

$$\begin{aligned} d_{\text{i-max}} &= 2 \cdot \frac{4.47 \times 10^{-3}}{1} \tan(25°) \\ &= 4.17 \times 10^{-3}\,. \end{aligned}$$

Stellenbosch University http://scholar.sun.ac.za

Thus the source beam diameter is calculated to be between 2.73 mm and 4.17 mm.

The next part of the optical setup is the combined beam expander and pinhole filter. The beam expander must introduce as little as possible deformation to the wave front at the sampling space. With this in mind high performance lenses must be chosen. Let's first look at the beam expander as it determines the required lens before the pinhole filter. The expansion ratio of the beam is determined by the focal lengths of the lens pair which constitutes the beam expander and is given by

$$M_x = \frac{f_2}{f_1} \tag{4.13}$$

where

$$\begin{aligned} M_x &= \text{Expansion ratio of the beam incident on lens one} \\ f_1 &= \text{Focal length of the first lens} \\ f_2 &= \text{Focal length of the second lens.} \end{aligned}$$

The relation in describing the magnification of beam diameter given by Eq. (4.13) assumes the beam to start from the source, be incident on the first lens and then on the second lens.

One would like to keep the optical setup as short as possible. This requires the use of lenses with short focal lengths, therefore the f/# of the lenses must be small. The f/# is the ratio of the effective diameter of a lens to the focal length of the lens. Standard lens performance decreases as the f/# of the lens becomes smaller. This is not a problem for the first lens as one can use an aspheric lens to be sure the pinhole filter performs optimally, thus only the second lens need to be considered. In order to have good lens performance and limit the size of the optical setup a lens with f/# of three was chosen. This is a small f/# and as a standard lens would not perform well enough we selected an achromatic doublet with focal length of 75 mm and diameter of 25 mm. In order to know the required focal length of the first lens in the beam expander one must first calculate the

Stellenbosch University http://scholar.sun.ac.za

required beam expansion.

$$\begin{aligned} M_{\text{x-min}} &= \frac{25 \times 10^{-3}}{2.73 \times 10^{-3}} \\ &= 9.16 \end{aligned}$$

$$\begin{aligned} M_{\text{x-max}} &= \frac{25 \times 10^{-3}}{4.17 \times 10^{-3}} \\ &= 5.995 \end{aligned}$$

The magnification formula Eq. (4.13) can be used to calculate the required focal lengths of the objective in front of the pinhole filter as,

$$\begin{aligned} f_{\text{min}} &= \frac{75 \times 10^{-3}}{9.16} \\ &= 8.19 \times 10^{-3} \end{aligned}$$

$$\begin{aligned} f_{\text{max}} &= \frac{75 \times 10^{-3}}{5.995} \\ &= 12.51 \times 10^{-3}. \end{aligned}$$

To satisfy all the requirements an aspheric lens with a focal length of 11 mm was selected and placed before the pinhole. This choice allows one to easily replace the achromatic doublet at the sampling space with a lens with focal length of 100 mm if one needs a bigger beam expansion ratio, allowing the minimum diameter beam to be sufficiently expanded. The diameter of the aspheric lens before the pinhole is 5.5 mm. If the beam before the beam expander is the maximum diameter, the collimating lens would be over illuminated to an acceptable degree with this lens choice.

The collimated light from the laser diode must be focused through a pinhole by the aspheric lens chosen. The size of the pinhole is determined by the parameters of the beam expander which consists of the chosen lens pair. The objective required by the beam expansion has a diameter of 5.5 mm and an EFL of 11 mm. The beam diameter was calculated to be between 2.73 mm and 4.17 mm, thus one can calculate the required size of the pinhole filter using Eq. (A.60) from Ap-

Stellenbosch University http://scholar.sun.ac.za

pendix A.6 as

$$\begin{aligned} d_1 &= 4 \cdot \frac{635 \times 10^{-9} \cdot 11 \times 10^{-3}}{\pi \cdot 2.73 \times 10^{-3}} \\ &= 3.26 \times 10^{-6} \end{aligned}$$

$$\begin{aligned} d_2 &= 4 \cdot \frac{635 \times 10^{-9} \cdot 11 \times 10^{-3}}{\pi \cdot 4.17 \times 10^{-3}} \\ &= 2.13 \times 10^{-6}\,. \end{aligned}$$

At the time when we ordered the pinholes the final design of the setup was not complete. As such we selected pinholes on the basis of the approximate lens that we would use before the pinhole. The lens was estimated to have a diameter of 5 mm and a focal length of 15 mm. The pinhole diameter can be calculated for such a lens using Eq. (A.59) from Appendix A.6. If one chooses a value for the cutoff constants such that neither lens nor pinhole will be overfilled such as $N_\mathrm{l} = N_\mathrm{p} = \frac{3}{\sqrt{2}}$ then we can calculate the size of the pinhole as,

$$\begin{aligned} W_\mathrm{p} &= \frac{2N_\mathrm{p}N_\mathrm{l}\lambda f}{\pi W_\mathrm{l}} \\ W_\mathrm{p} &= \frac{2 \cdot \frac{3}{\sqrt{2}} \cdot \frac{3}{\sqrt{2}} \cdot 635 \times 10^{-9} \cdot 15 \times 10^{-3}}{\pi \cdot 5 \times 10^{-3}} \\ &= 5.46 \times 10^{-6}\ . \end{aligned}$$

In theory the smaller the pinhole, the better the resultant beam quality would be. One has to take into account however that it gets increasingly difficult to focus the beam through smaller pinholes and the intensity of the beam is attenuated. A range of pinholes was therefore ordered with diameters 5 µm, 8 µm and 10 µm with the knowledge that smaller pinholes are available if needed.

In order to design the Fourier optical system a ray tracing program written in Matlab, see Appendix B, was used which gives flexibility in data analysis which commercial software does not necessarily give at a much lower price. The main optical element to perform the Fourier optical transform has been selected as an aspheric lens with a diameter of 25.2 mm and a focal length of 31.25 mm.

We also considered the possibility of obtaining the optical Fourier transform of the sample in reflection. Such a system would be more compact. The modified setup is illustrated in Fig. 4.11. For this purpose we purchased a beam splitter block (Thorlabs CM1-BS1) which is polarization insensitive.

Stellenbosch University http://scholar.sun.ac.za

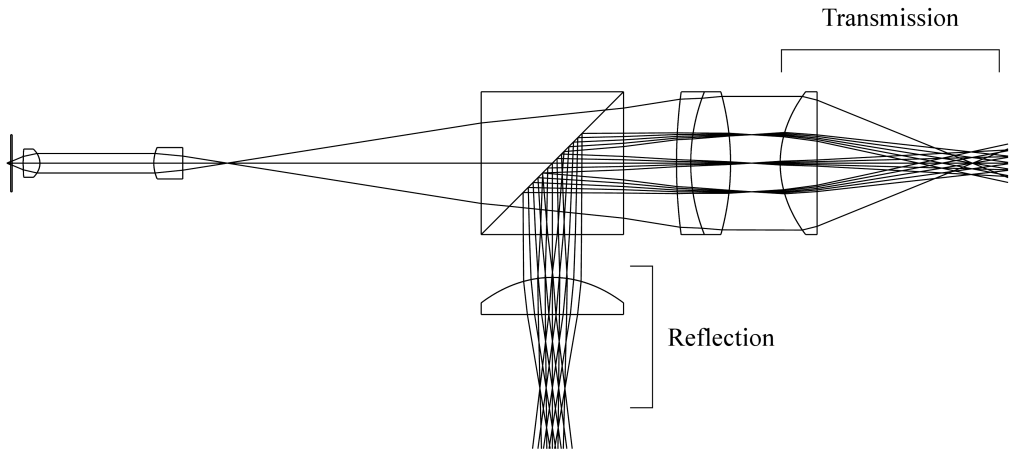

Figure 4.11: Schematic view of the optical system for observing the Fourier transform in both transmission and reflection

4.2.1 Positioning of elements

In order to determine the accurate positions of the optical elements the developed ray tracing software was used to calculate the intersection position of converging bundles of rays.

The method we used was to trace a set of parallel rays through the optical element and determine it's focal point by locating the geometrical waist where the set of rays converge as is illustrated in Fig. 4.12.

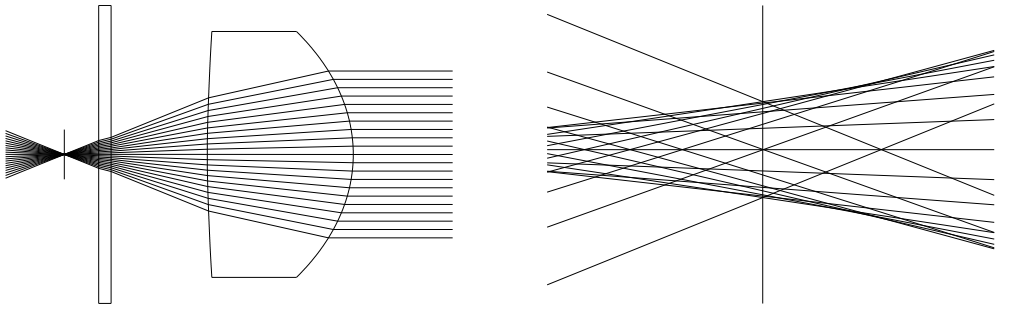

(a) Overview

(b) Magnified view of the geometrical waist

Figure 4.12: Example illustrating how the geometric waist is determined.

In Fig. 4.13 and Fig. 4.14 the focal positions calculated by means of ray tracing are indicated.

The exact positioning is not a requirement for all components except for the pinhole. In order to position the pinhole with micron precision a X-Y translation stage in combination with a z-axis mount piece is used.

Positioning the elements to the precise positions in practice would be very

Stellenbosch University http://scholar.sun.ac.za

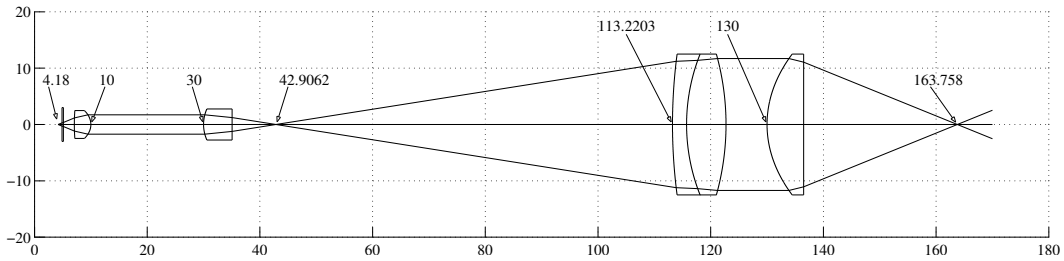

Figure 4.13: Schematic of the transmission optical setup with the positions of elements indicated.

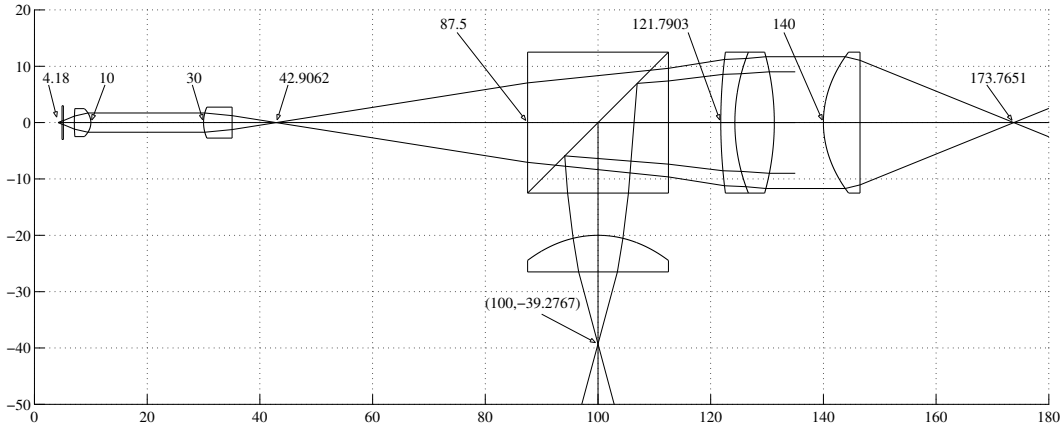

Figure 4.14: Schematic of the reflection optical setup with the positions of elements indicated.

difficult and time consuming or alternatively very expensive. Taking into account that one only needs a collimated beam at the sample space allows us to position elements such that the required function of each stage of the setup is attained. For example, the collimating lens after the laser diode is moved backwards or forward until the resultant beam is more or less collimated. The lens before the pinhole filter is then adjusted such that it focuses the light through the pinhole and we then position the doublet after the pinhole filter such that a collimated beam at the sampling space results.

Stellenbosch University http://scholar.sun.ac.za

5

The Fourier optical setup

In this Chapter the initial evaluation of both the transmission optical setup and the reflection optical setup as described in Chapter 4.2 is discussed. The problems encountered are discussed and possible solutions. A modified design where the solutions are applied is then discussed where the problems encountered with the initial design of the transmission optical setup are solved.

5.1 Light source

Assembling the light source, it was found that the 8 μm pinhole was adequate for the purpose of filtering. The expanded beam slightly overfilled the 75 mm diameter achromatic doublet, giving a beam of sufficient diameter. All experiments were performed using the source in this configuration.

5.2 Evaluation of the transmission setup

The CCD camera was placed at the Fourier plane of the transmission setup and a sample held between two glass plates in the sampling space. Two problems were identified with this arrangement:

- It was apparent that the slides holding the sample caused additional noise in the system.
- The intensity of the zero order of the pattern was many orders of magnitude greater than that of the side lobes as can be seen on Fig. 5.1.

Solving the problem of the additional system noise caused by reflections from the slides turned out to be quite simple. If the slides are a necessity in the system one possible solution would be to use anti reflection coated slides and placing

Stellenbosch University http://scholar.sun.ac.za

(a) Low intensity illumination.

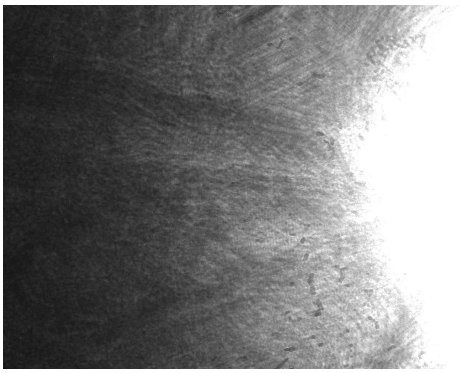

(b) High intensity illumination with the zero order peak located to the side of the CCD sensing area.

Figure 5.1: Images captured with the CCD camera using the transmission optical setup with the same fibre sample inserted into the sampling space illustrating the resultant images from different intensity illumination.

them at angles such that the zero order reflection of the source is diverted away from the sensing area. However placing the sample between slides complicates the operation of the device and the slides do not contribute to the measurement other than to hold the fibre sample in position. This can just as easily be done by hand thus the glass slides can be removed. The sample is then suspended in mid air, see Fig. 5.2.

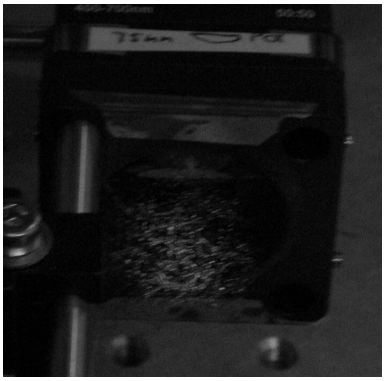

Figure 5.2: Image of the wool sample suspended in mid air.

In practice the implication is that one would have an opening in the device and the operator inserts the ends of a sample into the opening to take a measurement.

The second problem is that of the intensity of the zero order light which is many orders of magnitude larger than that of the pattern causing light to be reflected back into the system as well as saturating the CCD camera. It was clear that the zero order light had to be removed or diverted.

Stellenbosch University http://scholar.sun.ac.za

It was confirmed that removal of the zero order light would improve pattern definition in a crude experiment. In this experiment a lens with a focal length of 75 mm was used to perform the Fourier optical transform. A screen was placed at the focal plane of the lens which had a hole at the position of the zero order of the pattern. A hand held camera was used to photograph the resultant pattern which formed on the screen. The resultant image is illustrated in Fig. 5.3.

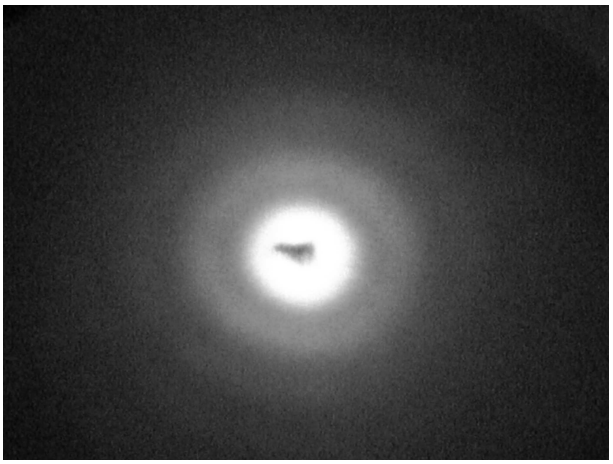

Figure 5.3: Image of the resultant Fourier optical pattern on a screen with a hole for the zero order light to pass through taken with a hand held camera.

In the resultant image the pattern is discernable with the naked eye. It was then concluded that removal of the zero order would make pattern analysis possible with the equipment available. Let's define any system which removes the zero order light from a Fourier optical system as a *zero order filter*. In Section 5.4 we will describe the application of a zero order filter to the transmission optical setup.

5.3 Evaluation of the reflection setup

The CCD camera was placed in the Fourier plane of the reflection optical setup. A sample was placed between the sampling plates and inserted into the sampling space. The resultant images for a clear sample and a sample with wool are shown in Fig. 5.4.

A lot of noise was observed and further investigation showed that the beam splitter block caused a double beam reflection effect. Looking at the observed pattern obtained with a sample, Fig. 5.4(a), it can be seen that reflected light causes serious degradation of the observable pattern. If one removes the sample two focal spots can clearly be observed, see Fig 5.4(b). We verified that the two

Stellenbosch University http://scholar.sun.ac.za

focal spots were caused by the beam splitter block by shining a collimated laser beam through it without any other optical elements present and observed a double beam emerging from its reflection. This result lead to the conclusion that the particular beam splitter block was not suited for the application.

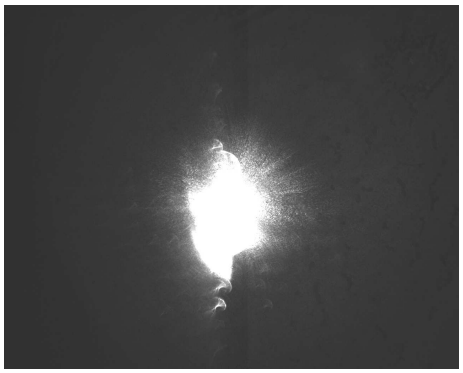

(a) A random sample present at the sampling space.

(b) No sample present at the sampling space.

Figure 5.4: Images captured with the CCD camera using the reflection optical setup, with a fibre sample present and without a fibre sample present at the sampling space.

Further investigation into the possible application of the reflection principle was put aside. Several key issues will need to be looked at critically if this possibility is to be investigated in the future.

- Light incident on wool or animal hair fibre is reflected by the surface of the fibre. It is therefore intuitive that the shape of the fibre would greatly influence the way light originating from different points on the fibre surface interferes at the focal plane.
- The intensities of reflections from the optical elements in the system must be sufficiently small such that the pattern could be easily distinguished if a pattern is formed in reflection.

5.4 The revised transmission setup

In this Section we will discuss possible zero order filters and show how we applied such a zero order filter to the transmission optical setup.

Application of a zero order filter requires removal of the zero order light before or at the CCD camera. Since the latter option is impractical we decided to remove the zero order light before the CCD. To remove the zero order light from

Stellenbosch University http://scholar.sun.ac.za

the diffracted light emerging from the sampling space we focus the light at a preliminary Fourier optical plane and block or deflect the zero order light by placing an opaque or a reflecting spot at the position of the zero order light. Let's refer to an opaque spot which blocks the zero order light as a *zero order blocker* and a reflector which can deflect the zero order light away in an off-axis direction as a *zero order reflector*.

Each option has it's own advantages. The zero order blocker is cheap and relatively simple to implement. The advantage of using a zero order reflector is that the intensity of the zero order light could be measured and compared with the source beam intensity to determine the density of the sample using the sample density model discussed in Section 4.1.

The zero order reflector was ruled out as it would have to be specially manufactured which would be costly and time consuming. Instead we opted for the zero order blocker option by placing an opaque spot in the path of the zero order light effectively removing it from the pattern observed at the CCD camera.

The size of the zero order filter is restrained by a minimum and a maximum value. If the size of the zero order filter is below the minimum then the zero order filter will no longer remove all the zero order light and some light will pass the filter to reach the CCD camera. If the size of the zero order filter is above the maximum value the filter would start to obstruct relevant data points on the pattern image observed by the CCD camera to an extent which would make it difficult or impossible to evaluate the captured pattern image.

The minimum diameter of the zero order filter is determined by a combination of factors, chief among these, the beam diameter, the focal length of the lens and the lens performance. If the lens performance is diffraction limited, the minimum value would be in the region of 10 μm as we are imaging the pinhole filter with a one to one ratio. This value only serves to give us an idea of the minimum required diameter of the zero order filter. Since such a small diameter is practically difficult to implement and the size of the central lobe for the maximum diameter fibre will be larger than the minimum zero order filter diameter, thereby satisfying the minimum requirement, we rather use the size of the central lobe for the maximum diameter fibre to determine the size of the zero order filter.

It is known that the bigger the fibre diameter the smaller the spacing between the minima will be on the resultant image pattern and therefore the smaller the central lobe of the resultant pattern. Since one is not allowed to obstruct an area bigger than the smallest possible central lobe of the image pattern, the maximum

Stellenbosch University http://scholar.sun.ac.za

size of the zero order filter is determined by the maximum fibre diameter.

The pattern image which is obtained from a random sample of wool or animal hair fibre is equivalent to the pattern observed for a disc with the same diameter as the mean diameter of the fibres. The solution to find the position of the n'th minimum for a disc inserted into the sampling space of a Fourier optical system is given by Eq. (A.64) in Appendix A.7 from which we can write,

$$x_{\mathrm{f}} = \frac{n\lambda f}{d} \tag{5.1}$$

where

x_{f} = The distance from the pattern centre to the nth minimum of the pattern
d = The diameter of the disc
f = The focal length of the optical system
n = Indicates the nth minima in the resultant pattern.

The size of the zero order filter can be calculated from the relation, given by Eq. (5.1), by choosing an arbitrary maximum fibre diameter value of 125 μm and calculating the position of the first pattern minimum as the limiting radius,

$$\begin{aligned} x_{\mathrm{f}} &= \frac{n\lambda f}{d} \\ &= \frac{1 \cdot 635 \times 10^{-9} \cdot 75 \times 10^{-3}}{125 \times 10^{-6}} \\ &= 381 \times 10^{-6} \end{aligned}$$

Thus the required maximum radius is 381 μm making the maximum diameter of the zero order blocker 762 μm. In the experiment we expected to measure fibres up to a maximum of 40 μm, thus for the purposes of the experiment we simply took a transparency and put a dot of paint on it with a fine paint brush approximately half a millimeter in diameter knowing if needed we could refine the zero order blocker.

With the use of the ray tracing software and available optics we assembled a revised optical setup which would be able to perform the filtering. The revised transmission optical setup is illustrated in Fig. 5.5. The effective focal lengths of the lenses are *(A)* 75 mm, *(B)* 100 mm, *(C)* 100 mm, *(D)* 200 mm and *(E)* 31.25 mm and the diameters are *(A)* 25 mm, *(B)* 25 mm, *(C)* 50 mm, *(D)* 50 mm and *(E)* 25.2 mm. With reference to the first or only curved surface of the lenses

Stellenbosch University http://scholar.sun.ac.za

their positions are *(A)* 0 mm, *(B)* 90 mm, *(C)* 120 mm, *(D)* 150 mm and *(E)* 180 mm and the zero order blocker is located at 75.3 mm.

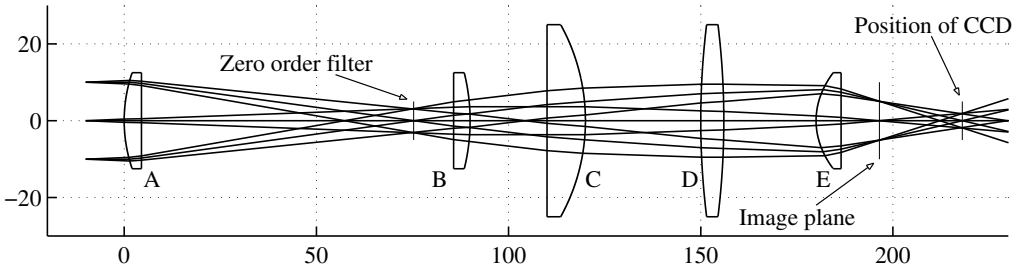

Figure 5.5: Schematic of the revised transmission setup.

The elements were positioned such that we were able to place the CCD camera in the image plane as well as at the Fourier optical plane as can be seen in Fig. 5.5.

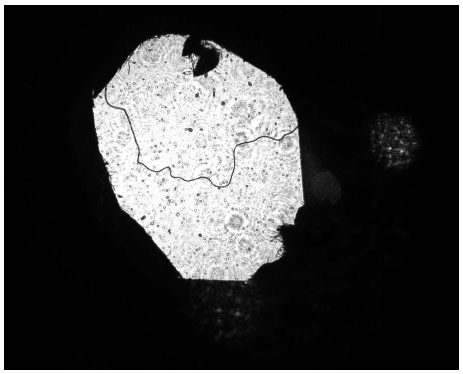

(a) Without the zero order filter in position.

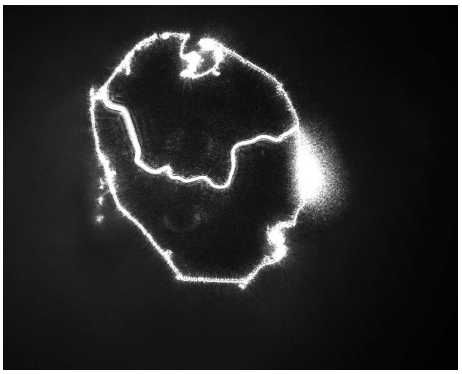

(b) With the zero order filter in position.

Figure 5.6: Images captured with the CCD camera at the image plane of the transmission optical setup using a sample consisting of a paper with a hole and an acrylic fibre placed across it illustrating the effect when the zero order filter is present or not.

The effect of the zero order filter is neatly demonstrated in Fig. 5.6 by showing an image without the filter in position, see Fig. 5.6(a), and an image with the filter in position, see Fig. 5.6(b).

Placing the CCD camera at the Fourier optical plane and inserting a random sample of wool into the sampling space with the zero order blocker in position, we obtained the resultant image as illustrated in Fig. 5.7. One can clearly see the ring structure on the captured pattern image with the naked eye.

Obtaining a Fourier optical pattern with the transmission optical setup was a success. We will refer to the resultant pattern obtained by placing a sample into the sampling space as a *fibre pattern image*. In the following chapters we will describe how we can extract the mean diameter from a fibre pattern image.

Stellenbosch University http://scholar.sun.ac.za

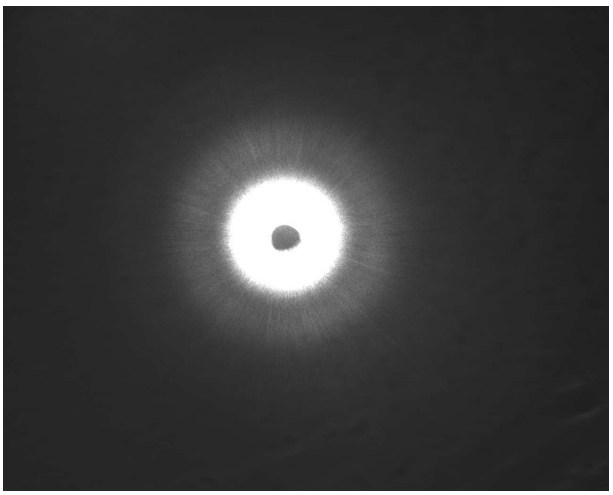

Figure 5.7: The fibre pattern image obtained for a sample of wool inserted into the sample space of the revised transmission setup with the zero order blocker in position.

Stellenbosch University http://scholar.sun.ac.za

6 Quantification of the system

In this Chapter we explain how to determine the parameters of the Fourier optical system and we discuss how to analyse the fibre pattern image obtained from said system.

6.1 System parameters

Parameterising the system refers to the process of gathering all the unknown parameters of the Fourier optical system which one needs in order to analyse a fibre pattern image.

In order to analyse a fibre pattern image, the following parameters are needed, referred to as the *system parameters*:

- The effective focal length of the Fourier optical system.
- The centre co-ordinate of the fibre pattern image.
- The static background image for an empty sample space.

In the following sections we discuss each of these in more detail.

6.1.1 Determining the effective focal length of the system

The adapted optical arrangement is a Fourier optical system with some undetermined focal length. It is possible to calculate the effective focal length of the system but this yields a theoretical result. We need an experimental method to determine the effective focal length of the system in an way which could be automated to allow the device to be calibrated automatically without the need of input from the operator.

In order to achieve this we insert a sample with a known mean diameter such as a wire, into the sampling space. It is known that the spacing between the

Stellenbosch University http://scholar.sun.ac.za

minima or the period of the minima of the resultant fibre pattern image is equal to the distance between the centre of the fibre pattern image and the first minima. Further it is known that the position of the minima is the same for a disc with a diameter equal to the mean diameter of a fibre sample. The relation between the positions of the minima for a disc is given by Eq. (A.64) from Appendix A.7.

Manipulation of Eq. (A.64) by substituting $x_f = T$ and $n = 1$ and solving for f gives,

$$f = \frac{Td}{\lambda} \tag{6.1}$$

where

$$T = \text{The period in meter of the recurring minima.}$$

Inserting a wire of known diameter into the input of the system one can determine the spacing between the minima of the resultant fibre pattern image. From this spacing one can calculate the effective focal length of the system by means of Eq. (6.1). The method used to determine the spacing of the minima of a fibre pattern image is looked at in detail in Section 6.2.

6.1.2 Determining the centre co-ordinates of the pattern

A fibre pattern image captured by the CCD camera for any input at the sampling space will always be centred about the optical axis of the system. We therefore need a method to find the centre of the fibre pattern image experimentally which could be automated.

The procedure used in our experiment is as follows. Adjust the output of the laser diode to a very low level and remove the zero order blocker. Increase the output intensity of the laser diode until a tiny spot can be seen on the CCD camera. Capture and store this image. This image, referred to as a *centre image*, is used to determine the centre co-ordinates of the Fourier optical system and any subsequent fibre pattern images, see Fig. 6.1.

When determining the centroid of an image, the non zero static background tends to shift the co-ordinate found. One can counter this effect by setting the value for all static noise below a cutoff threshold to zero. In our case the focal spot on the centre image saturates the CCD camera, thus the cutoff threshold could be chosen such that it is 80 % of the maximum intensity of the fibre pattern image.

Stellenbosch University http://scholar.sun.ac.za

The centroid of the image can then be accurately calculated as the resultant co-ordinates are not shifted by the static background noise.

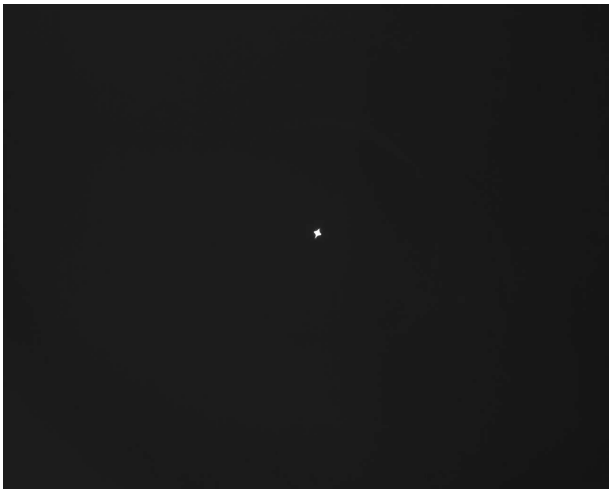

Figure 6.1: Example of a centre image.

6.1.3 Determining the static background noise

Image quality of a captured sample pattern can be improved by removal of static background noise. The light intensity is adjusted to a fixed level where one is able to capture a sample image. In theory if the zero order blocker is perfectly absorbing one should capture a uniformly dark image consisting of only static background noise. Let's refer to the image obtained when the zero order blocker is in position with an empty sample space as a *null image*. Such a null image can be captured and subtracted from the captured fibre pattern image. It has to be understood that the source light intensity must be held constant during the process of capturing the null image and the fibre pattern image.

In our experimental setup the zero order blocker was not completely absorbing since it was made by placing of a dot of blue paint on a piece of transparency. We argued that should we find the performance to be poor we could easily improve on the filter by using a more absorbing colour of paint and using a different brush to get a better spot size. We did, however, not need to modify the filter as the noise from our zero order blocker was found to be within manageable levels.

The following is a brief description of the side effects of the zero order blocker. Some of the sharply focused light on the zero order blocker scatters backwards through the system illuminating the metal plate of the pinhole filter. The Fourier plane where the CCD camera is located images the pinhole filter and the zero order blocker. The result is that we can see the pinhole filter as well as the zero

Stellenbosch University http://scholar.sun.ac.za

order blocker imaged on the CCD at the Fourier optical plane. The intensity of the null image with the pinhole filter visible due to back reflection from the zero order blocker was, however, low and static. The image quality of the fibre pattern images obtained was improved by subtracting the null image as is illustrated in Fig. 6.2. It has to be noted that the light scattering backwards through the system will be attenuated by the sample and will therefore not be exactly the same as the null image. The difference in intensity between the null image and the pinhole filter due to attenuation by the sample would cause a step to be observed when analysing the pattern. No such step was observed and we therefore conclude that the attenuation due to the sample is negligibly small.

The scattered light from the zero order filter will illuminate the sample causing it to scatter light forward through the system and leading to additional unwanted light reaching the CCD camera. This forward scattered light will have a low intensity and an even distribution and its effect will therefore be negligible as long as its intensity is low in comparison with that of the pattern.

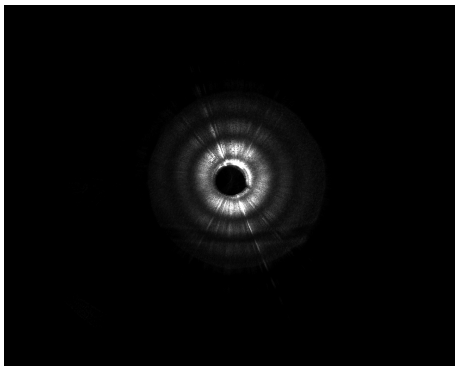

(a) Image before subtracting the constant background image.

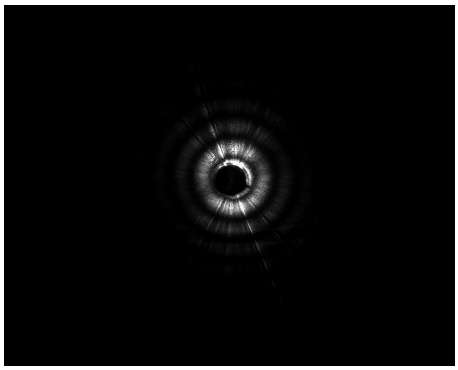

(b) Image after subtracting the constant background image.

Figure 6.2: Image of the resultant Fourier optical pattern for a 60 μm wire in a loop shape inserted in the sampling space of the transmission optical setup. The images shows the effect of removal of the constant noise background image.

6.1.4 Sampling procedure

From the preceeding discussion, the steps that must be taken before measuring and analysing samples for the transmission experimental setup are as follows:

- Position the optical components approximately as indicated in Fig. 5.5. It does not need to be very precise as the system will be parameterized exactly in the next steps.

Stellenbosch University http://scholar.sun.ac.za

- Capture and store the centre image and calculate the centre of any potential fibre pattern image for the current position of the CCD camera.
- Set the output power of the laser diode to a level which allows us to capture Fourier optical patterns for a sample inserted in the sampling space.
- Capture and store the null image.
- Determine the focal length of the optical system.

If these parameters have been determined we are ready to analyse a fibre pattern image in order to determine the mean diameter of a sample.

6.2 Sample analysis

Sample analysis describes the steps which are taken to determine the spacing of the minima in a fibre pattern image. These are then used to calculate either the effective focal length of the Fourier optical system or the mean diameter of the sample if the system parameters are known.

The method used to determine the focal length of the system differs from the method used to determine the mean diameter of a fibre sample due to pattern quality, more specifically the number of clearly visible minima in the fibre pattern image. We will first look at the basic processing which is common to the determining of the systems effective focal length and the mean diameter of a sample. We then look at the specific processing required to determine the spacing of the minima for each of these individually.

6.2.1 Basic pattern processing

In order to simplify the procedure to analyse a fibre pattern image the following steps are performed[1].

- Load the fibre pattern image in a matrix referred to as a *pattern matrix*.
- Transform the pattern matrix into a vector referred to as a *pattern vector*.
- Improve the pattern vector through fixed scaling and filtering.

[1]It has to be noted that we are only interested in the position of features in the subsequent graphs and therefore the scale of the y-axis is not important.

Stellenbosch University http://scholar.sun.ac.za

To transform the pattern matrix into a pattern vector the radius between each cell co-ordinate and the centre of the pattern matrix is calculated. The radius is used as the index in the pattern vector to store the mean value of all cells within the pattern matrix located at an equal radius. To do this the number of values added to each index in the pattern vector is counted and stored in a counter array. When the totals for the pattern vector have been added up the pattern vector is divided by the number of values as indicated by the counter array for each index. Fig. 6.3 shows an example of the resultant pattern vector extracted from the fibre pattern image in Fig. 6.2(b).

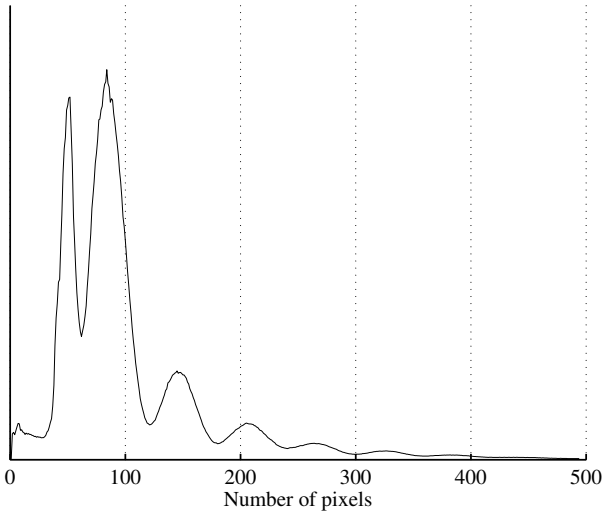

Figure 6.3: Graph of the pattern vector for the fibre pattern image of Fig. 6.2(b) .

Since we are looking at intensity what we see is the result from $|E|^2$. Each fibre section causes a pattern resembling a $\text{sinc}^2 x$ function which is perpendicular to the angle of the fibre section at the sampling space. If one has many fibres then the sum of all these will give a pattern resembling a circularly symmetric $\text{sinc}^2 x$ function. Noise or unwanted signal is caused by the fibre crossings and will cause the pattern to lose definition. Since a $\text{sinc}^2 x$ function is by definition $\frac{\sin^2 x}{x^2}$ the clarity of the pattern can be improved by multiplying the pattern vector by x^2, referred to as the *scaled pattern vector*. Fig. 6.4 shows an example of the scaled pattern vector for Fig. 6.3.

Up to this point the procedure to determine the minima spacing of the calibration wire of known thickness and a fibre sample is the same. In the following sections we will look separately at how one can further analyse the scaled pattern vector for a fibre sample and a wire of known thickness to determine the spacing of the minima.

Stellenbosch University http://scholar.sun.ac.za

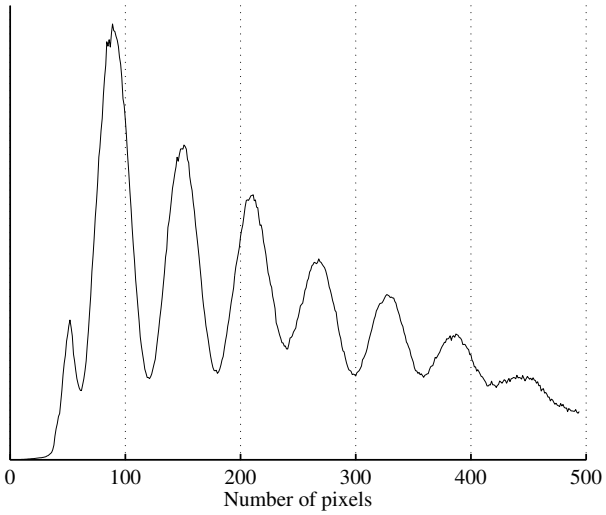

Figure 6.4: Graph of the scaled pattern vector from the pattern vector in Fig. 6.3.

6.2.1.1 Pattern analysis for a wire of known diameter

In order to determine the spacing between the minima of the scaled pattern vector which results when one inserts a wire of known diameter into the sampling space one must first differentiate the scaled pattern vector. Differentiating simplifies determining the dominant spectral component in the scaled pattern vector as the process of differentiating acts to suppress the slow varying spectral components and to magnify faster varying spectral components. Fig. 6.5 illustrates the differentiated scaled pattern vector of the pattern vector illustrated in Fig. 6.4.

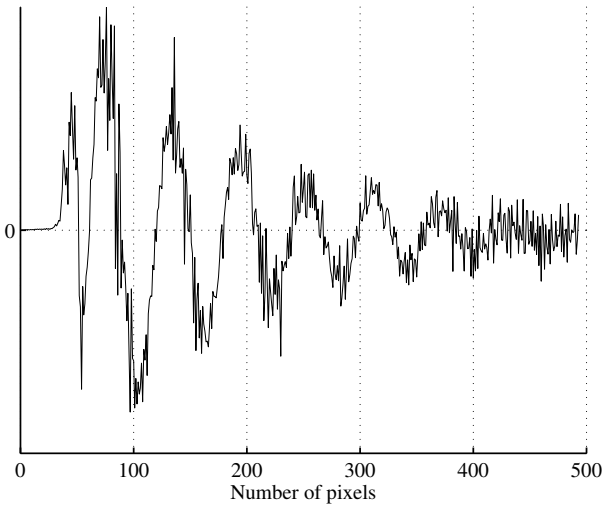

Figure 6.5: Graph of the differentiated scaled pattern vector illustrated in Fig. 6.4.

The signal quality of the differentiated scaled pattern vector for a wire of known thickness is good enough such that the Fourier transform could simply

Stellenbosch University http://scholar.sun.ac.za

be used to determine its dominant spectral component. This can be accurately achieved by zero padding the differentiated scaled pattern vector to approximately ten times it's original length in order for the Fourier transform to be interpolated. Fig. 6.6 shows the Fourier transform of the padded differentiated scaled pattern vector for the vector in Fig. 6.5.

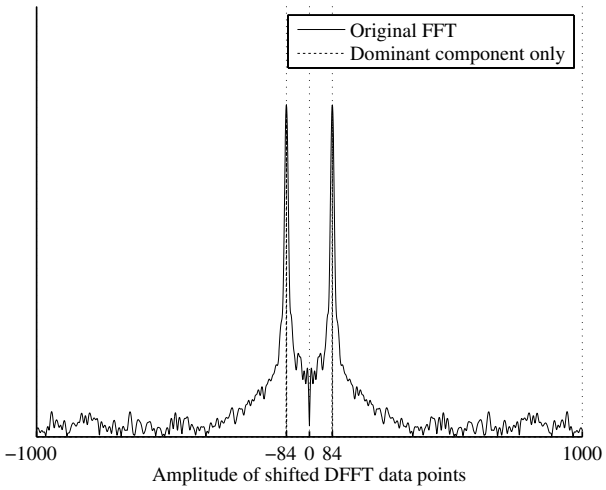

Figure 6.6: Discrete padded Fourier transform of the differentiated scaled pattern vector of Fig. 6.5.

The dominant frequency component can easily be determined from a graph such as the one in Fig. 6.6 by finding the index of the maximum valued element in the vector. Having the index of the dominant spectral component X_p it is known from discrete Fourier theory that the period of the dominant spectral component can be found by,

$$T_p = \frac{N}{X_p} \tag{6.2}$$

where

T_p = The period of the dominant spectral component in unit pixel.
X_p = The dominant spectral component.
N = The number of elements in the padded shifted DFT.

The pattern matrix results in a vector with indices in pixel units. The pixel units can be converted to meter by,

$$d_a = w_{pix} d_{pix} \tag{6.3}$$

Stellenbosch University http://scholar.sun.ac.za

where

$$\begin{aligned} d_{\mathrm{a}} &= \text{Distance in meter} \\ d_{\mathrm{pix}} &= \text{Distance in unit pixels} \\ w_{\mathrm{pix}} &= \text{The width of the pixels of the CCD camera.} \end{aligned}$$

Eq. (6.3) can now be used by noting that $d_{\mathrm{pix}} = T_{\mathrm{p}}$ and the distance found is the recurring period of the minima in meter, thus $T = d_{\mathrm{a}}$. Now substituting Eq. (6.2) into Eq. (6.3) and solving for T one finds

$$T = \frac{N w_{\mathrm{pix}}}{X_{\mathrm{p}}}. \tag{6.4}$$

The period of recurring minima found with Eq. (6.4) could then be substituted into Eq. (6.1) to determine an expression for the effective focal length of the Fourier optical system as,

$$f = \frac{N w_{\mathrm{pix}} d}{\lambda X_{\mathrm{p}}}. \tag{6.5}$$

With Eq. (6.5) one is able to calculate the effective focal length of a Fourier optical system from the resultant pattern matrix of a wire of known diameter. A computer program was developed which is capable of doing the image pattern analysis in order to determine the effective focal length of the system, see the code listing C.7 in Appendix C.3.

6.2.1.2 Pattern analysis of a fibre sample

The pattern matrix obtained when inserting a fibre sample into the sampling space of the system will not be defined as clearly as that of a wire of known thickness. If wool and animal hair fibres with small diameters are measured there will generally be only one minimum visible, due to the inverse relationship between fibre diameter and Fourier optical pattern size. As such one cannot reliably use a Fourier transform to determine its position as had been done for a wire of known diameter in Section 6.2.1.1. Instead we developed a method which differs from the method used for a wire of known diameter, which could reliably extract the position of the first minimum from the resultant sample pattern of a fibre sample.

In order to determine the location of the first minimum of the scaled pattern vector for a random fibre sample a differentiation technique can be used. In a

Stellenbosch University http://scholar.sun.ac.za

Cartesian co-ordinate system it is known that, if a function is differentiated, the positions of the maxima and minima are located at the positions on the x-axis where the differentiated function crosses the x-axis, referred to as the *zero crossings*. To determine if a zero crossing is a maximum or a minimum we look at the gradient of the differentiated function at that point. If the differentiated function has a positive gradient we know it is a minimum and if it has a negative gradient we know it is a maximum.

The scaled pattern vector obtained from the pattern matrix is not smooth. If such a signal is differentiated the differentiation acts to suppress slow spectral components and to amplify fast spectral components which could result in erroneous zero crossings. Thus the scaled sample vector should be as smooth as possible such that the differentiated signal could be processed to locate the first minimum of the scaled pattern vector. As such a filter can be applied. Since certain filters can introduce additional minima into a signal which could complicate determining the spacing between them, a type of filter is chosen which does not have the property of introducing unwanted minima into the signal. We chose to use a spectral sinc filter. A spectral sinc filter is simple to implement as it translates to a convolution of the temporal signal with a rect function.

The equation to determine the width of a rect function in the temporal domain, which translates to a sinc function in the spectral domain, is given in Appendix A.8 as,

$$T_{\mathrm{f}} = \frac{N \operatorname{sinc}^{-1}(k_{\mathrm{f}})}{\pi X_{\mathrm{p}}} \tag{6.6}$$

where

$$\begin{aligned} T_{\mathrm{f}} &= \text{The period of the minima of a spectral sinc filter} \\ k_{\mathrm{f}} &= \text{The attenuation value at the attenuation frequency} \\ X_{\mathrm{p}} &= \text{The attenuation frequency} \\ N &= \text{The number of elements in the vector.} \end{aligned}$$

The width of a rect function to be convolved with the signal in the temporal domain is equal to the period of the minima of the sinc function in the spectral domain. Thus the equation given by, Eq. (6.6), can be used to determine the width of a rect function which if convolved with the scaled pattern vector is equivalent to application of a sinc filter in the spectral domain. The maximum fibre diameter would result in a pattern vector with the shortest period due to the inverse

Stellenbosch University http://scholar.sun.ac.za

relation between sampling and Fourier optical space. We would like to relate the maximum fibre diameter to the width of an applicable sinc filter in order to be sure we do not filter our scaled pattern vector such that we are unable to determine the location of its first minimum in the case of a fibre sample of maximum diameter.

For any given fibre sample, the spacing of the minima for the resultant pattern matrix can be calculated if the position of the first minimum is known, thus one can rewrite Eq. (5.1) with T as the subject and $n = 1$ to find

$$T = \frac{\lambda f}{d}. \tag{6.7}$$

Eq. (6.7) can be used to calculate the period of the dominant spectral component for a disc with known diameter inserted into the sampling space and one can calculate the period of the dominant spectral component if the data is in discrete vector format using Eq. (6.4). Thus setting Eq. (6.7) equal to Eq. (6.4) and solving for the dominant frequency component in discrete space X_p one finds

$$X_\mathrm{p} = \frac{Nd}{w_\mathrm{pix}\lambda f}. \tag{6.8}$$

Now substituting Eq. (6.8) into Eq. (6.6) and solving for the period of the zero crossings of the spectral sinc filter T_f one finds

$$T_\mathrm{f} = \frac{\mathrm{sinc}^{-1}(k_\mathrm{f})\lambda f}{w_\mathrm{pix}\pi d}. \tag{6.9}$$

The width of the block function with which one must convolve the scaled sample vector is equal to T_f, thus one could easily calculate the required width of a spectral sinc filter by defining its attenuation properties using Eq. (6.9).

We define *our primary* filter such that it must attenuate the dominant spectral component of the scaled sample vector by a factor of no more than 0.5 for the maximum fibre diameter. Substituting the solution for $\mathrm{sinc}^{-1}(0.5)$ (see Eq. (A.75) in Appendix A.8) into Eq. (6.9) one finds

$$w_\mathrm{fp} = \frac{0.6\lambda f}{w_\mathrm{pix}d} \tag{6.10}$$

Stellenbosch University http://scholar.sun.ac.za

where

$$w_{\text{fp}} = \text{The width of the required primary rect function in pixel units.}$$

After application of the primary filter to the scaled pattern vector the we found that the resultant vector still exhibits noise when differentiated, see Fig. 6.7(a). Thus we apply a spectrally wider sinc filter such that it does not affect the slow varying spectral components but filters out faster varying ones. We choose this filter such that it attenuates the dominant spectral component by a factor of no more than 0.9. Substituting the solution to $\text{sinc}^{-1}(0.9)$ (see Eq. (A.75) in Appendix A.8) into Eq. (6.9) one finds

$$w_{\text{fs}} = \frac{0.25\lambda f}{w_{\text{pix}} d} \tag{6.11}$$

where

$$w_{\text{fs}} = \text{The width of the required secondary rect function in pixel units.}$$

We will refer to this filter as the *secondary filter*. We apply this filter twice with a resulting attenuation of the dominant spectral component of no more than 0.81. The result is effectively a sinc^2 filter. An example of the resultant differentiated signal is illustrated in Fig. 6.7(b).

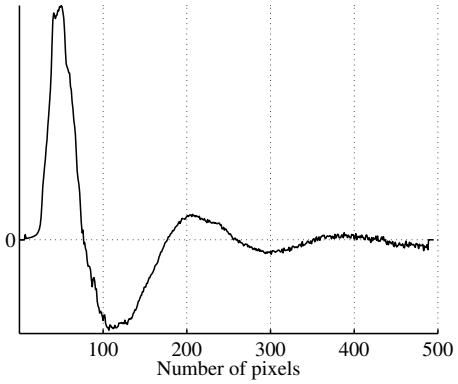

(a) Application of the primary filter.

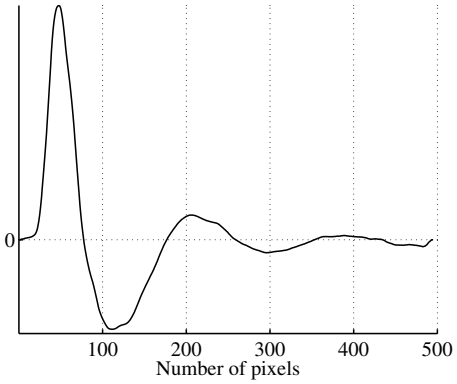

(b) Application of the primary and secondary filters.

Figure 6.7: Example of a differentiated scaled pattern vector for different stages of filtering.

The final filtered differentiated scaled pattern vector can then be used to determine the position of the first minimum of the pattern vector in pixel units. This gives us the spacing of the pattern minima which is inversely proportional to the

Stellenbosch University http://scholar.sun.ac.za

mean diameter of the fibre sample.

In the application of the program we have found the zero order blocker would sometimes introduce false minima into the differentiated signal which must be ignored. For this reason a mask was used which allows us to ignore the data points near the origin of the pattern vector. The size of the mask is determined by the size of the zero order blocker in the pattern vector which in turn is determined by the biggest mean diameter fibre sample. From this one can determine the location of the first minimum in order to know the maximum size of the mask. For a disc of equivalent diameter, as given by Eq. (A.65) in Appendix A.7, the period of the minima is equal to the location of the first minimum, thus one can use Eq. (6.7) to determine the position of the first minimum. One then has to scale the value to pixel units using Eq. (6.3) and by setting $W_{\text{mask}} = T$ in Eq. (6.7), $W_{\text{mask}} = d_{\text{a}}$ in Eq. (6.3) and manipulating one finds

$$W_{\text{mask}} = \frac{\lambda f}{d_{\text{a}} w_{\text{pix}}}. \tag{6.12}$$

The resultant equation, given by Eq. (6.12), is used to calculate width of the mask which is used to ignore possible erroneous data points in the scaled pattern vector.

After the filters and the mask is applied to the scaled pattern vector we are able to determine location of the first minimum by differentiating and finding the first zero crossing with a positive gradient. The method we used to do this linearly interpolates the data point below the axis and above the axis such that the zero crossing position is very accurately determined. The position of the first minimum is equal to the period of the minima of the scaled pattern vector from which one can derive the mean diameter of a sample. One can now derive an equation relating the period of the minima in the scaled pattern vector to the mean fibre diameter of the sample. The equation for a Fourier optical system relating a disc as input to the pattern spacing between its minima is given by Eq. (A.65) (see Appendix A.8). The determined period of the minima must be converted from the scaled pattern vector to meters using Eq. (6.3) before one can substitute it into Eq. (A.65). Thus setting $d_{\text{a}} = T$ and $d_{\text{pix}} = T_{\text{p}}$ in Eq. (6.3) and substituting the result into Eq. (A.65) and solving for d one finds

$$d = \frac{\lambda f}{T_{\text{p}} w_{\text{pix}}}. \tag{6.13}$$

A program was written and used to determine the spacing between the min-

Stellenbosch University http://scholar.sun.ac.za

ima of the pattern matrix, see the code listing C.6 in Appendix C.3. Having found the spacing between the minima using the program one can insert it into Eq. (6.13) to calculate the mean diameter of the fibre. Fig. 6.8 shows an example of the first minimum found for a random wool sample.

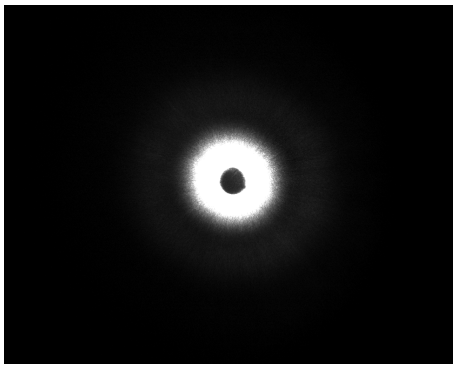

(a) Image with the static background removed.

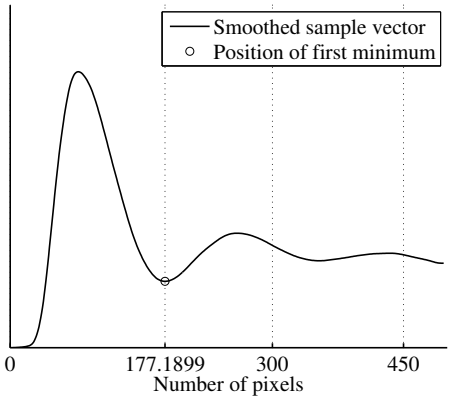

(b) Smoothed differentiated pattern vector with the first minimum as detected indicated.

Figure 6.8: Processing of a wool sample to detect the first minimum.

The interpolation techniques used in determining the effective focal length and the position of zero crossings and consequently mean fibre diameter is such that the system is limited only by sample noise and possibly aberrations. If aberrations introduces a non-linear effect on measurements one could determine a calibration curve for a range of sample diameters to solve the problem.

Stellenbosch University http://scholar.sun.ac.za

7

Sample measurement experiment

In this Chapter we will determine the system parameters for the Fourier optical system as used in our experimental setup. We will then discuss the experiment done which allowed us to compare measurements made with our system to those made by an independent laboratory.

7.1 Calculation of actual system parameters

In the previous chapters we have developed the theory which allows us to parameterise our system. This requires determining the system parameters as described in Section 6.1 and calculating the limits of the filters and the mask which will be used to analyse a pattern vector from a fibre sample as described in Section 6.2.1.2.

7.1.1 System parameters

The system parameters consist of the effective focal length of the system, the co-ordinates of the optical centre of the system on the CCD camera and the static background for each sample. Before a pattern image can be analysed the optical centre of the image must be determined and the optical system adjusted such that a pattern image can be obtained. A single centre image which is applicable to all pattern images taken in the experiment was stored and a null image was stored for each sample. The optical centre of the system is determined from the centre image, thus the centre co-ordinates are effectively contained within the centre image. Each pattern image is improved by subtracting the null image relevant to that sample from the pattern image. Thus having a centre image and a null image for each pattern image one only needs to determine the effective focal length of the system in order to have a parameterised system. Of course the filter parameters needs to be calculated, but this is done only once for the device and is fixed.

Stellenbosch University http://scholar.sun.ac.za

A copper wire was used with a diameter of 60 µm bent into a loop shape to determine the effective focal length of the system. The focal length was found by processing the resultant pattern image using the developed code (see listing C.7 in Appendix C.3) to determine the dominant frequency component X_p and substituting the value found into Eq. (6.5). We found the dominant frequency component located at $X_p = 82.795$ and calculated the focal length as,

$$\begin{aligned} f &= \frac{N w_p d}{\lambda X_p} \\ &= \frac{5000 \cdot 6.7 \times 10^{-6} \cdot 60 \times 10^{-6}}{635 \times 10^{-9} \cdot 82.795} \\ &= 38.2 \times 10^{-3}. \end{aligned}$$

The effective focal length of the system was found to be 38.2 mm.

7.1.2 Filter parameters

The analysis of the resultant pattern vector obtained for a fibre sample needs to be filtered as explained in Section 6.2.1.2. It is known that the width of the filter is determined by the biggest diameter fibre sample which one would like to be able to measure. We chose the maximum diameter to be 125 µm.

Inserting the chosen maximum into Eq. (6.10) to determine the width of a rect function for the primary filter which must be convolved with the scaled sample vector one finds

$$\begin{aligned} w_{fp} &= \frac{0.6 \lambda f}{w_p d} \\ &= \frac{0.6 \cdot 635 \times 10^{-9} \cdot 38.2 \times 10^{-3}}{6.7 \times 10^{-6} \cdot 125 \times 10^{-6}} \\ &= 17 \end{aligned}$$

In the same way the width of a rect function for our secondary filter is determined as

$$\begin{aligned} w_{fs} &= \frac{0.25 \lambda f}{w_p d} \\ &= \frac{0.25 \cdot 635 \times 10^{-9} \cdot 38.2 \times 10^{-3}}{6.7 \times 10^{-6} \cdot 125 \times 10^{-6}} \\ &= 7 \end{aligned}$$

Stellenbosch University http://scholar.sun.ac.za

Thus we know we must not exceed a width of 17 pixel units for the primary filter and 7 pixel units for the secondary filter if they are to have the correct attenuation properties.

Thus we chose,

$$\begin{aligned} w_{\text{fp}} &= 15 \\ w_{\text{fs}} &= 7 \end{aligned}$$

In order to be sure we do not get incorrect results due to erroneous minima introduced into the scaled pattern vector by the zero order filter we ignore minima found according to a mask which starts at the origin and extends to a width limited again by the thickest diameter fibre sample we would like to be able to measure.

We insert a thickest diameter value of 125 µm into Eq. (6.12) to find,

$$\begin{aligned} W_{\text{mask}} &= \frac{\lambda f}{d_{\text{a}} w_{\text{p}}} \\ &= \frac{635 \times 10^{-9} \cdot 38.2312 \times 10^{-3}}{125 \times 10^{-6} \cdot 6.7 \times 10^{-6}} \\ &= 29 \end{aligned}$$

The width of the mask is chosen as

$$W_{\text{mask}} = 29$$

All the required parameters are now known for the system and we are able to perform our experiment. During the setup of the experiment we found that apart from the complete source as illustrated in Fig. 4.10, the position of the elements are not sensitive to exact placement to such an extent that we could move elements 1 mm backwards or forwards as long as we maintained the CCD camera at the focal plane and the zero order blocker in position to remove the zero order light. Of course if the position of the elements change one must determine the effective focal length of the system again.

7.2 Experiment

At this point we have established a method which allows us to analyse a sample without the need of hand selecting values, thus we are able to automatically anal-

Stellenbosch University http://scholar.sun.ac.za

yse a set of samples. We only need to capture the relevant images. We received a sample set of wools from Cape Mohair and Wool which had been analysed with the OFDA 2000.

The samples had already been prepared to be analysed by the OFDA 2000, as such the wool is clean. The minimum of sample preparation was done during the capturing of the images. Each sample was simply, with its ends spread out slightly, inserted into the sample space of the transmission optical setup. It has to be noted that this procedure only takes a small part of the entire sample into consideration. The resultant images were saved in files corresponding to the sample number as indicated on the measurement sheets from the OFDA 2000 system.

Having determined the parameters of the system, the program developed was used to do the sample analysis, see Appendix C.2. The resultant data is illustrated in Fig. 7.1.

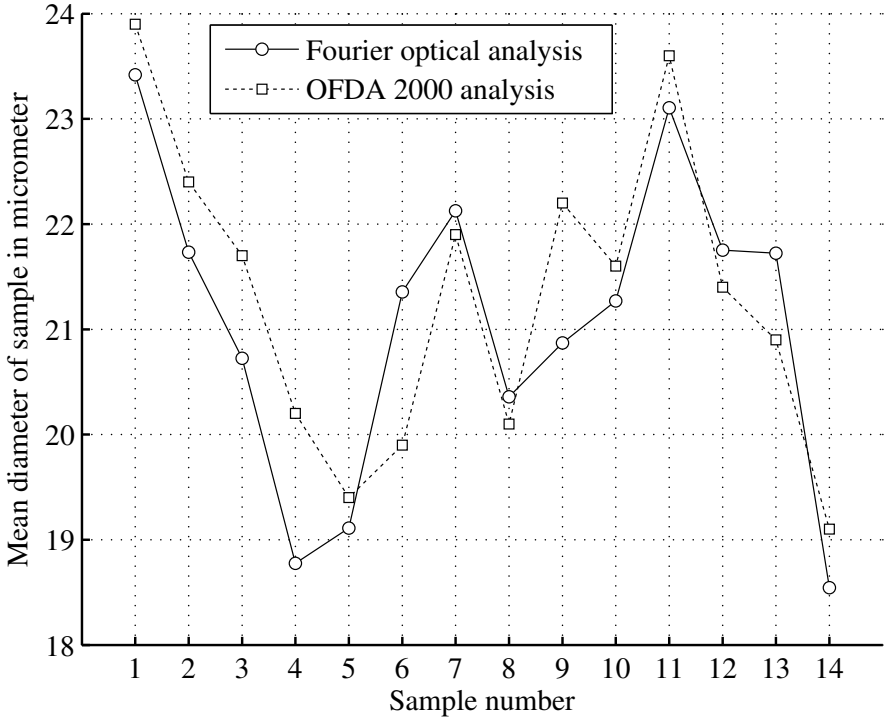

Figure 7.1: Comparison of OFDA 2000 measurements to the measurements of the transmission Fourier optical setup.

The acquired results are surprisingly good for the comparatively simple experimental setup taking into consideration that the sampling technique used only takes a small section of the entire sample into consideration. Fig. 7.1 clearly shows that there is a definite very close correlation between the data sets with an average absolute difference of 0.69 μm for the particular sample set.

Stellenbosch University http://scholar.sun.ac.za

8

Conclusion

A functioning system for measuring fibre diameters of wool samples which utilises the principle of Fourier optics was developed and tested during this thesis. The system was assembled in the form of an experimental table top setup. The resultant data obtained from a comparison with wool samples measured with one of the current standard techniques, the OFDA 2000 system, shows very close correlation with the developed system. The developed system works in principle and shows good potential for further development. The advantages of the device is its ability to rapidly make measurements, its relative compactness and robustness.

It is clear from the literature study that all instruments to be used in the process of wool certification must comply to certain stringent standards. The viability of the present instrument can, therefore, only be evaluated by collaborating with a faction of the IWTO. One particular requirement to be able to compete in the laboratory setting, is the ability of a device to determine not only the mean but also the variation of the mean. Since we now understand the relationship between sample density and measurability and we know that there exists a relationship between clarity of definition of a pattern and the variation of the mean, see Edmunds [77], further research in this avenue could be done. If the device could be developed to successfully determine the variation then combined with the rapid measurement rate such a device would be very competitive in the laboratory market segment.

It could also be possible to fill a niche market segment. At present wool samples from specific areas on sheep are sent to be analysed by a certified laboratory for shearing purposes by the farmers before the wool is shorn. A hand held device performing well enough to replace this step by direct measurement on the farm would potentially have a big market. It is here that the present instrument could certainly find its application.

Stellenbosch University http://scholar.sun.ac.za

Appendices

Stellenbosch University http://scholar.sun.ac.za

A

Mathematical derivations

A.1 The Helmholtz equation

The Helmhotz equation can be derived with the functions as defined in Section 2.1.5.

Given

$$u_c(P,t) = U_c(P)\, e^{-j2\pi\nu t} \tag{A.1}$$

where

$$U_c(P) = U(P)\, e^{-j\phi(P)}. \tag{A.2}$$

Now consider the wave equation

$$\nabla^2 u - \frac{1}{c^2}\frac{\partial^2 u}{\partial t^2} = 0 \tag{A.3}$$

where ∇^2 is the Laplacian operator

$$\nabla^2 = \frac{\partial^2}{\partial x^2} + \frac{\partial^2}{\partial y^2} + \frac{\partial^2}{\partial z^2}. \tag{A.4}$$

Stellenbosch University http://scholar.sun.ac.za

Substituting Eq. (A.1) into Eq. (A.3) one finds

$$\nabla^2 U_c(P)\, e^{-j2\pi vt} = \frac{1}{c^2}\frac{\partial^2}{\partial t^2} U_c(P)\, e^{-j2\pi vt} \tag{A.5}$$

$$e^{-j2\pi vt}\nabla^2 U_c(P) = \frac{-j2\pi v}{c^2} U_c(P)\, \frac{\partial}{\partial t} e^{-j2\pi vt} \tag{A.6}$$

$$e^{-j2\pi vt}\nabla^2 U_c(P) = -\left(\frac{2\pi v}{c}\right)^2 U_c(P)\, e^{-j2\pi vt} \tag{A.7}$$

$$\left(\nabla^2 + \left(\frac{2\pi v}{c}\right)^2\right) U_c(P) = 0 \tag{A.8}$$

now given

$$k = \frac{2\pi v}{c} = \frac{2\pi}{\lambda} \tag{A.9}$$

and substituting Eq. (A.9) into Eq. (A.8) one finds

$$\left(\nabla^2 + k^2\right) U_c(P) = 0 \tag{A.10}$$

which is known as the Helmholtz equation.

A.2 Solution to the diffraction problem using an in-phase Green's function

The in-phase solution to the Rayleigh-Sommerfeld integral as defined in Section 2.5.1.2 can be derived in a similiar fashion to the out of phase solution by choosing an in-phase Green's function. Given

$$U_c(P_0) = \frac{1}{4\pi} \iint_S \left(\frac{\partial U_c}{\partial n} G_c - U_c \frac{\partial G_c}{\partial n}\right) ds \tag{A.11}$$

and taking the Green's function as

$$G_{c\phi+} = \frac{\exp(jkr_{01})}{r_{01}} + \frac{\exp(jk\widetilde{r}_{01})}{\widetilde{r}_{01}}. \tag{A.12}$$

Stellenbosch University http://scholar.sun.ac.za

The derivative of $G_{c\phi+}$ is

$$\frac{\partial G_{c\phi+}}{\partial n} = \cos(\bar{\mathbf{n}}, \bar{\mathbf{r}}_{01}) \left(jk - \frac{1}{r_{01}} \right) \frac{\exp(jkr_{01})}{r_{01}} + \cos(\bar{\mathbf{n}}, \widetilde{\bar{\mathbf{r}}}_{01}) \left(jk - \frac{1}{\widetilde{r}_{01}} \right) \frac{\exp(jk\widetilde{r}_{01})}{\widetilde{r}_{01}}. \quad \text{(A.13)}$$

Now taking the following into account

$$r_{01} = \widetilde{r}_{01} \quad \text{(A.14)}$$

$$\cos(\bar{\mathbf{n}}, \bar{\mathbf{r}}_{01}) = -\cos(\bar{\mathbf{n}}, \widetilde{\bar{\mathbf{r}}}_{01}) \quad \text{(A.15)}$$

by substituting Eq. (A.14) and Eq. (A.15) into Eq. (A.12) and Eq. (A.13) one finds

$$G_{c\phi+} = \frac{2\exp(jkr_{01})}{r_{01}} \quad \text{(A.16)}$$

$$\frac{\partial G_{c\phi+}}{\partial n} = 0. \quad \text{(A.17)}$$

Substituting Eq. (A.16) and Eq. (A.17) into Eq. (A.11) and taking the boundary conditions into account one finds

$$U_c(P_0) = \frac{1}{4\pi} \iint_{\Sigma} \frac{2\exp(jkr_{01})}{r_{01}} \frac{\partial U_c}{\partial n} ds. \quad \text{(A.18)}$$

If one assumes the aperture is illuminated by a single spherical wave then

$$U_c(P_1) = \frac{A\exp(jkr_{21})}{r_{21}} \quad \text{(A.19)}$$

Now taking the derivative of Eq. (A.19) one finds

$$\frac{\partial U_c}{\partial n} = A\cos(\bar{\mathbf{n}}, \bar{\mathbf{r}}_{21}) \left(jk - \frac{1}{r_{21}} \right) \frac{\exp(jkr_{21})}{r_{21}}. \quad \text{(A.20)}$$

Given that $k \gg \frac{1}{r_{21}}$ one can simplify Eq. (A.20) to find

$$\frac{\partial U_c}{\partial n} \cong jkA\cos(\bar{\mathbf{n}}, \bar{\mathbf{r}}_{21}) \frac{\exp(jkr_{21})}{r_{21}}. \quad \text{(A.21)}$$

Stellenbosch University http://scholar.sun.ac.za

Substituting Eq. (A.21) into Eq. (A.18) one finds

$$\begin{aligned} U_c(P_0) &= -\frac{A}{j\lambda}\iint_{\Sigma}\frac{\exp(jkr_{01})}{r_{01}}\frac{\exp(jkr_{21})}{r_{21}}\cos(\bar{\mathbf{n}},\bar{\mathbf{r}}_{21})ds \\ &= -\frac{A}{j\lambda}\iint_{\Sigma}\frac{\exp(jk\left[r_{01}+r_{21}\right])}{r_{01}r_{21}}\cos(\bar{\mathbf{n}},\bar{\mathbf{r}}_{21})ds \end{aligned} \tag{A.22}$$

which is the in-phase solution of the Rayleigh-Sommerfeld diffraction theorem.

A.3 The thin lens as a Fourier optical system

Consider Fig. A.1. Given a thin lens and a hypothetical input function at the y plane as indicated. It is known that a plane wave traveling through a thin lens will be focused at a point (f,d). If one considers that the transformation of the thin lens is such as to produce a perfectly spherical wave front which converges to the point (f,d) then the inverse must be true, that a point source located at a point (f,d) would generate perfectly spherical wave fronts which would be transformed by a thin lens into perfect planar waves.

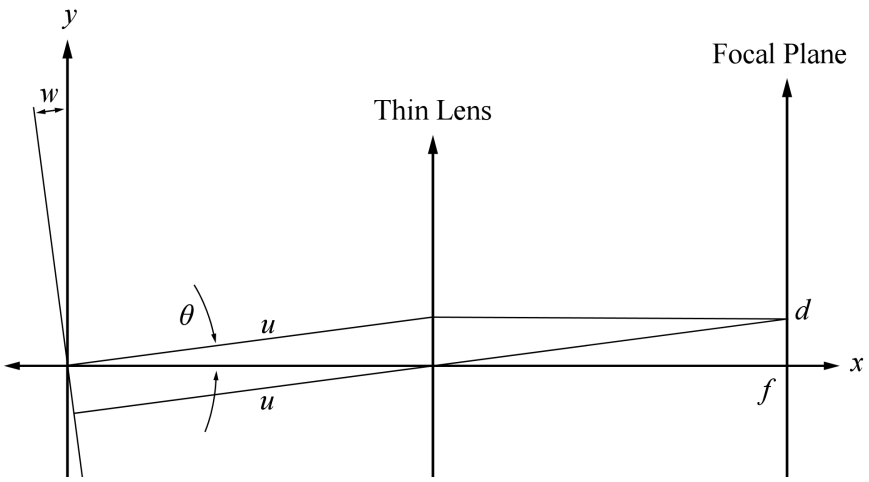

Figure A.1: Geometry of a thin lens optical system

Again working in the first order approximation, one has

$$\begin{aligned} \sin\theta &\cong \theta \\ \cos\theta &\cong 1 \\ \tan\theta &\cong \theta \\ \tan^{-1}\theta &\cong \theta. \end{aligned} \tag{A.23}$$

Stellenbosch University http://scholar.sun.ac.za

From Fig. A.1 with application of Eq. (A.23) one has

$$\tan u \cong u \cong \theta. \tag{A.24}$$

Now consider w as the difference in distance a ray with gradient u travels with respect to the ray originating at the origin of the axis with gradient u,

$$w = y \sin\theta \cong yu. \tag{A.25}$$

Rewriting (A.25) in terms of wavelength ϕ one finds

$$\phi = \frac{2\pi}{\lambda} yu. \tag{A.26}$$

The difference between path lengths r_1 and r_2 for two parallel rays from two points on the y-axis to the corresponding point of convergence (f, d) is approximately the same. Further one can assume that within the paraxial approximation the path length between any ray from the input plane y to the focal plane f is the same. Attenuation due to path length is therefore a constant factor referred to as K_{A}.

Now calculating the interference at any point (f, d) as the sum of all the parallel rays from the input plane y to any point on the focal plane by taking their phase into account one finds

$$f(u) = K_{\mathrm{A}} \int_{-\infty}^{\infty} f(y) e^{j\phi} dy. \tag{A.27}$$

Substituting Eq. (A.26) into Eq. (A.27) one finds

$$f(u) = K_{\mathrm{A}} \int_{-\infty}^{\infty} f(y) e^{j\frac{2\pi}{\lambda} yu} dy. \tag{A.28}$$

The resultant equation is one dimensional, and can be easily expanded to two dimensions by defining ϕ as

$$\phi = \frac{2\pi}{\lambda}(yu_{\mathrm{y}} + xu_{\mathrm{x}}). \tag{A.29}$$

Now the input function could be defined on the $(x_{\mathrm{i}}, y_{\mathrm{i}})$ plane as $f(x_{\mathrm{i}}, y_{\mathrm{i}})$ and substituting the relation $u_{\mathrm{x}} = \frac{x_{\mathrm{o}}}{f}, u_{\mathrm{y}} = \frac{y_{\mathrm{o}}}{f}$ thereby defining a coordinate on the

Stellenbosch University http://scholar.sun.ac.za

output plane as (x_o, y_o) one finds

$$f(x_o, y_o) = K_A \iint_{-\infty}^{\infty} f(x_i, y_i) e^{j\frac{2\pi}{\lambda f}(y_i y_o + x_i x_o)} dx_i dy_i. \quad (A.30)$$

From Eq. (A.28) it is clear that the ideal thin lens performs a Fourier transformation.

A.4 The plane wave

In order to understand better the definition of a plane wave in Cartesian co-ordinates let's consider the two dimensional case[1] as illustrated in Fig. A.2.

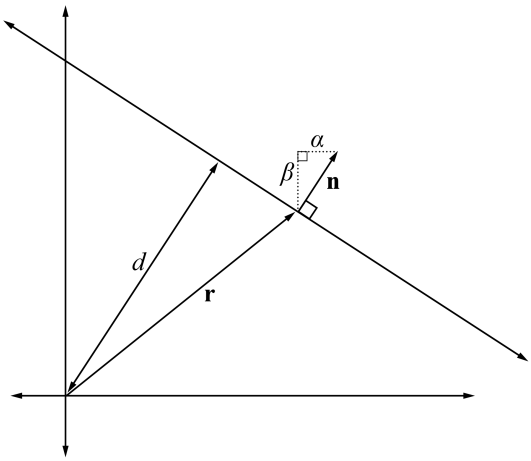

Figure A.2: A line in two dimensional Cartesian co-ordinates

The line in Fig. A.2 in Cartesian co-ordinates can be defined by the equation,

$$\mathbf{n} \cdot \mathbf{r} = d. \quad (A.31)$$

With this in mind a plane wave can be defined as illustrated in Fig. A.3 by

$$\mathbf{B}(x, y) = \exp\left[j\frac{2\pi}{\lambda}(\alpha x + \beta y)\right]. \quad (A.32)$$

From Fig. A.3 it is clear that

$$n^2 = 1 = \alpha^2 + \beta^2. \quad (A.33)$$

[1] For background regarding vector calculus see Zill and Cullen [78]

Stellenbosch University http://scholar.sun.ac.za

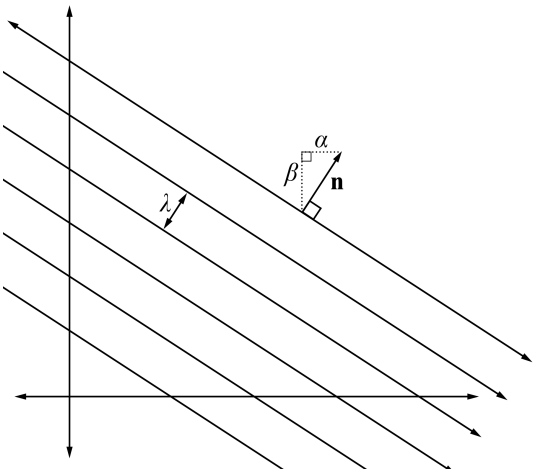

Figure A.3: Plane waves in two dimensional Cartesian co-ordinates

Now expanding this to three dimensions one finds

$$\mathbf{B}(x,y,z) = \exp\left[j\frac{2\pi}{\lambda}(\alpha x+\beta y+\gamma z)\right] \tag{A.34}$$

$$1 = \alpha^2+\beta^2+\gamma^2. \tag{A.35}$$

Eq. (A.35) can now be rewritten as

$$\gamma = \sqrt{1-\alpha^2-\beta^2} \tag{A.36}$$

A.5 Variation of the mean

Given a random variable X of which the variance σ is known. If N samples are taken of X then the mean is determined by

$$\bar{X} = \frac{1}{N}\sum_{i=1}^{N} X_i. \tag{A.37}$$

Thus if $\mathrm{var}(Y)$ is a function which determines the variance of a random variable Y then one can write the variance of the mean given by Eq. (A.37) as follows

$$\begin{aligned}\sigma^2_{\text{mean}} = \mathrm{var}(\bar{X}) &= \mathrm{var}\left(\frac{1}{N}\sum_{i=1}^{N} X_i\right)\\ &= \frac{1}{N^2}\sum_{i=1}^{N}\mathrm{var}(X_i).\end{aligned} \tag{A.38}$$

Stellenbosch University http://scholar.sun.ac.za

Since the variance of the sample is given and is constant, irrelevant of sample size, one can substitute σ^2 into Eq. (A.38) to find

$$\begin{aligned} \sigma^2_{\text{mean}} = \text{var}(\bar{X}) &= \frac{1}{N^2}\sum_{i=1}^{N}\sigma \\ &= \frac{\sigma^2}{N}. \end{aligned} \tag{A.39}$$

Taking the square root of Eq. (A.39) one finds

$$\sigma_{\text{mean}} = \frac{\sigma}{\sqrt{N}}. \tag{A.40}$$

A.6 Gaussian beam calculations

The equation describing the radius of the Gaussian laser beam a distance z from the origin is given by, see Brooker [79][2]

$$w(z) = w_0\sqrt{1+\left[\frac{z}{z_{\text{R}}}\right]^2} \tag{A.41}$$

where

$$\begin{aligned} w(z) &= \text{The radius of a Gaussian beam at a distance } z \text{ from the origin} \\ w_0 &= \text{The radius of the waist at the origin} \\ z &= \text{The distance from the origin along the axis of the beam} \\ z_{\text{R}} &= \text{The Rayleigh range about the origin of the beam.} \end{aligned}$$

The Raleigh range is where the wave front of the beam is no longer approximately spherical and where the waist of the Gaussian beam begins to form, and is given as

$$z_{\text{R}} = \frac{\pi {w_0}^2}{\lambda}. \tag{A.42}$$

The ratio of actual beam diameter to ideal beam diameter is referred to by M^2

[2] Brooker [79] on page 154

Stellenbosch University http://scholar.sun.ac.za

and is incorporated into Eq. (A.41) describing the beam radius as follows

$$w(z) = w_0\sqrt{1+\left[M^2\frac{z}{z_R}\right]^2} \tag{A.43}$$

where

$$M^2 = \text{The beam quality factor.}$$

From Eq. (A.43) which describes beam diameter we can derive an equation for the beam divergence as follows

$$\lim_{z\to\infty} w(z) = M^2 w_0\frac{z}{z_R}. \tag{A.44}$$

Substituting (A.42) into (A.44) one finds

$$\lim_{z\to\infty} w(z) = M^2\frac{z\lambda}{\pi w_0}. \tag{A.45}$$

Now taking the derivative of Eq. (A.45) one finds

$$\lim_{z\to\infty} \frac{d}{dz}w(z) = M^2\frac{\lambda}{\pi w_0}. \tag{A.46}$$

Noting that the derivative is equal to $\tan\theta$ one can write

$$\tan\theta = M^2\frac{\lambda}{\pi w_0} \tag{A.47}$$

and finally rewriting Eq. (A.47) with θ as the subject of the equation to find the equation for the divergence of a Gaussian laser beam as,

$$\theta = \tan^{-1}\left(M^2\frac{\lambda}{\pi w_0}\right) \tag{A.48}$$

$$\cong M^2\frac{\lambda}{\pi w_0} \tag{A.49}$$

where Eq. (A.49) is an approximation which holds for small values of $M^2\frac{\lambda}{\pi w_0}$.

If the angle at which a Gaussian beam diverges is known and the focal length to a lens which collimates the beam is known then one can calculate the beam

Stellenbosch University http://scholar.sun.ac.za

diameter after the lens as

$$w_l = f \tan \theta M^2 \tag{A.50}$$

where

$$w_l = \text{The collimated } \frac{1}{e} \text{ beam radius.}$$

The diameter of the waist can be found with the simple relation

$$d_l = 2\, w_l \tag{A.51}$$

where

$$d_l = \text{The collimated } \frac{1}{e} \text{ beam daimeter.}$$

The beam waist for a Gaussian beam can be calculated using Fourier optical theory. A Gaussian beam is illustrated in Fig. A.4.

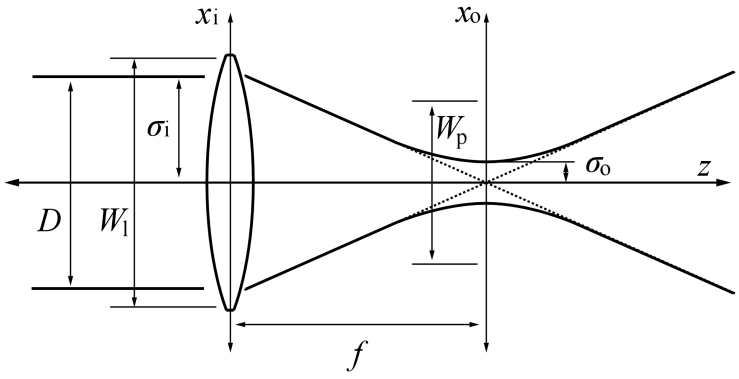

Figure A.4: Gaussian beam waist

From Fourier theory the general scaling property of the Fourier transform of a function is, see Peebles [46][3]

$$f\left(\frac{x}{\alpha}\right) \quad \underset{\longleftrightarrow}{\mathcal{F}} \quad |\alpha| F\left(\alpha\omega\right) \tag{A.52}$$

and the Fourier transform of a Gaussian function is, see Peebles [46][4]

$$\exp\left(-\frac{x^2}{2\sigma^2}\right) \quad \underset{\longleftrightarrow}{\mathcal{F}} \quad \sigma\sqrt{2\pi}\exp\left(-\frac{\sigma^2\omega^2}{2}\right). \tag{A.53}$$

[3] Peebles [46] on page 426
[4] Peebles [46] on page 434

Stellenbosch University http://scholar.sun.ac.za

In Fourier optics the resultant output can be scaled to meters by the relation

$$\omega = \frac{2\pi}{\lambda f} x_o \tag{A.54}$$

where

$$\begin{aligned} x_o &= \text{The co-ordinate in the lens plane} \\ f &= \text{The focal length of the lens} \end{aligned}$$

thus the scaled optical Fourier transform of a Gaussian function becomes

$$\exp\left(-\frac{x_i^2}{2\sigma_i^2}\right) \overset{\mathcal{F}}{\longleftrightarrow} \sigma\sqrt{2\pi}\exp\left(-\frac{\sigma_i^2\left[\frac{2\pi}{\lambda f}x_o\right]^2}{2}\right) \tag{A.55}$$

where

$$\begin{aligned} x_o &= \text{The co-ordinate in the focal plane} \\ \sigma_i &= \text{The Gaussian beam radius before the lens.} \end{aligned}$$

From Eq. (A.55) the Gaussian radius of the waist can be determined as

$$\sigma_o = \frac{\lambda f}{2\pi\sigma_i} \tag{A.56}$$

where

$$\sigma_o = \text{The Gaussian beam radius at the focal plane.}$$

Defining the Gaussian beam diameter in terms of the the cutoff diameter in front of the lens one can write

$$\frac{W_l}{2} = N_l\sigma_i \tag{A.57}$$

where

$$\begin{aligned} W_l &= \text{Cutoff diameter before the lens} \\ N_l &= \text{The lens cutoff constant.} \end{aligned}$$

The lens cutoff constant can be chosen such that the beam is affected as little

Stellenbosch University http://scholar.sun.ac.za

as possible by the diameter of the lens.

If one focuses a Gaussian beam through a pinhole then the diameter of the pinhole can be defined as follows

$$\frac{W_p}{2} = N_p \sigma_o \tag{A.58}$$

where

$$\begin{aligned} W_p &= \text{Cutoff diameter at the focal plane} \\ N_p &= \text{The pinhole cutoff constant.} \end{aligned}$$

With the pinhole diameter defined as given by Eq. (A.58) we can choose the pinhole cutoff constant such that most of the beam energy passes through the pinhole.

Now we can manipulate and substitute Eq. (A.58) and Eq. (A.57) into Eq. (A.56) to find a general expression which relates lens diameter to pinhole diameter as

$$W_p = \frac{2 N_p N_l \lambda f}{\pi W_l} \tag{A.59}$$

If one wants to calculate the $\frac{1}{e}$ waist diameter for a beam passing through a lens one can use Eq. (A.59) by choosing $N_p = N_l = \sqrt{2}$. This choice for the cutoff constants will have the result such that $\frac{W_l}{2} = w_l$ and $\frac{W_p}{2} = w_p$ and substitution of these into Eq. (A.59) results in

$$w_p = \frac{\lambda f}{\pi w_l} \tag{A.60}$$

where

$$\begin{aligned} w_l &= \text{The } \frac{1}{e} \text{ beam radius before the lens} \\ w_p &= \text{The } \frac{1}{e} \text{ beam radius at the focus} \end{aligned}$$

which describes the relation between the $\frac{1}{e}$ beam radius at the lens and at the focal plane.

Stellenbosch University http://scholar.sun.ac.za

A.7 The Fourier optical pattern for a disc sample

The Fourier optical pattern for a mask $t_{oc}(x,y)$ placed in front of a Fourier optical system where one measures only intensity and are only interested in the position of features on the resultant pattern as explained in Section 2.5.4 is given by

$$U_{\mathrm{fc}}(x_{\mathrm{f}},y_{\mathrm{f}}) = K \iint_{-\infty}^{\infty} t_{\mathrm{oc}}(x,y) P\left(x_{\mathrm{o}}+\frac{d_{\mathrm{o}}}{f}x_{\mathrm{f}}, y_{\mathrm{o}}+\frac{d_{\mathrm{o}}}{f}y_{\mathrm{f}}\right) \exp\left[-j\frac{2\pi}{\lambda f}(x_{\mathrm{o}}x_{\mathrm{f}}+y_{\mathrm{o}}y_{\mathrm{f}})\right] dx_{\mathrm{o}}dy_{\mathrm{o}}. \quad \text{(A.61)}$$

Assuming the mask is small enough such that the pupil function could be ignored then the function becomes the same as that for a sample placed against the lens. Further assuming rotational symmetry one can rewrite Eq. (A.61) as

$$U_{\mathrm{fc}}(r_{\mathrm{f}}) = K \iint_{-\infty}^{\infty} t_{\mathrm{oc}}(r_{\mathrm{o}}) \exp\left[-j\frac{2\pi}{\lambda f}r_{\mathrm{o}}r_{\mathrm{f}}\right] dr_{\mathrm{o}}. \quad \text{(A.62)}$$

For a disc of diameter d at the input of the Fourier optical system one can calculate the resultant pattern at the output of the system using Eq. (A.62) as

$$U_{\mathrm{fc}}(r_{\mathrm{f}}) = \mathrm{sinc}\left(\frac{r_{\mathrm{o}}\pi d}{\lambda f}\right) \quad \text{(A.63)}$$

Consider the intensity of the pattern which results from Eq. (A.63) then the minima are given by

$$\frac{r_{\mathrm{o}}\pi d}{\lambda f} = n\pi. \quad \text{(A.64)}$$

From Fourier theory it is known that the diameter of the disc is proportional to the spacing of the minima. It is also known that the position of the first minimum is equal to the spacing between the minima thus one can find an expression to determine the diameter of the disc and the focal length of the system by substituting $T = r_{\mathrm{o}}$ and $n = 1$ into Eq. (A.64) to find

$$d = \frac{\lambda f}{T} \quad \text{(A.65)}$$

$$f = \frac{Td}{\lambda}. \quad \text{(A.66)}$$

Stellenbosch University http://scholar.sun.ac.za

A.8 The spectral sinc filter

Let's first define a spectral sinc filter as a sinc function which is multiplied with the spectrum of some arbitrary signal. One can derive the width of a rect function which must be convolved with the temporal signal to have the same effect as the multiplication of the signal spectrum with a sinc function.

Let's define the spectral sinc filter such that it attenuates a specific spectral component in the spectral domain by a specified amount.

It is known from Fourier theory that the spacing between the spectral zeros of a $\text{sinc}(X)$ function can be used to determine the width of the $\text{rect}(x)$ function in the temporal domain.

Let's define the $\text{rect}\left(\frac{x}{w}\right)$ function as

$$\text{rect}\left(\frac{x}{w}\right) = \begin{cases} 1, & \text{for } -\frac{w}{2} < x < \frac{w}{2} \\ 0, & \text{elsewhere.} \end{cases} \tag{A.67}$$

Starting from the spectral domain one can write an expression for an arbitrary sinc function which will serve to attenuate an arbitrary chosen spectral frequency X_f by a chosen factor k_f due to being scaled in it's width by a constant a,

$$\text{sinc}\left(\frac{X_\text{f}}{a}\right) = k_\text{f}. \tag{A.68}$$

Using Eq. (A.68) one can solve for a to find,

$$a = \frac{X_\text{f}}{\text{sinc}^{-1}(k_\text{f})}. \tag{A.69}$$

Now an expression for the spectral sinc filter with the required attenuation properties can be written as

$$F(X) = \text{sinc}\left[\frac{X\,\text{sinc}^{-1}(k_\text{f})}{X_\text{f}}\right] \tag{A.70}$$

From Fourier theory it is known that the width of the resultant rect function when performing an inverse Fourier transform on a sinc function is inversely proportional to the spacing between the zeros of the sinc function. It is also known that the spacing between the zeros of a sinc function is equal to the distance from the origin to the first zero of the sinc function, thus from Eq. (A.70)

Stellenbosch University http://scholar.sun.ac.za

we can calculate the spacing of zeros by finding the position of the first zero at $X = X_s$ where $n = 1$,

$$\begin{aligned} \frac{X_s \operatorname{sinc}^{-1}(k_f)}{X_f} &= n\pi \\ \Rightarrow X_s &= \frac{\pi X_f}{\operatorname{sinc}^{-1}(k_f)}. \end{aligned} \tag{A.71}$$

Now one can determine the width of a rect function that would result from the inverse discrete Fourier transform, given

$$T_s = \frac{N}{X_s} \tag{A.72}$$

and substituting Eq. (A.71) into Eq. (A.72) one finds

$$T_s = \frac{N \operatorname{sinc}^{-1}(k_f)}{\pi X_f}. \tag{A.73}$$

One can use Eq. (A.73) to calculate the width of a rect function in discrete space which must be convolved with the temporal signal in order to have the correct spectral attenuation. Rewriting Eq. (A.73) with w as defined in Eq.(A.67) one finds

$$w = T_s. \tag{A.74}$$

For the purposes of this thesis we have determined from a graph the following values for the inverse *sinc* function,

$$\begin{aligned} \operatorname{sinc}^{-1}(0.5) &= 0.6034\pi \\ \operatorname{sinc}^{-1}(0.9) &= 0.2504\pi \end{aligned} \tag{A.75}$$

Stellenbosch University http://scholar.sun.ac.za

B

Ray Tracer

The ray tracing program was implemented in Matlab. In this appendix we describe the basic data types used and give a list of the functions and describe their functionality.

B.1 Data types

The following is a descriptive list of the data types used.

ray - An array containing the position and angle of a ray.

base element - A set of parameters which defines an optical element without fixing it's position and orientation.

element - An *element* is a collection of arrays each of which contains the parameters describing the surface shape, it's position and orientation for each surface which makes up an optical element.

trace data - A collection of arrays containing the position of intersection for a ray passing through a collection of *elements* as well as the index of refraction for each section and the propagation angle of the ray.

B.2 Functions

The following is a list of functions and their descriptions.

elements - Globally defines a collection of *base elements* with correct index of refraction for the wavelength 635 nm. The index of refraction was obtained from OSLO Lite Software.

Stellenbosch University http://scholar.sun.ac.za

create_element - Uses base optical element data such as is defined by the "elements" procedure to generate *elements* located at specified positions and orientations through the following functions:

- ***define_zemax_apcx -*** Generates the *element* data set for a Plano convex spheric or aspheric lens for a specified position and orientation.
- ***define_beam_split -*** Generates the *element* data set for a beam splitter plate for a specified position and orientation.
- ***define_beam_split_box -*** Generates the *element* data set for a beam splitter box for a specified position and orientation.
- ***define_achromat -*** Generates the *element* data set for an achromat lens for a specified position and orientation.
- ***define_zemax_adcx -*** Generates the *element* data set for a double convex spheric or aspheric lens for a specified position and orientation.

genray_array_th - Generates a specified number of parallel *rays* equally spaced within a specified width with their origins centered about a specified point at a specified orientation.

genray_point - Generates a specified number of *rays* originating from a specified point. The rays are spread out in a cone of a specified angle and the centre of the cone is aimed at a specified angle.

genrays - Generates *rays* originating from a specified point traveling at angles calculated for the zero field orders of the far field diffraction pattern for a slit of given width. The number of rays depends on the specified number of orders.

genrays_tpt - Generates a set of *rays* corresponding to a given set of angles such that each ray in the set starts at a specified position on the x-axis and passes through a specified point.

draw_element - Draws an optical element according to its defined *element* data set on a Cartesian axis.

draw_elements - Draws a set of optical elements according to their respective *element* data set definitions.

draw_plane - Base function to draw a plane as defined in an *element* data set.

Stellenbosch University http://scholar.sun.ac.za

draw_zemax - Base function to draw a spheric or aspheric surface as defined in an *element* data set.

draw_rays - Draws a set of *rays* extending each up to a specified length.

ray_trace_I - Generates *trace data* for a specified set of rays through a specified collection of *elements*.

ray_trace_esurf_I - Generates *trace data* for a specified collection of *elements* up to a specified *element* and a specified surface within the *element*. The function additionally generates *rays* as reflected by the specified surface of the *element*.

plot_rays_xstop - Draws *trace data* and extends the data to end at a specified position on the x-axis.

plot_rays_ystop - Draws *trace data* and extends the data to end at a specified position on the y-axis.

plot_rays_esurf - Draws *trace data* up to a specified surface and element.

find_best_waist - Generates the co-ordinates of a line across the minimum point of convergence for specified *trace data*.

ray_cross - Calculates the intersection points of a *ray* crossing an *element*.

Stellenbosch University http://scholar.sun.ac.za

C

Pattern analysis code

In this appendix the functions used to analyse a pattern image is listed with a brief description of the parameters for each function.

C.1 Example code to analyse a pattern image

The following code listing C.1 is a code example of the commands used to determine the effective focal length from a sample pattern with known diameter. The functions used are listed in Appendix C.2.

Listing C.1: Matlab code example to determine the effective focal length from the pattern image of a sample with known diameter.

```
directory = '..\..\Final Experiments\exper\';
[cx,cy] = get_cx_cy([directory '60um Wire'],'cen');
im_pat = double(imread([directory '60um Wire\60um 14.5mA.bmp'
    ]));
im_nul = double(imread([directory '60um Wire\60um 14.5mA
    nowool.bmp']));
im_cen = double(imread([directory '60um Wire\cen.bmp']));
f = analyse_fixed_pat(im_cen, im_nul, im_pat, 635e-9, 60e-6,
    6.7e-6);
```

The following code listing C.2 is a code example of the commands used to determine the mean diameter of a sample pattern from a random sample of wool.

Listing C.2: Matlab code example to determine the diameter of a sample.

```
directory = '..\..\Eksperimente\Experiment 18 - Image analysis
    \three images\';
im_cen = double(imread([directory 'thin 13.7mA cen.bmp']));
im_nul = double(imread([directory 'thin 13.7mA nowool' '.bmp'
    ]));
```

Stellenbosch University http://scholar.sun.ac.za


```
im_pat = double(imread([directory 'thin 13.7mA' '.bmp']));
d = analyse_sample_pat(im_cen, im_null, im_pat, 635e-9,
    37.6827896512936e-003, 6.7e-6);
```

C.2 Example of code used to process the final experiment

If the effective focal length of the system has been determined we can use the following code to process a batch of pattern images. The functions used assume a file name with the following format: a prefix 'back' followed by the sample number, in the case of the null image there is no suffix and in the case of the pattern image a suffix of 'a'. A single centre image is shared between all samples named 'cen.bmp'.

The following code listing C.3 starts the batch processing of the experiment.

Listing C.3: Matlab code example to evoke the batch processing of the final experiment.

```
dias_a = proc_exper('..\..\Final Experiments\exper',
    38.2312055921414e-003, 635e-9, 6.7e-6);
```

The following is a code listing of the following two functions C.4 and C.5 which does the batch processing of the pattern images.

Listing C.4: Matlab code to analyse a sample set.

```
function dias = proc_exper(directory,f,lambda,pix_W)
%directory - The location of the batch of pattern images
%f - The effective focal length of the system
%lambda - The wavelength of the light source
%pix_W - The width of a CCD pixel
%dias - The returned array of diameters for the batch of
%       pattern images
min_count = 0;
for n = 1:15;
    try
        disp(['current sample number : ' num2str(n)]);
        [im_cen, im_null, im_pat] = load_back(directory,n);
        dias(n-min_count) = analyse_sample_pat(im_cen,im_null,
            im_pat,lambda,f,pix_W);
    catch
```

Stellenbosch University http://scholar.sun.ac.za


```
            disp(['There is no sample number (' num2str(n) ')
                ignoring...']);
            min_count = min_count + 1;
        end;
    end;
```

Listing C.5: Matlab code to load an image set for a sample set.

```
function [im_cen, im_null, im_pat] = load_back(directory,
    back_nr)
%directory - The location of the batch of pattern images
%back_nr - The number in the batch to load
%im_cen - The returned centre image
%im_null - The returned null image
%im_pat - The returned pattern image
im_pat = double(imread([directory '\back' num2str(back_nr) 'a.
    bmp']));
im_null = double(imread([directory '\back' num2str(back_nr) '.
    bmp']));
im_cen = double(imread([directory '\cen.bmp']));
```

C.3 Pattern image analysis functions

Listing C.6: Matlab code to analyse the image pattern and return the mean diameter.

```
function [dia] = analyse_sample_pat(im_cen, im_null, im_pat,
    lambda, f, pix_W)
%im_cen - Centre image
%im_null - Null image
%im_pat - Pattern image of the sample
%lambda - The wavelength of the light source
%f - The effective focal length of the system
%pix_W - The width of a pixel on the CCD camera
%dia - The returned mean diameter of the sample
[cx, cy] = find_center(im_cen);
im = im_pat - im_null;
s_vect = sample2vect_xy(im,cx,cy);
s_vect_scale = s_vect.* [1:length(s_vect)].^2;
s_vect_scale = smoothen(s_vect_scale,8);
s_vect_scale = smoothen(s_vect_scale,3);
```

Stellenbosch University http://scholar.sun.ac.za


```
s_vect_scale = smoothen(s_vect_scale,3);
tzer = imgetzeros(s_vect_scale,[zeros(1,28)],1);
pos = tzer(1);
pos_mm = pos*pix_W;
dia = lambda * f / pos_mm;
```

Listing C.7: Matlab code to analyse the image pattern and return the effective focal length.

```
function [f, pos] = analyse_fixed_pat(im_cen, im_null, im_pat,
    lambda, W, pix_W)
%im_cen - Centre image
%im_null - Null image
%im_pat - Pattern image of the sample
%lambda - The wavelength of the light source
%W - The mean diameter of the sample
%pix_W - The width of a pixel on the CCD camera
%f - The returned effective focal length of the system
%pos - The returned position of the first minima in the
%      pattern vector
[cx, cy] = find_center(im_cen);
im = im_pat - im_null;
s_vect = sample2vect_xy(im,cx,cy);
s_vect_scale = s_vect.* [1:length(s_vect)].^2;
d_s_vect_scale = diff(s_vect_scale);
VECT = abs(fftshift(fft(d_s_vect_scale,5000)));
index = -2500:2500-1;
[v,i] = max(VECT);
minima_1 = 5000/abs(index(i)) * pix_W;
pos = 5000/abs(index(i));
f = minima_1 * W / lambda;
```

Listing C.8: Matlab code to find the centre of a centre image.

```
function [cx,cy] = find_center(im)
%im - The centre image
%cx - The returned centre of the image on the x-axis
%cy - The returned centre of the image on thy y-axis
I = find(im<200);
im2 = im;
im2(I) = 0;
```

Stellenbosch University http://scholar.sun.ac.za


```
[cx,cy] = expected_2D(im2);
```

Listing C.9: Matlab code to find the centroid of an image.

```
function [ex,ey] = expected_2D(im)
%im - The centre image
%ex - The returned centre of the image on the x-axis
%ey - The returned centre of the image on the y-axis
[i j] = size(im);
by = 0;
bx = 0;
a = 0;
for m = 1:i
    for n = 1:j
        by = by+m*im(m,n);
        bx = bx+n*im(m,n);
        a = a+im(m,n);
    end
end
ey = by / a;
ex = bx / a;
```

Listing C.10: Matlab code to convert a pattern image to a pattern vector.

```
function [values] = sample2vect_xy(A,x,y)
%A - The pattern image
%x - The centre of the pattern image on the x-axis
%y - The centre of the pattern image on the y-axis
%values - The returned pattern vector
[i j] = size(A);
values = zeros(1,round(min([x y]))-1);
ncount = zeros(1,round(min([x y]))-1);
for n = 1:i
    for m = 1:j
        dst = sqrt( (n-y)^2 + (m-x)^2 );
        pos = round(dst+1);
        if pos <= min([x y])
            try
                values(pos) = values(pos) + A(n,m);
                ncount(pos) = ncount(pos) + 1;
            catch
```

Stellenbosch University http://scholar.sun.ac.za


```
                values2 = [values 0];
                ncount2 = [ncount 0];
                values = values2;
                ncount = ncount2;
                values(pos) = values(pos) + A(n,m);
                ncount(pos) = ncount(pos) + 1;
            end
        end;
    end;
end;
I = (ncount == 0);
ncount(I) = 1;
values = values./ncount;
```

Listing C.11: Matlab code to find the position of the zeros of a vector.

```
function [zero] = imgetzeros(vect, mask, grad)
%vect - The vector which must be processed to find its zero
%      crossings
%mask - A mask which allows us to ignore certain areas of
%      the vector
%grad - A value of 1 returns zero crossings where the
%      gradient is bigger than zero, a value of -1 returns
%      zero crossings where the gradient is smaller than
%      zero and a value of 0 returns both.
dvect = diff(vect);
D = size(dvect);
count = 0;
if length(mask) < length(vect)
    mask = [mask ones(1,abs(length(mask)-length(vect)))];
end;
for n = 1:D(2)-1
    if mask(n) == 1
        if grad == 0 || grad == -1
            if ((dvect(n) > 0) && (dvect(n+1) <0)) || (dvect(n
                ) == 0)
                count = count + 1;
                zero(count) = (dvect(n+1)*n - dvect(n)*(1+n))
                    /(dvect(n+1) - dvect(n)) +0.5;
            end
        end;
```

Stellenbosch University http://scholar.sun.ac.za


```
            if grad == 0 || grad == 1
                if ((dvect(n+1) > 0) && (dvect(n) <0)) || (dvect(n
                    ) == 0)
                    count = count + 1;
                    zero(count) = (dvect(n+1)*n - dvect(n)*(1+n))
                        /(dvect(n+1) - dvect(n)) +0.5;
                end
            end;
        end;
    end
```

Stellenbosch University http://scholar.sun.ac.za

D

Cool beard

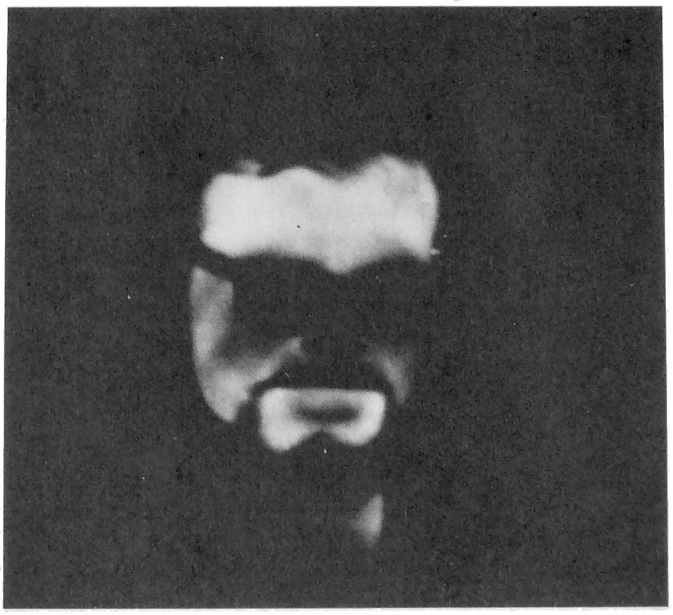

Figure 3.37 Thermograph of the author. Note the cool beard.

Figure D.1: Scan of Figure 3.37 on page 71 from Hecht [1]

Stellenbosch University http://scholar.sun.ac.za

References

[1] Hecht, E.: *Optics* . World Student Series, 3rd edn. Addison-Wesley, Reading, Mass., 1998. ISBN 0-201-30425-2.

[2] Goodman, J.W.: *Introduction to Fourier Optics*. Roberts & Company, 2005.

[3] von Bergen, W. and Krauss, W.: *Textile Fiber Atlas*. American wool handbook company, 1942.

[4] Perich, J., Rivett, D. and Johns, R.: Modification of wool-fibre properties by phosphorylative treatment. *Journal of the Textile Institute*, vol. 83, no. 4, pp. 498–506, 1992.

[5] Sommerville, P.: Fundamental principles of fibre fineness measurement. AWTA Ltd. Newsletter, March 2004. Part 12 - Porosity.

[6] Lynch, L.J. and Michie, N.A.: Optical shadowing method and apparatus for fibre diameter measurement. 1973.

[7] Lynch, L.J. and Michie, N.A.: An instrument for the rapid automatic measurement of fiber fineness distribution. *Textile Research Journal*, vol. 56, pp. 653–660, 1976.

[8] Cantrall, C.J., Dabbs, T.P., Glass, M., Humphries, W. and Wills, L.J.: Method for apparatus for determining measurement parameter of a fibrous object and whether the object is a valid object. 1996.

[9] Sommerville, P.: Fundamental principles of fibre fineness measurement. AWTA Ltd. Newsletter, August 2006. Part 13 - Photometry.

[10] Matthew, J.A.: 6-measurement of fibre and yarn diameters by diffraction method. *The Journal of the textile institute transactions*, vol. 23, no. 3, pp. T55–T70, 1932.

Stellenbosch University http://scholar.sun.ac.za

[11] Boshoff, M.C. and Kruger, P.J.: The mikronmeter - an instrument for the rapid measurement of mean fiber diameter. *Textile Research Journal*, vol. 41, pp. 573–576, 1971.

[12] Marler, J.W. and Harig, H.: A comparison of diameter measurement technologies from interwoollabs international round trials for wool tops. Technology and Standards Committee Report No. 10, International Wool Textile Organisation, Dresden, June 1998.

[13] Gaskill, J.D.: *Linear systems, Fourier transforms, and optics*. John Wiley & Sons Inc., 1978.

[14] Hibbeler, R.C.: *Statics and Mechanics of Materials*. Prentice-Hall Inc., 1991.

[15] Carlson, F.P.: *Introduction to Applied Optics for Engineers*. Academic Press, 1977.

[16] Born, M. and Wolf, E.: *Principles of optics*. 7th edn. Cambride University Press, 1999.

[17] Silver, S.: Microwave aperture antennas and diffraction theory. *Journal of the Optical Society of America*, vol. 52, p. 131, 1962.

[18] Collins english dictionary - complete & unabridged. HarperCollins Publishers, Feb 2011.
Available at: `http://dictionary.reference.com/browse/wool`

[19] Dictionary.com unabridged. Random House, Inc, Feb 2011.
Available at: `http://dictionary.reference.com/browse/wool`

[20] D'Arcy, J.B.: *Sheep Management and Wool Technology*. 3rd edn. New South Wales University Press Ltd, 1990.

[21] Dictionary.com unabridged. Feb 2011.
Available at: `http://dictionary.reference.com/browse/woolly`

[22] Hill, J.A.: Micrometer calipers for teaching the discrimination of the fineness of wool. *Journal of Animal Science*, vol. 1922, pp. 8–11, 1922.

[23] Burns, R.H.: Wool measurement technic. *Journal of Animal Science*, vol. 1930, pp. 111–121, 1930.

[24] Fairbanks, B.W.: Variation in the fineness of duplicate wool samples. *Journal of Animal Science*, vol. 1932, pp. 244–246, 1932.

Stellenbosch University http://scholar.sun.ac.za

[25] Stobart, R.H., Russell, W.C., Larsen, S.A., Johnson, C.L. and Kinnison, J.L.: Sources of variation in wool fiber diameter. *Journal of Animal Science*, vol. 62, pp. 1181–1186, 1986.

[26] Dunlop, A.A. and McMahon, P.R.: The relative importance of sources of variation in fibre diameter for australian merino sheep. *Australian Journal of Agricultural Research*, vol. 25, pp. 167–181, 1974.

[27] McNicholas, H.J. and Curtis, H.J.: Measurement of fiber diameter by the diffraction method. *Review of scientific instruments*, vol. Vol 2, May 1931, No 5, pp. 263–286, 1931.

[28] Simpson, W.S., Crawshaw, G.H., Höcker, D.H., Hearle, J.W.S., Halliday, L.A., Hunter, L., Parton, K., Russell, K., McDowell, D., Ryder, I., Smith, C., Russell, S., Myers, S.A. and Killduff, P.D.F.: *Wool: Science and technology*. Woodhead Publishing Ltd, 2002.

[29] Baxter, P.: Report on the 2004/05 ofda4000 and almeter/ofda100/laserscan round trial. Technology & Standards Committee Report No: SG 02, International Wool and Textile Organisation, April 2005. Sliver Group.

[30] Heath, W., Barkhuizen, J. and Wright, O.: The relationship between mean fibre diameter measurements by airflow and laserscan for south african wools. Technology & Standards Committee Report No: RWG 03, International Wool Textile Organisation, Cairo, May 2006. Raw Wool Group.

[31] The australian superfine woolgrowers' association inc. 2009.

[32] Baxter, B.P.: Examination of the differences between ofda and laserscan on ultrafine wools. Technology & Standards Committee Report No: 6, International Wool Textile Organisation, Nice, December 1997.

[33] Baxter, B.P.: Technical note: 5 micron fibres found in an ultrafine grower lot - implications for diameter distribution measurement. Technology & Standards Committee Report No: RWG 02, International Wool Textile Organisation, Shanghai, May 2001. Raw Wool Group.

[34] von Bergen, W.: Cashmere. *The Melliand*, vol. 1, no. 6, pp. 855–859, 1929.

[35] Tonin, C., Bianchetto, M. and Vineis, C.: Differentiating fine hairs from wild and domestic species: Investigations of shatoosh, yangir, and cashmere fibers. *Textile Research Journal*, vol. 72, pp. 701–705, 2002.

Stellenbosch University http://scholar.sun.ac.za

[36] von Bergen, W.: Musk-ox wool and its possibilities as a new textile fiber. *The Melliand*, vol. 3, no. 2, pp. 553–556, 1931.

[37] Rowell, J.E., Lupton, C.J., Robertson, M.A., Pfeiffer, F.A., Nagy, J.A. and White, R.G.: Fiber characteristics of qiviut and guard hair from wild muskoxen (ovibos moschatus). *Journal of Animal Science*, vol. 79, pp. 1670–1674, 2001.

[38] von Bergen, W.: Vicuna. *The Melliand*, vol. 2, no. 3, pp. 353–357, 1930.

[39] Boos, A.D., Naylor, G., Slota, I. and Stanton, J.: The effect of the diameter characteristics of the fibre ends on the skin comfort and handle of knitted wool fabrics. Technology & Standards Committee Report No: CTF 01, International Wool Textile Organisation, Nice, November 2001. Commercial Technology Forum.

[40] Baxter, B. and Brims, M.: Linearity and focus independence of the ofda. Technical Committee Report no.: 9, International Wool Textile Organisation, Nice, December 1992.

[41] Glass, M.: Fresnel diffraction from curved fiber snippets with application to fiber diameter measurement. *Applied Optics*, vol. 35, no. 10, pp. 1605–1616, April 1996.

[42] Cardamone, J.M., Nuñez, A., Garcia, R.A. and Aldema-Ramos, M.: Characterizing wool keratin. *Research Letters in Materials Science*, vol. 2009, p. 5 pages, 2009. Article ID 147175.

[43] Sommerville, P.: Fundamental principles of fibre fineness measurement. AWTA Ltd. Newsletter, January 2002. Part 2 - Understanding Fiber Diameter Measurement.

[44] Lundberg, J.L.: Light scattering from large fibers at normal incidence. *Journal of Colloid Interface Science*, vol. 29, Issue 3, pp. 565–583, March 1969.

[45] Lynch, L.J. and Thomas, N.: Optical diffraction profiles of single fibers. *Textile Research Journal*, vol. July, pp. 568–572, 1971.

[46] Peebles, P.Z.: *Probability , Random Variables and Random Signal Principles*. 4th edn. McGraw-Hill, 2001.

[47] Burns, R.H.: Fleece analysis in sheep. *Journal of Animal Science*, vol. 1932, pp. 246–258, 1932.

Stellenbosch University http://scholar.sun.ac.za

[48] Buchanan, M.L. and Bolin, D.W.: Wool fiber measurements. *Journal of Animal Science*, vol. 11, pp. 631–637, 1952.

[49] Koehler, W.F.: *Comparison of microscopic and micrometer caliper measurements*. Master's thesis, University of Wyoming, 1924.

[50] Sommerville, P.: Fundamental principles of fibre fineness measurement. AWTA Ltd. Newsletter, October 2002. Part 5 - Gravimetry.

[51] Sommerville, P.: Fundamental principles of fibre fineness measurement. AWTA Ltd. Newsletter, February 2002. Part 3 - Technologies for measuring the fineness of wool.

[52] Sommerville, P.: Fundamental principles of fibre fineness measurement. AWTA Ltd. Newsletter, December 2003. Part 11 - Sedimentomitry.

[53] Sommerville, P.: Fundamental principles of fibre fineness measurement. AWTA Ltd. Newsletter, July 2003. Part 9 - Harmonics.

[54] Sommerville, P.: Fundamental principles of fibre fineness measurement. AWTA Ltd. Newsletter, December 2003. Part 10 - Conductometry.

[55] Sommerville, P.: Fundamental principles of fibre fineness measurement. AWATA Ltd. Newsletter, May 2003. Part 8 - Radiometry.

[56] Burns, R.H.: Methods of instruction in the wool laboritory. *Journal of Animal Science*, vol. 1927, pp. 103–108, 1927.

[57] Hardy, J.I.: Cross sectional variability of wool fibers. *Journal of Animal Science*, vol. 1936a, pp. 144–146, 1936.

[58] Wilson, J.F.: The need of new units of measurement in wool research. *Journal of Animal Science*, vol. 1933, pp. 187–189, 1933.

[59] International Wool Textile Oragnisation, February 2011. Available at: `http://www.iwto.org/publications/iwto-standard-specifications/`

[60] IWTO: Method of test for the determination of the mean diameter of wool fibres in combed sliver using the airflow apparatus. International Wool Textile Organisation, March 2009. IWTO-6-98.

[61] IWTO: Determination by the airflow method of the mean fibre diameter of core samples of raw wool. International Wool Textile Organisation, March 2009. IWTO-28-00.

Stellenbosch University http://scholar.sun.ac.za

[62] IWTO: Method of determining fibre diameter distribution parameters and percentage of medullated fibres in wool and other animal fibres by the projection microscope. International Wool Textile Organisation, March 2009. IWTO-8-04.

[63] IWTO: Measurement of the mean and distribution of fibre diameter using the sirolan-laserscan fibre diameter analyser. International Wool Textile Organisation, March 2009. IWTO-12-09.

[64] IWTO: Measurement of the mean and distribution of fibre diameter of wool using an optical fibre diameter analyser (OFDA). International Wool Textile Organisation, March 2009. IWTO-47-09.

[65] IWTO: Determination of fibre length, length distribution, mean fibre diameter and fibre diameter distribution of wool top & slivers by the OFDA4000. International Wool Textile Organisation, January 2011. IWTO-62-10.

[66] Sommerville, P.: Fundamental principles of fibre fineness measurement. AWTA Ltd. Newsletter, May 2002. Part 4 - The Projection Microscope.

[67] Cassie, A.: The porous plug and fibre diameter measurement. a practical method of wool fibre diameter measurement. *Journal of the Textile Institute*, vol. 1942, no. 23, pp. 195–204, 1942.

[68] Anderson, S. and Warburton, F.: The porous plug and fibre diameter measurement. effect of fibre orientation and use of plugs of randomised fibres. *Journal of the Textile Institute*, vol. 1949, no. 40, pp. 749–758, 1949.

[69] Sommerville, P. and Teasdale, D.: Introduction of SIROLAN-LASERSCAN as the standard service for certification of mean fibre diameter by AWTA ltd: Commercial and technical implications. Technology & Standards Committee Report No: RWG 03, International Wool Textile Organisation, Florence, May 1999. Raw Wool Group.

[70] Baxter, B., Brims, M. and Taylor, T.: Description and performance of the optical fibre diameter analyser (ofda). *Journal of the Textile Institute*, vol. 83, no. 4, pp. 507–526, 1992.

[71] Sommerville, P.: Fundamental principles of fibre fineness measurement. AWTA Ltd. Newsletter, April 2007. Part 14 - Image Analysis.

[72] Baxter, P.: An evaluation of the performance of the ofda2000 instrument operating in ofda 100 mode. Technology & Standards Committee Report No:

Stellenbosch University http://scholar.sun.ac.za

RWG 03, International Wool Textile Organisation, Barcelona, May 2002. Raw Wool Group.

[73] Baxter, P. and Brims, M.: Performance of OFDA4000 instruments in three mill laboratories. Technology & Standards Committee Submission No: SG 01, International Wool Textile Organisation, Beijing, April 2008. Sliver Group.

[74] David, H.G. and Connell, J.P.: Confidence limits for the measurement of fiber diameter using the mikronmeter. *Textile Research Journal*, vol. 42, pp. 377–379, 1972.

[75] Wiktionary, October 2009.
Available at: `http://en.wiktionary.org/wiki/erio-`

[76] Ewles, J.: A simple optical method for determining rapidly the mean diameters of a number of fibers. *Journal of Textile Science*, vol. 1928, pp. 101–102, 1928.

[77] Edmunds, I.: A diffraction method for the estimation of average diameter and standard deviation of diameter in a fibre sample. *Journal of the Textile Institute*, vol. 60, no. 4, pp. 161–164, 1969.

[78] Zill, D.G. and Cullen, M.R.: *Advanced Engineering Mathematics*. Jones and Bartlett Publishers, 2000.

[79] Brooker, G.: *Modern Classical Optics*. Oxford University Press, 2003.